OPTIMAL-VELOCITY MODELS OF MOTORWAY TRAFFIC

By
Peter Berg
School of Mathematics

December 2001

A dissertation submitted to the University of Bristol
in accordance with the requirements of the degree
of Doctor of Philosophy in the Faculty of Science

Abstract

This thesis deals with the mathematical description of motorway traffic by optimal-velocity (OV) models. To date, any OV type is classified as one of two classes, which are considered independent: discrete car-following and continuum models.
In this work, it is shown that a transformation exists that relates these two classes so that under certain circumstances an analogous continuum version of a given car-following model can be derived. Correspondingly, certain continuum models can be transformed into their car-following counterpart.
This formalism is then applied to two cases of simulations. Firstly, the types of waves which connect traffic flow of two different fluxes are investigated in an OV car-following model. They can be interpreted in the analogous continuum picture. Secondly, an on-ramp simulation of an OV car-following model reveals, qualitatively, the same results as previous simulations of OV continuum models. This underlines the idea of their mathematical analogy and in the case of solitary waves, this can be shown explicitly.
Even though the correspondence between these two types of models is strictly shown for only one specific case, the Bando model, it can be generally assumed that they predict similar results for similar traffic situations. Hence, this work establishes a link between the microscopic (car-following models) and the macroscopic (continuum models) description of traffic.

Acknowledgements

My special thanks to all of those who made my PhD an enjoyable time.
Most of all to Rhona, whose smile makes up for any lack of sunshine in this rainy place. Thanks to my family for any support they have given me, Max and Gaëlle for their catering and caring services, Niels "Aaldäär" Wergin for keeping up the good mood, Robert and Luisa for just being themselves, Christian, Sabine, Ilja and Elke for getting here, Heiko, Terry and Andy for the matches, Duncan for his place, Julian for his "Spanish" lessons, Javier for standing by me at the Adams family and the Mendips for being perfect hills to cycle through.
This piece of work would have neither been started, nor finished without the financial support of the Alfried Krupp von Bohlen und Halbach-Stiftung. Here, most credits go to Herrn Seidenfus, Herrn Marheineke and Herrn Kempf for their acknowledgement of my special circumstances.
The work itself was made possible by the help of my supervisor, Professor Andy Woods, whose ideas and support have been essential, and whose personal engagement opened up my future opportunities in R&D. Moreover, Eddie Wilson played an important part in being my local reference person, and Boris Kerner delivered vital arguments for the on-ramp simulation.
The environment at work was unique due to the mixture of various cultures: Hakim and his views on life, Robert and his computational knowledge, Dave "Braveheart" Pritchard and his lessons in HTML and British history. An unforgettable bunch! Thanks to all of you.

Financial Support

Diese Arbeit wurde im Stipendienprogramm der Alfried Krupp von Bohlen und Halbach-Stiftung zur Förderung von Doktoranden auf dem Gebiet der Verkehrswissenschaften gefördert.

This dissertation has been supported financially by Alfried Krupp von Bohlen und Halbach-Stiftung. The author is a grateful recipient of this foundation's scholarship for PhD students in traffic research.

Author's Declaration

I declare that the work in this thesis was carried out in accordance with the Regulations of the University of Bristol. The work is original except where indicated by special reference in the text and no part of the dissertation has been submitted for any other degree. Any views expressed in the dissertation are those of the author and in no way represent those of the University of Bristol. The thesis has not been presented to any other University for examination either in the United Kingdom or overseas.

Peter Berg

Date: 05 December 2001

Contents

List of Tables

List of Figures

Chapter 1

Introduction

> *Road congestion may not be the most efficient solution to transport problems, but as an equitable solution it is hard to beat!* [74]

This dissertation comprises the scientific modelling of road traffic, with special regard to motorways, and its aim is to deliver further insight into the features of this road type. A powerful tool in revealing such deeper understanding is the application of simple flow models based on a mathematical description of the system. The study of complex computational simulations of these models, combined with an analytical analysis of some of their characteristics, should then ideally provide a better picture of how traffic works.
To date, the phenomena and processes which are involved in traffic flow are investigated by approaches which can be qualitatively divided into three classes: on a microscopic level we find *discrete car-following* and *stochastic* models, whereas the macroscopic scale is represented by the *continuum* models.
The features predicted by either of these classes show numerous similarities and it is a major purpose of this thesis to pull two of them together, the car-following and the continuum approach. This is in particular achieved by focusing on a special type that is found in both classes called the *optimal-velocity* model. This closes a gap between discrete modelling of the flow, which enables quick numerical simulations including reaction time and other individual driver characteristics, and continuum modelling, which provides easy means of analysing some phenomena through the extraction of asymptotic solutions and other analytical techniques.
In principle, one could also find an analogous way to link the stochastic to the deterministic models of this work. Therefore, the results of this dissertation should be regarded as a first step on which further work can be based.

The remainder of this chapter briefly assesses motorway traffic in modern transport infrastructure and gives reasons why we concentrate on this type of road. Then

it describes what mathematical modelling of traffic flow means, what applications have already been implemented or are currently being tested and, last but not least, what the objectives of this dissertation are in this framework.

1.1 Aspects and Relevance of Motorway Traffic

There are both economic and scientific reasons to focus on motorway traffic when it comes to traffic research, a few of which might be given here.
Speaking of the wider aspects of traffic, an efficient infrastructure is a prerequisite of a powerful economy [83] and it is, therefore, of great importance that it should be in an optimal condition. However, it seems that in most European countries the upper bounds of the dimension and the capacity of the road network is almost reached. This is likely to remain, because the road network of the Western world is so advanced that it is impossible to shift its entire volume to alternative means of transport. In the coming years, a rising demand for roads and their efficiency seems to be inevitable, but the growing environmental consciousness of the 1980s and 90s has set boundaries of this immense extension of road networks. Hence, the increase in congestion in urban and rural areas and car use may lead to serious social, economic and environmental problems, unless new technology is incorporated.
In this context, the European motorway network plays an important role. At 50 000km, it comes to less than five percent of the entire interurban road system, but accounts for more than thirty per cent of the annual mileage of all vehicles [21]. The economic use of motorways compared to other roads is far bigger in particular when considering their lengths. Correspondingly, the average throughput of a German autobahn reaches 43 940 vehicles per day, whereas the throughput of an ordinary interurban road remains just below 9 500 [21].
For all road types, traffic jams are an important aspect, because their environmental and economic costs increase from year to year. Politicians have begun to realize the enormous amounts of money which are wasted by congestion. Figures for the German road system lead to estimated annual costs of up to seventy billion pounds [3] of which motorways form a major part. This equals several per cent of the GDP. The vehicular traffic volume of the European Union has doubled between 1970 and 1993, and the European Conference of the Ministers of Transportation (ECMT) predicts an annual rise in traffic volume from 1.5 to 2.8 per cent for the next two decades [25]. At the same time, the UK's road congestion is forecast to increase by up to seventy per cent in the next 15 years [82].
The car industry and public institutions noticed as early as 1970 that the rising traffic volumes can only be managed by the current road system if more research is

carried out. This is not only an engineering task and, hence, a matter of technical applications; there is also a need for basic research including mathematical models of traffic flow which should provide a better understanding of the intrinsic features of the system. What all these measures have in common is that they try to maximize the throughput of the existing roads and minimize the travel times. This could be achieved by a combination of, for example,

- intelligent data response systems that make use of traffic flow modelling and its predictions, delivering rules of thumb of how to operate these systems,
- understanding of how to collect, interpret and use online traffic data that could identify the current flow regimes,
- tolling systems based on both current traffic levels and future predictions for various time scales.

As well as the practical applications of traffic modelling, the range of patterns and processes on motorways has raised the attention of applied mathematicians. The formation and propagation of *shock waves* (rapid transitions along the road between two zones of different flows), *stop-and-go traffic* (in which cars come to a total standstill in some regions and travel at intermediate speed in others), unstable flow that breaks down under sufficient perturbation near on-ramps, and transitions between different types of flow such as free flow, stop-and-go jams and *synchronized flow* (in which overtaking is almost non-existent and vehicles drive at intermediate and similar speed on all lanes with high flux) are all well observed phenomena. A natural question is whether they can be described and reproduced as results of simple mathematical models.
In fact, most of them have been successfully interpreted using *continuum models*, which are based on the traffic parameters car density and speed, and which focus on the macroscopic features of the flow. However, car traffic is a rather dilute system and, therefore, a common argument is that the flow should be regarded as a *discrete system*. The governing equations of these models are based on the distance between adjacent vehicles rather than on the density of vehicles.
In this work, a theory is derived of how to link these two descriptions. This is achieved by the development of a new approach to relate spatial car density and the distance between the vehicles. It turns out that the relation found in the literature is only a lowest order approximation which does not apply to non-homogenous flow situations. By analysing the correspondence of these models, we gain a deeper understanding of traffic flow modelling and are able to assess the validity of different models by investigating their mathematical structures and numerical predictions. One of these predictions is the range of transitions (wave types) between different

flows as they occur along the motorway, in particular, in the vicinity of ramps. Here, a closer examination of the wave types reveals which terms are important in certain flow regimes, when nonlinearity dominates and when it does not dominate. One may then try to identify real flow patterns with these theoretical predictions and, thereby, to obtain a better insight into traffic phenomena, which may lead to improved models of both the continuum and the discrete type.
Among the impacts and consequences for real motorway traffic are a broader understanding of flow regimes and how they are triggered, the forecast of maximum throughput and how to control the flow to obtain it, and the simulation of slow and fast lanes including different lane or vehicle characteristics, resulting in a better lane usage.

Considering the link between car-following and continuum models, there is a technical reason why the latter can only be successfully applied to motorways and highways. Due to the different density and speed regimes, the large number of junctions, traffic lights and roundabouts, the simulation of urban traffic flow requires different techniques from those described here. The complexity of urban road networks can be tackled by discretized models such as the cellular automaton (CA), for example. These models, which discretize both space and time, take the stochasticity of traffic into account but they usually imply extensive numerical simulations. In contrast, we do not focus on randomness but on some deterministic key parameters of the flow such as inertia. To date, this coincides with methods of most traffic engineers who base their work on deterministic car-following and continuum models. This is another major justification for concentrating on these two types of models.

These arguments show us that the need for traffic research is immense, which leads us to the next topic.

1.2 Mathematical Modelling of Traffic Flow

Improved management and control of traffic flow are counted among the great technological challenges [4]. Applied mathematics has an important role to play by providing a basis to describe a complex stochastic system by a few mathematical equations. This way, it forms a platform for online information, predictions of the effects of new projects such as lane extensions or speed limits, and the understanding of traffic flow as a physical process of interacting particles, namely cars and lorries.

We will now briefly present some problems of traffic modelling, what features it contains and what practical implementations are already under way.

In traffic flow, we deal with an additional level of complexity compared to the de-

terministic physical sciences, since it is not a fully controlled or determined system, due to the considerable variation in human behaviour patterns, personal skills and driving attitudes. The driver's behaviour and attention towards traffic events change with time, and the properties (physical size, maximum speed and acceleration) of different vehicles vary randomly. At first sight, traffic flow is a stochastic rather than a deterministic process, and in fact Adams regarded *road traffic as a random series* as early as in 1936 [1]. In this context, mathematical modelling could be defined as describing an intricate system by a few fundamental equations which are based on averaging over numerous parameters.

Various complex stochastic processes in nature such as trail formations [76] or group decision making [33] are already modelled by simple deterministic equations with increasing success. With regard to traffic, *car-following*, *granular flow* and *continuum* models are the different ways of simulating the flow, and each type has its specific advantages and disadvantages. The first two classes are called *microscopic* models, since they simulate each vehicle individually, whereas the latter belongs to the *macroscopic* picture, making use of locally averaged quantities like speed or car density, which represents the distance between the vehicles. Micro- and macroscopic models give rise to some very important results. A stability analysis, for example, demonstrates how the state of a platoon of cars depends on parameters such as *inertia* and *reaction time*, which are the basic parameters of the models to simulate the vehicle's behaviour.

The simplest case, a one-lane model without any on- or off-ramps, is rather easy to simulate, whereas the modelling of multi-lane flow is a much harder task. The coupling of lanes seems to be crucial for the simulation and because it is also a stochastic process, it is not clear how it is to be incorporated and how the lanes are to be linked.

Traffic flow modelling may be used in understanding the effects and consequences of local speed controls and autonomous headway control systems, which are already implemented in various cars. Both have the task of maximizing the throughput of the current road network as an alternative to increasing capacity by the extension of further lanes.

DaimlerChrysler, for example, has already set up radar systems in recent S-class models and has coupled lorries on a test track by using this technology [77]. The major objective of this project, named *Promote Chauffeur*, is to find the most appropriate algorithm that controls the acceleration and the deceleration of the interacting vehicles. It should be a compromise between individual benefits and the overall stabilization of the flow.

Another result of flow simulations might be a reduction of fuel consumption because a steady continuous flow saves energy in comparison with an irregular one, not to mention the effect of jams. It is estimated that up to 200 billion litres of fuel are

wasted in traffic congestion in the USA alone [42].
The potential of these measures seems to be immense. In fact, there are various EC, public and privately funded projects which aim for making use of it [77]:

- Vita: test vehicle of DaimlerChrysler using a video camera to recognize road marks, obstacles and traffic signals
- University of Berkeley: magnetic transmitters on the road surface allowing vehicles to drive in a convoy on the Interstate Highway No.15
- EU plans to set up a satellite network to determine the exact position of cars by GPS navigation system
- MAN runs the Adaptive Cruise Control (ACC) project in cooperation with private companies, universities and the German Ministry of Transportation.

Since these driver supporting systems suit commercial and private as well as public interests, it is a promising future market.

As already mentioned, traffic flow models reveal various nonlinear features including *shock waves*, *travelling waves*, *limit cycles*, *periodic orbits*, *solitons* and *phase transitions*. The analogy to other physical systems such as granular flow, many-particle systems and shallow water theory delivers powerful tools to tackle the nonlinear governing equations. Therefore, this subject is not only a promising candidate for real applications, but also a field of research in which new mathematical methods are developed and tested. This is where a major contribution of this dissertation lies, which brings us finally to the aims of this thesis.

1.3 Targets of this Work

Motivated by the importance of traffic modelling, in this thesis we examine a series of flow situations to uncover some of the fundamental aspects of traffic flow. There are several approaches to traffic modelling as described above, and these are explored and compared in chapter 3 where we focus on using discrete car-following and continuum descriptions of the flow. We identify a series of objectives for the modelling in this thesis and this is reflected in the structure of the dissertation. It generally contains research on single-lane flow on motorways, which is presented in the following six chapters and four appendices. The main results and numerical calculations are carried out for one specific, simple model which, nevertheless, contains most generic features of the flow.

First a historical summary of the **principles of traffic flow modelling** is given. Every model aims to reproduce some characteristic features of traffic such as flow

breakdown, shock waves and stop-and-go jams. Depending on the purpose, the roads (urban, interurban, motorway) and the speed regimes considered, different models can be applied: continuum, car-following or cellular automata (CA). Each type has similarities with data and observations of real traffic flow.
We provide this rather comprehensive overview of the literature for two reasons: firstly, it presents the background on which this work is based and puts it into its context, and secondly, it gives some motivation for our decision to use a particular model throughout the course of this dissertation.

The **third chapter** reveals how to **relate car-following and continuum models** by developing a transformation between *headway* (the distance between two successive cars, which is the key variable in car-following models) and car density which is the key parameter in the continuum picture. It is revealed that the former is not simply the inverse of the latter unless we have uniform flow conditions. This theory is established for a specific model, known as the *Bando model* [8], which was introduced in 1995. It is a very generic model in the sense that it is based on the assumption that there exists an *optimal-velocity* function, which describes a desired speed as a function of the headway, to which the traffic adjusts over some relaxation time. The numerical and analytical results of the Bando model support the idea of the equivalence of continuum and car-following models, where the correspondence is more accurate when there are no sharp density gradients in the flow.
This concept can be used to derive continuum analogues of car-following models, and vice versa. However, even if every model is analogous to a continuous or discrete counterpart, the explicit time delay of car-following models complicates the simulation of time lag in the corresponding continuum models, which shows the advantage of the car-following over the continuum formulation with respect to delay terms.
The main work of this chapter has been published in [11, 33].

The **fourth chapter** gives an **overview of analogous car-following and continuum models** using the transformation that is derived in the previous chapter. This list is presented for reasons of completeness and to uncover some differences and similarities between the models. Lastly, it reveals some interesting effects when a discrete model is turned into its continuum equivalent, and vice versa.

The following two chapters employ the insight that discrete and continuum models are analogous to carry out a comprehensive numerical study of a range of steady and unsteady flow structures in a car-following model.

Accordingly, in the **fifth chapter, wave types in the stable Bando model** are classified. For different up- and downstream fluxes of vehicles, there exists a transition region along the road, in which cars adjust to the downstream flow regime depending on their inertia. Among various transition zones, in some regimes it may

take the form of a steady travelling wave, in others it may be dispersive or may even assume a nonlinear wave type. Here, an analysis establishes a connection between the latter and the wave fronts of stop-and-go jams. In addition, all wave types are explained with the help of the flow-density curve (fundamental diagram), as well as with the analogous continuum model.
The results have important consequences for varying sensitivities and autonomous cruise control systems (ACCS). A changing sensitivity, equivalent to a more realistic composition of a convoy, reveals that only a small portion of cars might cause a change in flow conditions leading to increasing travel times of the following cars. Likewise, this has to be taken into account when implementing ACCS. The algorithms which control the cars should avoid these nonlinear wave solutions in order to optimize travel time and throughput as well as safety. The interpretation of these results may ultimately lead to the design of more suitable control algorithms.
The main results have been presented in [13, 14].

In the **penultimate chapter**, we look at an **on-ramp simulation in the car-following Bando model**, where cars enter a motorway of initially homogenous density and speed with a constant flux. We classify different regimes of the system: they resemble those of the previous chapter, because they can again be interpreted as a transition zone between a stream of different flows. Hence, we build on existing results to present a diagram which summarizes the states near a ramp. The analysis of this system might deliver a better understanding of how to set up appropriate on-ramp metering.
Depending on the upstream flux and the ramp flux that sets in, various solutions are found. Among these are homogenous congested and oscillatory congested traffic, as well as *solitary waves*. These have also been found in previous on-ramp simulations of continuum models and further underline the analogy between these two types. In the case of the solitary wave solution, this is shown analytically.
This correspondence might be a bit surprising at first sight because the on-ramp simulation is a continuous process in space and time when considering a continuum model, whereas it becomes discrete in both dimensions when turning to a car-following model.
The main parts have been published in [12].

The **first appendix** briefly introduces **cellular automata** (CA) as another class of traffic flow models. This is mainly done for reasons of completeness rather than further relevance for this dissertation because CA are becoming increasingly popular in various applications such as simulations of pedestrians, urban and interurban traffic or avalanches.

Appendix B contains some remarks on the transformation of chapter 3 relating car-following and continuum models. It stresses in particular how to apply the

inverse transformation.

Appendix C explains how time delay is incorporated into car-following models by changing ordinary differential equations into **differential delay equations**. A simple example shows that these two systems have entirely different formulations and that one may expect new types of wave solutions. A few reasons are presented, which support the idea of explicit time delay in traffic flow models.

The **last appendix** summarizes the **numerical techniques** that were used to simulate the models. A remarkable difference in CPU time occurs when calculating travelling wave solutions in the car-following and the analogous continuum model.

Chapter 2

Principles of Traffic Flow Modelling

The mathematical modelling of road traffic has passed through a rapid development over the last decade. The general increase of computer power enables system simulations of rising complexity so that real time traffic simulation is no longer fiction, but applied reality. However, these simulations are based on simple mathematical models and without a deeper understanding of these, not only might the predictions be unrealistic, but the interpretation of the results would be a very difficult task.
Various approaches are used depending on the corresponding traffic regimes, urban (city) or interurban (motorway) traffic. The first is usually described by microscopic models in which the trajectory of every single vehicle is given by its individual governing equation or algorithm. Among these, cellular automata (CA) and car-following models are the most common [35], where the former are stochastic and the latter deterministic.
In contrast, interurban traffic is described not only by microscopic but also by continuum models, which give a macroscopic picture of the events in terms of the density and the velocity of cars. Since their governing equations show similarities to those of other physical systems such as gas flow, various techniques to investigate their solutions are already known. This helps to understand the underlying effects in these models.
This dissertation mainly deals with motorway traffic. The basic difference from city traffic is that neither junctions, traffic lights nor roundabouts are taken into account. On- and off-ramps are regarded as sinks and sources of vehicles along the road, in both continuum and car-following models.

The main objectives for road management are to increase throughput, avoid jams, toll drivers, use data intelligently, cut pollution, etc. Empirical surveys, for example,

have shown that the profitability of traffic projects depends strongly on their ability to avoid congestion [9].
Here, simple mathematical models provide insight into the effects of road building, lane blockage, speed limits, ramp metering and other measures on road use.

This chapter presents an overview of some of these models, in particular the deterministic car-following and continuum models on which the remaining work is built. By synthesizing the literature and comparing it with new results, we are then able to draw new conclusions.
Another important aspect is that we focus on models that contain a relaxation term, mainly embodied by the Bando model, and this chapter gives reasons why this class is the main topic of this work.
However, we will first consider the characteristics of motorway traffic and how these are built into the models.

2.1 Features of Road Traffic

No matter what type of mathematical model is chosen to describe traffic, it should reproduce certain characteristics of real flow and real data. Unfortunately, the measurement of traffic flow itself is not a straigtforward process. Induction loops along motorways are only available every hundred meters, or even every few kilometers. Moreover, only spatially and temporally averaged values of the speed, the density and, hence, the flow are obtained. Typical average times are about 5 minutes due to a minimum of counted vehicles to yield representative average quantities [50]. In accordance, continuous variables are discretized in space and time as time series. The disadvantage of this procedure is obvious: lack of knowledge of the events between the loops, poor time resolution and high uncertainty of the estimated variables. It is, however, possible to extract three essential variables of traffic flow from this data: the speed v and density ρ of the vehicles, and the flow q, which equals the amount of cars that pass a fixed point per unit time.
Flow and speed can be measured easily at a given point, x, along the road by using one induction loop, or the combination of two, respectively. The density is then obtained by the most important relation of traffic flow modelling

$$q = \rho v. \tag{2.1.1}$$

When the data is plotted as the flow against the density, we obtain the **fundamental diagram** shown in Fig. 2.1. It is this diagram on which most traffic models are based.
If the speed of the vehicles depends uniquely on the density, the flow is also deter-

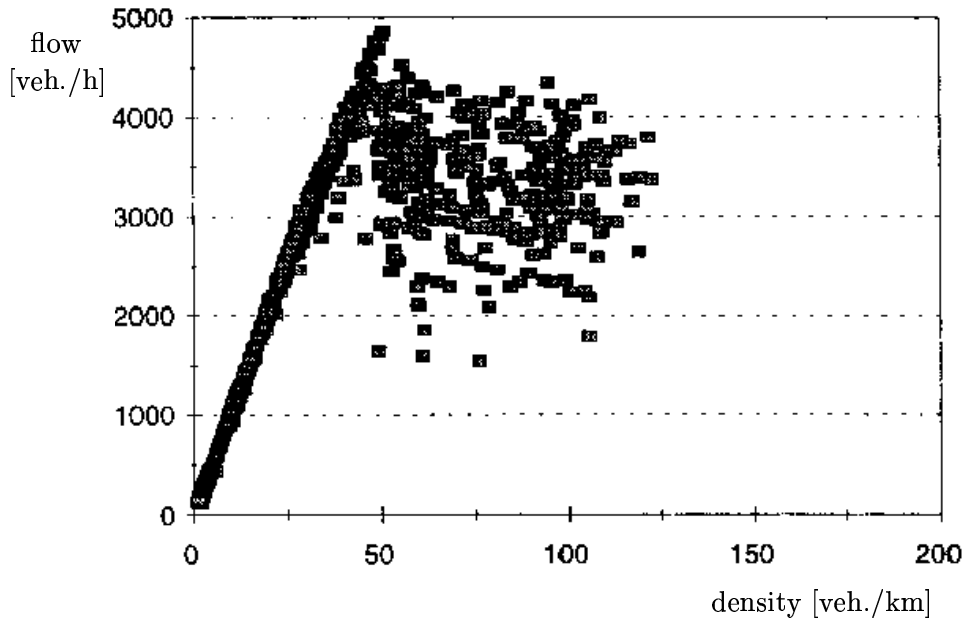

Figure 2.1: The fundamental diagram of two lanes in terms of real traffic data. The critical density, $\rho \approx 50$veh./km, can be clearly observed as well as the coexistence of two phases (hysteresis effect): free flow (straight line) and synchronized flow (scattered points) [4].

mined solely by the density, via

$$q(\rho) = \rho v(\rho). \tag{2.1.2}$$

Figure 2.1 shows that this is roughly fulfilled for low densities and, hence, free flow situations. However, for higher densities the data becomes more scattered. In the unstable regime ($\rho > 50$veh./km), the cloud of points does not allow a definite allocation of the density to the flow. This area is named the *synchronized flow* regime. The scattering gives a strong indication that the speed does not only depend on the density, but also on other variables such as the gradient of the car density or the traffic situation during some preceding time interval.
However, for stationary, homogenous and stable situations, Eq. (2.1.2) is regarded as a reasonable first-order approach and several conclusions can be drawn from it. The equilibrium velocity $v(\rho)$ should obviously be a monotonic decreasing function and, therefore, q turns out to be convex, at least in some density range. For non-homogenous flow conditions, this can lead to the formation of shock waves, if one assumes as a lowest-order approximation that the cars react instantaneously to the traffic situation. This is equivalent to a lack of inertia. Then the speed c of density waves is given by the gradient of the tangent in the fundamental diagram [84]

$$c(\rho) = q'(\rho) = v(\rho) + \rho v'(\rho) < v(\rho), \tag{2.1.3}$$

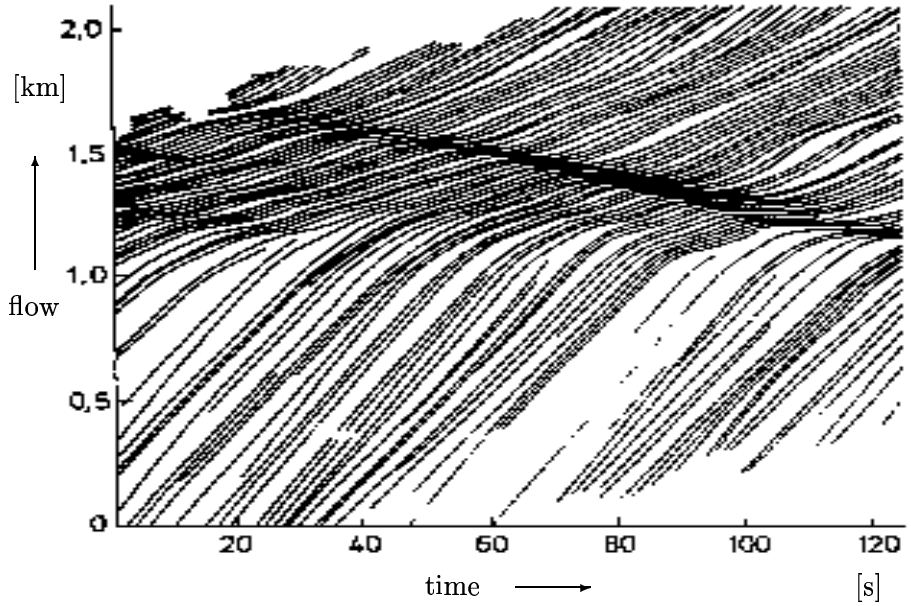

Figure 2.2: Data extracted from aerial photographs along a highway shows a shock wave travelling upstream [81].

as shown in subsection 2.2.1. In the convex regime of q, this is a monotonic decreasing function and, hence, regions of smaller densities catch up with those of higher densities until a shock forms. This is an essential result of traffic flow theory and avoiding these shocks in reality is a major task.
Moreover, Eq. (2.1.3) shows that density waves, and hence information, never travel faster than cars. This must certainly be fulfilled, or otherwise information would travel faster downstream than the cars. This would only be possible if the drivers could react to traffic events behind them which usually have no influence. In the context of Eq. (2.1.3), the function $v'(\rho)$ would have to increase monotonically in some density ranges, which contradicts the available data. More attention is drawn to this fundamental diagram later on.
However, there is more to traffic data than the fundamental diagram. We now describe some of the important observations and basic phenomena of road traffic data, which ideally should appear in a model also. Among these characteristics are:

- The **structures of stop-and-go clusters**: the velocity of cars in- and outside a jam, outflow of escaping vehicles, densities of the clusters and the intermediate regions of large headways, as well as the speed of the upstream moving cluster fronts, seem to be unique quantities [48, 50].
  These are reproduced very well by the car-following Bando model that we use in this dissertation.

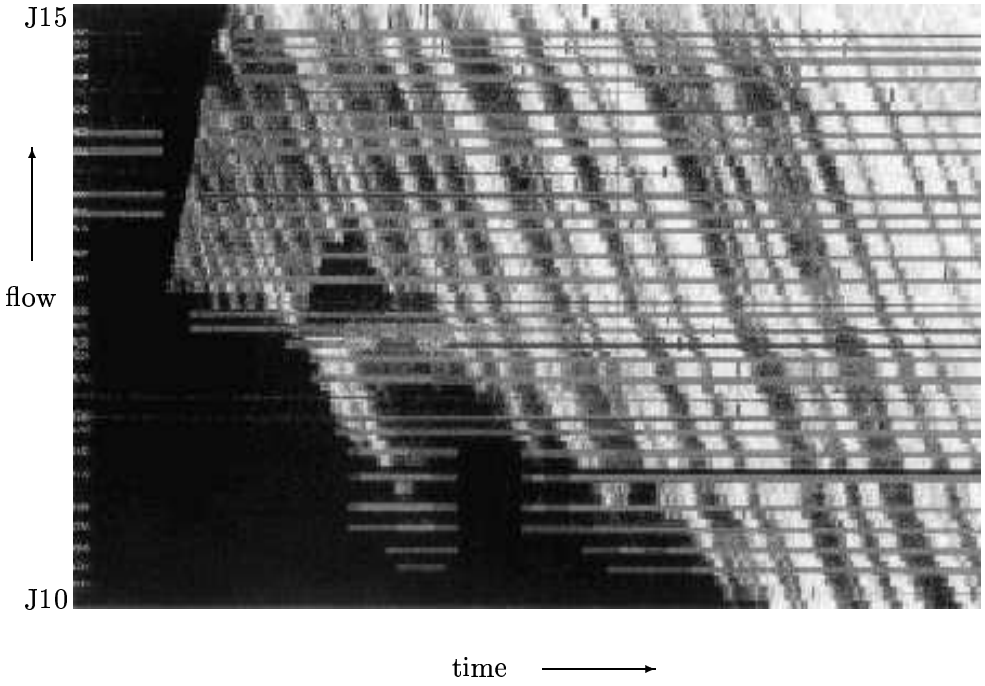

Figure 2.3: Jam waves of high (white) and low (black) density travelling upstream between junctions J10 and J15 on the M25 London ring [2]. The waves are parallel, and of constant gradient and, hence, constant speed.

- The **formation of stop-and-go traffic** ("phantom jams") without any obvious reason. Figure 2.2 reveals how a transformation from an originally dense, but rather homogenous flow (1.0km−1.5km) to a shock wave might occur. The latter travels upstream at a speed of approximately 10 miles/hour: this, according to worldwide traffic data, seems to hold for any motorway in any country and can, thus, be regarded as an intrinsic feature of the system (Fig. 2.3). The flow only becomes unstable in certain regimes of the density [28].
  Chapter 5 explores similar nonlinear waves that form a transition between zones of different flux.

- The **broadening of the speed distributions** when approaching the critical density of flow breakdown was first measured on the German autobahn A5 in 1976 [53]. On the onset of traffic jams the speed variance spreads out and returns to its Gaussian shape when the jam dissolves [51].
  This phenomenon is not investigated further in this thesis, but it remains an interesting question whether a car-following model can reproduce it.

- **Synchronized traffic** appears on motorways of rather high densities. The lanes are strongly coupled, which leads to a homogenous movement of vehicles on all lanes, with an overall low velocity but high throughput [34, 36]. Overtaking is impossible, and lane-changing rare compared to free flow or traffic

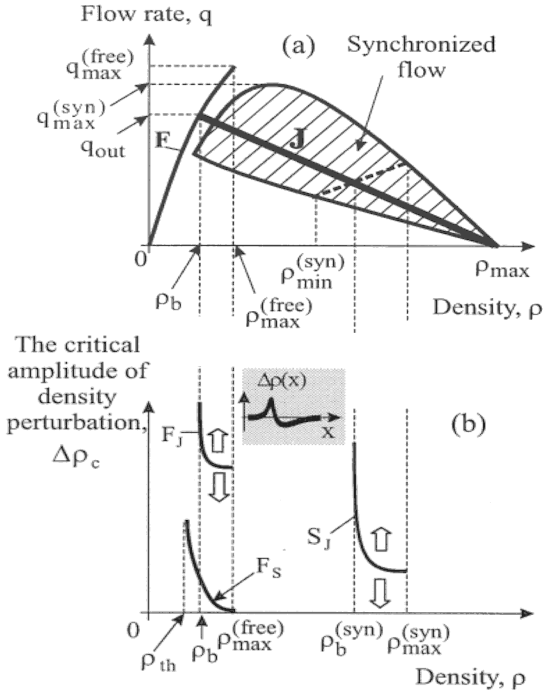

Figure 2.4: (a) A qualitative diagram of the occuring traffic states and their maximum (out)flows: free flow (F), jam (J) and synchronized flow (hatched region), as interpreted by Kerner [44]. (b) Phase transitions between these three states can only be caused by a sufficiently large density perturbation in the corresponding density regimes. In accordance, the likelihood of the transition free flow $\Leftrightarrow$ synchronized flow (F_S) between ρ_{th} and $\rho_{max}^{(free)}$ is the highest, of synchronized flow $\Leftrightarrow$ jam (S_J) transitions between ρ_b and ρ_{max} is less, and of free flow $\Leftrightarrow$ jam (F_J) transitions between ρ_b and $\rho_{max}^{(free)}$ is least. The form of S_J depends on the density of the synchronized flow and varies across the range $[\rho_b, \rho_{max}]$. Only one specific example S_J is shown here.

jams. It typically occurs at on-ramps where a localized perturbation causes a linearly stable free flow of high speed and flux to break down and move more slowly [49]. The transition back to free traffic occurs at lower density and higher average velocity than the original transition (a *hysteresis effect*). Motorway data shows that synchronized flow consists of a great number of steady state flows along the road. Each state is characterized by its density and its flux. However, these two variables are not related by a functional expression (2.1.2) any longer, which results in scattered data points in the fundamental diagram, when these steady state regions pass an induction loop.

Whether free flow turns into a synchronized flow, or into a stop-and-go jam, depends crucially on the initial conditions and it is not fully understood yet, though it might be explained by the nonlinearities involved in traffic flow [48]. However, it seems that the most likely transitions in traffic flow appear as free flow $\Leftrightarrow$ synchronized flow and synchronized flow $\Leftrightarrow$ jam formation. A tran-

sition from free flow straight to jams is rather unlikely due to the size of the perturbation that is required (Fig. 2.4).
In chapter 6, a traffic state near an on-ramp is discussed, which some authors have refered to as being synchronized.

- Traffic data from the Dutch freeway A9 Haarlem-Amsterdam suggest that adjacent **lanes** show a **strong correlation** with respect to the temporal evolution **of densities** $\rho_1(x,t)$ and $\rho_2(x,t)$, for given x [28]. Their difference is mainly a function of the overall density [30], and the same holds for the speed variances of both lanes, $\Theta_i(x,t) =< (v_i - \hat{v}_i)^2 >$. The latter is not only strongly correlated, but considerably lower for synchronized than for free flow [49].
However, multi-lane flow will not be of further relevance to this thesis.

- The governing equation of a car-following model should somehow represent the **experimental studies of driver behaviour** towards preceding cars carried out by Chandler *et al* in 1957 [16]. Their simple observations tried to assess the driver's response to vehicles one or two ahead. Similar work by Bando *et al* [7] led to the generic model used throughout this thesis.

A major task of research in traffic is to control the flow so that it does not assume some of the states presented above. Among these are shock waves, which can lead to dangerous driving manoeuvres, and transitions into states of lower throughput leading to increased travel times and higher pollution. In contrast, low travel times and a maximum flow represent the ideal state of the system and on-ramp metering, as well as online speed limits, might be future options to control this.

2.2 Mathematical Models

Owing to the problems in simulating traffic flow, three different approaches have been developed in parallel. The reasons for this arise from the observation of fundamental laws governing behaviour and interaction properties of the vehicles. In this section, we describe the two deterministic approaches in greater detail, and revise the historical development of each, leaving a brief description of the stochastic class to appendix A.

The first mathematical approach to traffic flow was Greenshield's *study of traffic capacity* as early as 1934 [24]. However, Lighthill and Whitham's *theory of traffic flow on long crowded roads* marks the beginning of the deterministic **macroscopic models** [58]. The authors explain the existence of shock waves and the evolution of density waves by a differential equation for the density ρ. Here, an explicit functional relation between the flow in terms of the density (fundamental diagram) is

used. This description is in full analogy to fluid motion such as, for example, fluid waves and glaciers [84]. Since average densities and velocities rather than discrete sets are used, this model embodies the basis of the so called **continuum models**. Later this approach was extended by Payne [71] and Kühne [53] to higher order models, which couple density, velocity and, in current models [29], even the speed variance in corresponding partial differential equations. Also, a Boltzmann-like approach has been suggested using the analogy between vehicles and molecules [73].
Simultaneously, **microscopic models** were developed, which examine the entire flow by looking at the movement of each vehicle. In these theories every car motion is coupled to the preceding car by either a deterministic equation or a probability of following within a certain distance. **Car-following, cellular automata**, queueing and mean-field models all belong to this class.
In 1958 Chandler *et al* carried out a multitude of experiments to determine the relation between acceleration, distance to the car in front and its temporal change [16]. Based on these results, the first car-following models were established. They were continuously improved and are now capable of reproducing most of the characteristic features of motorway traffic, as mentioned above. A governing equation that is of second order in time seems to be necessary to match these findings. These models have received considerable interest over the last 10 years owing to computers which enable the simulation of nonlinear flow regimes. This now provides a valuable complement to the continuum approach for which some analytical solutions have been found. The combination of the numerical modelling of car-following models with the analytical description of nonlinear phenomena using analogous continuum models forms a major aim of this thesis.
However, before we proceed with the deterministic models, it should be mentioned that increasing attention has been paid to granular flow theory in recent years. In certain regimes, the stochastic properties of traffic flow can be simulated successfully by cellular automata models. Among these, the Nagel-Schreckenberg model [68] gave rise to new ideas in this field of research. Even though we will not consider these models for simulations in this dissertation, a brief overview of the ideas and the theory of this ansatz is given in appendix A, for completeness.

There are several reasons why we confine our investigation to the deterministic models in this work. They are not only successful in describing certain aspects of the flow, but also give an insight into its underlying effects. There is even one application where randomness is not important at all: the study of automated vehicle control systems. In addition, the analytical link between continuum and car-following models in this publication might be considered and used as a basis to connect these to cellular automata, providing a better understanding of how stochastic features influence the flow.

2.2.1 Continuum Models

For road engineers, spatially and temporally averaged quantities, such as density and flow, are often of more interest than the tracking of individual drivers. Therefore, the impact of road geometries and speed controls on a large scale is often simulated by continuum models. They are based on the macroscopic traffic variables of density and speed, which evolve according to a coupled set of partial differential equations. The validity of these models can only be tested by comparison with traffic data, and it is this procedure that shows the limits of this theory. Formally, the flow in Eq. (2.1.1) is defined as the number of vehicles that passes a point along the road in unit time, and the density ρ is the number of cars per unit distance. Since traffic measurements are carried out by induction loops, only the flow and the speed are monitored. The direct measurement of the density would require aerial photographs. However, an obvious definition for the current flow q at time t, and position x along the road would be

$$q(x,t) = \lim_{\Delta t \to 0} \frac{N(x,t,\Delta t)}{\Delta t}, \tag{2.2.1}$$

with N being the number of vehicles passing during $[t, t+\Delta t]$. In reality, this limit will equal zero, since no car will pass the induction loop in an arbitrary small interval, but it can be approximated by a time averaged value (typically 1 to 5 minutes in traffic data), if the change in flow during this period is sufficiently small. This means that the continuum formulation is only accurate for traffic situations in which the change of traffic quantities only occurs on a length scale much bigger than the headway of cars. An explicit example is given in chapter 3, where the validity of a continuum approach to a car-following model breaks down for rather large spatial gradients of the density.

A speed measurement might be performed in two different ways: either at a given point in time along the road (instantaneous speed distribution), or at some point along the road during a time period Δt (local speed distribution). Their arithmetic averages are different for non-homogenous flows. The latter procedure counts relatively more vehicles of higher speed, since they pass a fixed point more often than slower ones relative to the composition of vehicles.

To take this into account, the space mean velocity of the local speed distribution is defined by its harmonic average

$$v(x,t) = \lim_{\Delta t \to 0} \frac{n}{\sum_{i=1}^{n} \frac{1}{v_i}} \tag{2.2.2}$$

where n vehicles of speed v_i are measured at x during a time interval $[t, t+\Delta t]$. This equals the arithmetic average of the instantaneous speed distribution [57], which is

most welcome because we can see by the definition of the latter

$$v(x,t) = \lim_{\Delta x \to 0} \left\{ \sum_{i=1}^{n} \frac{v(x_i,t)}{n} : \forall x_i \in [x, x+\Delta x] \right\}, \tag{2.2.3}$$

that this is the mean speed we are searching for. Here, x_i denotes the position of the i-th vehicle. The local density is then given by

$$\rho(x,t) = \frac{q(x,t)}{v(x,t)}, \tag{2.2.4}$$

and can, therefore, be extracted by the measurements of the flow and the velocity.

2.2.1.1 Lighthill-Whitham Model

The first research on the continuum formulation was based on a differential equation, the **conservation of cars**

$$\rho_t(x,t) + q_x(x,t) = \rho_t(x,t) + [\rho(x,t)v(x,t)]_x = Q(x,t). \tag{2.2.5}$$

It states that the number of cars on the road is a conserved quantity, unless there are sinks (off-ramps, $Q < 0$) or sources (on-ramps, $Q > 0$) along the road.
Lighthill and Whitham [58] transformed Eq. (2.2.5) into a single partial differential equation (PDE) for the density by assuming that the velocity, and hence the flow, is determined solely by the density

$$v = V(\rho) \Rightarrow q = q(\rho). \tag{2.2.6}$$

It means that no inertia is taken into account, since the cars adopt their speed instantaneously [39]. Even though this is an unrealistic assumption, it first established dynamic traffic modelling. The governing equation then turns into a nonlinear partial differential equation

$$\rho_t + q_\rho \rho_x = 0. \tag{2.2.7}$$

This yields that density waves travel with a local speed $c(x,t) = q_\rho(x,t)$. The speed may be interpreted as the first derivative of the flux as a function of density and is, therefore, the gradient of the tangent in the fundamental diagram (Fig. 2.7) at the corresponding density ρ. The waves which are governed by the single equation (2.2.7) are also known as *kinematic waves*. On the corresponding trajectories $X(t)$ with $X_t(t) = c(x,t)$, the density is constant since

$$\frac{d\rho(X(t),t)}{dt} = \rho_t(X(t),t) + \rho_x(X(t),t)X_t(t) = 0. \tag{2.2.8}$$

This is why the *method of characteristics* can be applied to solve this PDE: for any initial distribution $\rho(x,t_0)$, we can find the density distribution at later times

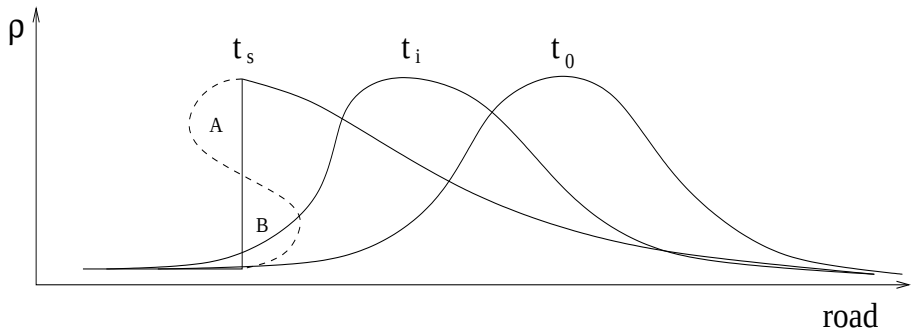

Figure 2.5: The formation of a shock only appears if $\frac{\partial}{\partial x}\left(\frac{\partial q}{\partial \rho}\right) < 0$ is at some point along the road. t_0: initial distribution, t_i: intermediate solution, t_s: shock wave formation.

by moving the local density with its corresponding speed $\dot{X}(t) = q_\rho(x,t)$ down the road.

Lighthill and Whitham give no explicit expression for the speed function $V(\rho)$, though they stipulate that it should be monotonically decreasing and $q(\rho)$ convex. The velocity of density waves is then a monotonic decreasing function of the density Eq. (2.1.3), which means that regions of low density travel faster than regions of higher density. (The speed of the cars should not be confused with the speed of the density waves; they are different.) In terms of Fig. 2.5, it implies that dispersion dominates where the density decreases downstream and that wave steepening dominates where it increases. In the latter case, the regions of higher density catch up with those of lower density and the method of characteristics no longer applies since $\rho(x,t)$ becomes multi valued. Instead, a shock wave forms, as presented in Fig. 2.5. Its speed c_s is given by the conservation of cars as

$$c_s = \frac{q_1 - q_2}{\rho_1 - \rho_2}, \tag{2.2.9}$$

and can be either negative or positive (up- or downstream propagating wave). Respectively, q_i and ρ_i are the upstream and downstream values of the jump [84]. In addition, the position of the shock front is determined so that the areas of region A and region B are equal in order to conserve the amount of cars.

The speed change that drivers encounter when passing a shock is immense, due to intense braking, as Fig. 2.5 suggests. In contrast, there is no discontinuity in real traffic. This can be taken into account by higher order terms (ρ_x, ρ_{xx}) in the model, which lead to shock smoothing and, hence, a more realistic picture [60].

The flow-density curve Eq. (2.2.6), which has to be substituted into the equation for the conservation of cars, is ambiguous. Numerous functions were proposed and fitted to data. It seems that there is no unique relation that can explain all the

effects which occur in traffic flow. However, the functions $q(\rho)$ and $v(\rho)$ have to fulfill three basic properties:

- $q(\rho = 0) = 0$: no flow without cars
- $q(\rho_{max}) = 0$: no flow when traffic assumes its jam density ρ_{max}
- $v'(\rho) < 0$: otherwise, vehicles could be overtaken by density waves as shown by Eq. (2.1.3).

Various functions are presented in the following sections. However, the model (2.2.7) always shows shock formation in the free flow regime if q fulfills these requirements. This instability is rather unrealistic since real traffic is only unstable for sufficiently large densities $\rho > \rho_c$. In contrast, the model does not account for the existence of some form of dispersion in the free flow regime, which represents the drivers' responses to fluctuations and smoothes out small perturbations.
Since the model is not applicable in the free flow regime, and since it cannot reproduce the downstream shock front of stop-and-go traffic clusters, it had to be extended to a higher order model including inertia.

2.2.1.2 Prigogine's Boltzmann-like Model

Before the Lighthill-Whitham model was extended to higher order, Prigogine and Andrews [73] proposed a Boltzmann-type ansatz for a velocity distribution function $f(x, v, t)$, similar to the Maxwell-Boltzmann collision theory of gases. The expression $f(x, v, t)\, dx\, dv$ represents the probability of a car being in the road element $[x, x + dx]$, and in the velocity range $[v, v + dv]$ at time t. This stochastic theory is based on two effects: a relaxation term for the driver's adjustment to an equilibrium velocity f_0, and a "collision" term which describes the interaction of vehicles. The former is similar to the relaxation terms used in later developed continuum models,

$$\frac{d}{dt} f^{(relax)}(x, v, t) = -\frac{f(x, v, t) - f_0}{T}, \tag{2.2.10}$$

so the traffic tends to assume the equilibrium state f_0 over some time interval T. The "collision" term is proportional to the deviation of the velocity distribution from its mean speed $\bar{v} - v$, weighted by the probability density $f(x, v, t)$ of finding a car in this regime, and the density c of the cars. Their product is proportional to the number of "collisions" per unit time

$$\frac{d}{dt} f^{(coll)}(x, v, t) = a\ c(x, t)\ f(x, v, t)\ (\bar{v} - v), \tag{2.2.11}$$

with some constant of proportionality a. If these terms are put together, they yield a nonlinear integro-differential equation for f,

$$\frac{d}{dt}f(x,v,t) = -\frac{f(x,v,t) - f_0}{T} + a\ c(x,t)\ f(x,v,t)\ (\bar{v} - v), \tag{2.2.12}$$

where $\bar{v}$ is given by

$$\bar{v} = \frac{\int v f(x,v,t)\, dv}{\int f(x,v,t)\, dv} = \frac{\int v f(x,v,t)\, dv}{c(x,t)}. \tag{2.2.13}$$

This model forms the basis for recently proposed models such as Helbing's (see following pages), which couples the density, velocity and its variance in a system of PDEs [10, 27].

2.2.1.3 The Payne Model

Based on the idea of Lighthill and Whitham, a higher order continuum model can be derived, if one assumes that the velocity is not only a function of the density, but also of its gradient ρ_x and possibly even higher order terms such as diffusion ρ_{xx}

$$v = V(\rho, \rho_t, \rho_x, \rho_{xx}, ...). \tag{2.2.14}$$

It means that drivers do not only adjust to a local traffic situation, but also to events further ahead. Their speed is different depending on whether there is more congested ($\rho_x > 0$), or less congested ($\rho_x < 0$) traffic ahead. The term ρ_t can be interpreted as an inertia term, because it relates the current speed to former traffic situations [72]. However, the adjustment is still instantaneous, and hence not realistic.
Payne [71] suggested that the speed obeys its own dynamical equation, rather than a relation like (2.2.14). It is determined by both the surrounding flow and its inertia, which occurs as a "retarded" reaction to a given traffic situation.
Payne uses a relaxation term similar to Prigogine's to represent the driver's tendency to adjust to an **optimal velocity** (OV) $V(\rho)$ which depends on the local density. $V(\rho)$ is the equilibrium velocity of a platoon of cars with density ρ: in other words, if a vehicle leads a platoon of cars with velocity v, the car behind follows in some safety distance (headway) $b(v) = 1/\rho(v) = 1/V^{-1}(v)$. Instead of assuming a general equilibrium velocity v_0, it now becomes a locally varying parameter, and the equation for the conservation of cars

$$\rho_t + (v\rho)_x = 0 \tag{2.2.15}$$

is closed by a partial differential equation for the velocity

$$v_t + v v_x = \frac{1}{T}\left[V(\rho) - v\right] - \mu\frac{\rho_x}{\rho}. \tag{2.2.16}$$

The velocity function was fitted to traffic data from several freeways in Los Angeles, obtaining the form

$$V(\rho) = \min(88.5, 172 - 3.72\rho + 0.0346\rho^2 - 0.00119\rho^3) \text{ km/h}, \tag{2.2.17}$$

and

$$T = \frac{1}{240}\text{h} = 15\text{s}, \tag{2.2.18}$$

$$\mu = 13\text{km}^2/\text{h}^2. \tag{2.2.19}$$

The last term of the dynamical equation represents the driver's anticipation to the preceding traffic events: increasing congestion ($\rho_x > 0$) reduces the acceleration, and vice versa. It can be written as

$$\frac{\mu\rho_x}{\rho} = \frac{1}{\rho}\frac{d}{dx}p(\rho) = \frac{p_\rho\rho_x}{\rho}. \tag{2.2.20}$$

p is called *traffic pressure*, because it is of a similar form to its gas-kinetic counterpart [62].
This model is unstable for small perturbations of arbitrary wavelength to an initial homogenous distribution ρ_0 for which

$$\frac{\rho_0}{\sqrt{\mu}}V_\rho(\rho_0) \geq 1 \tag{2.2.21}$$

holds [71]. This is a much more realistic result than Lighthill-Whitham's model, because it is stable in the free flow regime, and becomes unstable for $\rho > \rho_c$ towards congested flow. The critical density ρ_c is given by the root of Eq. (2.2.21), and is of the order of 25 vehicles/km, which is approximately 1/7 of the maximum density assumed in a jam [54]. However, this model is still not able to describe cluster formations, as observed in real traffic.

2.2.1.4 Kühne Model

Kühne included a dissipation term of the form νv_{xx} on the right hand side of the dynamical Eq. (2.2.16), to obtain a Navier-Stokes-like equation

$$v_t + vv_x = \frac{1}{T}[V(\rho) - v] - \mu\frac{\rho_x}{\rho} + \nu v_{xx}. \tag{2.2.22}$$

This term is of viscous nature and smears out the discontinuities that the Payne model still contains [53].
Kühne investigated roll wave solutions both of Payne's and his model (2.2.22). By doing so, he showed the similar nature of continuum models of traffic flow and flood waves in open channels. The shapes of the periodic roll wave solutions of the Payne model are fully determined by their minimum density (water height),

but since no continuous periodic travelling wave solutions exist, discontinuities have to be introduced to fit piecewise continuous solutions together. This changes with the dissipative term. Now continuous periodic solutions exist, which are similar to cluster shapes in traffic observations. Therefore, this model forms the basis for further developments.
Moreover, it has the same stability criterion as the Payne model [54], and Kühne showed that this system passes through Hopf bifurcations to form stop-and-go traffic.

2.2.1.5 The Kerner-Konhäuser Model

Kerner and Konhäuser discovered that the Kühne model reproduces most of the characteristic features of traffic flow [46, 47, 48, 50], if the dissipative term is slightly changed. Since their values do not depend on the initial conditions, the authors speak of self-organization, which always leads to a specific set of parameters determined by the nonlinearity of the system.
A modification yields

$$v_t + vv_x = \frac{1}{T}\left[V_{kk}(\rho) - v\right] - \mu\frac{\rho_x}{\rho} + \nu\frac{v_{xx}}{\rho} \tag{2.2.23}$$

with

$$V_{kk}(\rho) = v_0\left[\left(1+\exp\frac{(\rho-\rho_i)/\hat{\rho}}{\sigma}\right)^{-1} - \left(1+\exp\frac{1-\rho_i/\hat{\rho}}{\sigma}\right)^{-1}\right]. \tag{2.2.24}$$

The maximum speed at $\rho = 0$ is proportional to v_0, and at $\rho = \hat{\rho} = 180$veh./km, the traffic comes to a standstill ($v = 0$). $\rho_i = 36.5$veh./km and $\sigma = 0.02875$ are obtained by fitting to traffic data, which leads to a model that is unstable in a regime $\rho > \rho_c$, but stable in the free flow region.
However, cluster formation (Fig. 2.6) can appear in the linearly stable regions of the density as a nonlinear instability, if the perturbation is sufficiently large [44]. On the other hand, a cluster might also disappear in this regime. Therefore, this process is interpreted as a transition between different metastable states in a metastable regime.
The authors investigate the formation, shape and dynamics of these clusters in great detail. They argue that this model gives an explanation for *phantom traffic jams*, jams which occur without any obvious cause. Bevan [15] found similar features in the car-following Bando model of road traffic. We come back to this in chapter 3.
A typical shape of one of these developing clusters is illustrated in Fig. 2.6. It is an up- or downstream travelling congested region in which cars have to brake when entering, and accelerate when leaving it, followed by a tail of relatively free flowing traffic.
There are also "anticlusters", local regions of free flow traffic within congested traffic

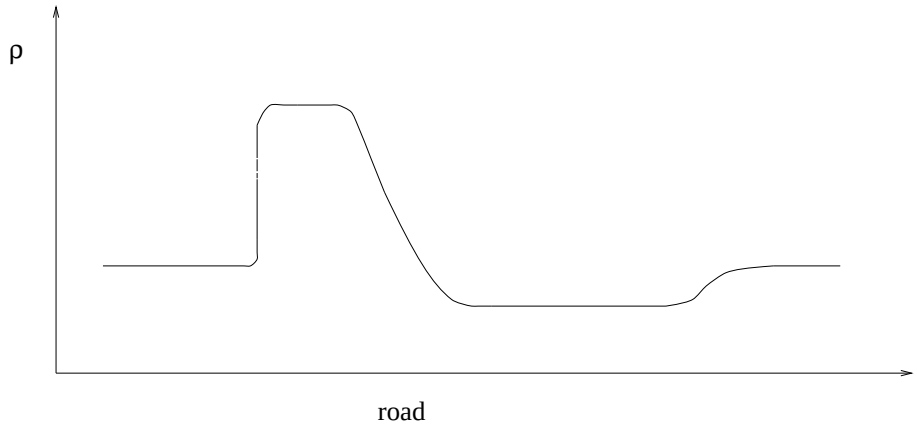

Figure 2.6: A qualitative cluster solution of the Kerner-Konhäuser model (2.2.23) in the metastable regime. The asymmetry is remarkable, with a consequence of the harsh braking when entering and a more moderate acceleration when leaving the cluster.

which remind one of the dark soliton solutions of the nonlinear Schrödinger equation. In fact, Kurtze and Hong [55] revealed that the Kerner-Konhäuser model can be transformed into a perturbed Kortweg-de-Vries (KdV) equation near the onset of instability, and that the traffic jam can be identified with a soliton solution of the KdV equation. A similar analysis was carried out by Komatsu and Sasa [52] for the Bando model (subsection 2.2.3). Here, the cluster fronts can be described as kink solitons of a modified KdV equation.

2.2.1.6 The Helbing Model

More complex models have also been developed starting from Prigogine's ideas of a velocity distribution function where traffic is simulated by a kinetic gas law. This introduces some aspects of stochasticity through the introduction of a granular temperature governed by a third equation, and this accounts for fluctuating traffic parameters and dispersive effects.

Helbing [27] constructed a gas-kinetic traffic model, based on individual driver behaviour, concerning acceleration and interaction of vehicles. The author derives macroscopic partial differential equations for the density, the velocity, its variance and higher moments. This system is open, and has to be closed by assuming that one of the higher moments adopts its equilibrium value. In this formulation, the Lighthill-Whitham model is a zeroth-order approximation.

First Helbing defines a phase space density $\hat{\rho}(x, v, v_0, t)$. It is a probability density which describes the probability of finding a car at x, with velocity v, and desired velocity v_0, at time t. The gas-kinetic traffic model is derived by assuming a conservation equation for the phase space density and once again, a relaxation term

for the speed is introduced. Together with a Gaussian form for the desired speed distribution, and a Boltzmann equation for the vehicle interactions, it leads to a system of equations of the form

$$\rho_t + (\bar{v}\rho)_x = 0, \tag{2.2.25}$$

$$\bar{v}_t + \bar{v}\bar{v}_x = \frac{1}{T}\left[V_e(\rho, \bar{v}, \Theta) - \bar{v}\right] - \frac{1}{\rho}(\rho\Theta)_x, \tag{2.2.26}$$

$$\Theta_t + \bar{v}\Theta_x = \frac{2}{T}\left[\Theta_e(\rho, \bar{v}, \Theta) - \Theta\right] - \frac{2\rho\Theta\bar{v}_x}{\rho}. \tag{2.2.27}$$

Here, the variables ρ, $\bar{v}$ and Θ are extracted from the phase space density $\hat{\rho}$ by their corresponding integral definitions as average quantities [27]. As in former models, the equilibrium velocity V_e, and the equilibrium variance Θ_e must be given explicitly. Again, the fundamental diagram has direct influence on the model via the function V_e.

The velocity distribution and the power spectrum of the time dependent vehicle density were measured along the Dutch freeway A9 [29]. It confirms that the assumption of a Gaussian velocity distribution is justified. However, its skewness varies with the density, and it is difficult to find an analytical expression to substitute into the model.

Helbing also showed that a slightly simplified version of the model (2.2.25)-(2.2.27) [79] describes the formation and phase transition of various traffic states on a single lane caused by ramps [36], as well as other nonlinear dynamical phenomena such as cluster formation of stop-and-go traffic, and its characteristic parameters.

This model is interesting because of the explicit relation between microscopic driver behaviour and macroscopic traffic equations [30]. The model can be used to examine which assumptions lead to which former models, and where the problems of the formulation of a consistent continuum model lie.[1]

Moreover, Helbing showed that some features of the flow, such as the broadening of the speed distribution at the onset of a traffic jam, are in good agreement with former measurements [53]. However, the question remains open of whether these features could also be contained in a car-following model that contains different vehicle and driver types or reaction time. Since this is still unclear, we restrict out attention to simpler models in this work, which brings us to the next subsection.

2.2.2 Car-following Models

We now focus on deterministic microscopic models of road traffic. They attempt to capture the discrete nature of the system, and simulate each vehicle individually by

[1] A final note on continuum models: it is of great doubt whether macroscopic traffic flow will ever be properly described by quantum mechanics [5].

its own dynamical equation. It is usually modelled using a differential delay equation of the form

$$\dot{v}_n(t+T) = V(b_n(t), \dot{b}_n(t), v_n(t)), \tag{2.2.28}$$

where T is the driver's reaction time, b_n the headway denoting the distance to the car in front, and v_n the car's velocity. The car-following models which have been proposed so far mainly differ through the function V. Here, we discuss several car-following laws and examine their stability and fundamental flow characteristics. However, for the main calculations of the thesis, we adopt the optimal-velocity model suggested by Bando *et al* [8] (subsection 2.2.3).
Car-following models can be studied both analytically and numerically. Much of the initial research was analytical since it predated powerful computers and examined the linear stability of perturbations for a steady flow [16]. The advent of modern computers, however, has enabled investigations of the associated nonlinear evolution of linearly unstable flow regimes and this approach is taken herein.
Table 2.1 gives an overview of the car-following models in chronological order, their stability criterion (next subsection) and the corresponding equilibrium flow-density curve, the fundamental diagram (next subsection but one).

2.2.2.1 Stability

In most models, an explicit time lag T is introduced to account for the driver's retarded reaction to current traffic situations. This leads to a differential delay equation (DDE) like Eq. (2.2.28).
Time delay and inertia are often confused, even though they are two different parameters. In the Bando model, for example, one might think of the *sensitivity* a as the inverse of the relaxation time $\bar{T} = 1/a$, which is the system's adjustment time to an equilibrium. However, the Bando model is not a DDE and strictly speaking, this relaxation time corresponds rather to the inverse of inertia than to reaction time since the response is proportional to a. In a given traffic situation, a car will brake more harshly the bigger this parameter is.
Therefore, inertia $1/a$ is explicitly incorporated in all second-order models ($\ddot{x}_n = \dot{v}_n$). In contrast, Newell's model is of first order in time ($\dot{x}_n = v_n$), and does not incorporate inertia at first sight. However, the cars do not assume their speed, which depends on the traffic situation, instantaneously. Like the vehicles of the second-order models, they need some time to adjust. This means that a first-order car-following model without an explicit inertia term might, nevertheless, incorporate some sort of *intrinsic inertia* due to the retarded reaction time of the driver.

Since the acceleration and deceleration are also functions of the density, we expect time delay, inertia and density to be the major parameters in a stability analysis.

CAR-FOLLOWING MODELS
Chandler model [16]: $\dot{v}_n(t+T) = a\dot{b}_n(t)$ Stability: $2Ta < 1$ Flow: $q(\rho) = a(1-\rho/\rho_{jam})$
Gazis model [23]: $\dot{v}_n(t+T) = \frac{a}{b_n(t)}\dot{b}_n(t)$ Stability: $2Ta\rho < 1$ Flow: $q(\rho) = a\rho\ln(\rho_{jam}/\rho)$
Pipes model [72]: $\dot{v}_n(t+T) = \frac{a}{b_n(t)^s}\dot{b}_n(t)\ ,\ s \in N$ Stability: $2Ta\rho^s < 1$ Flow: $q(\rho) = \frac{a}{1-s}\rho^s + c\rho$
(Advanced) Edie model [23]: $\dot{v}_n(t+T) = \frac{av_n(t+T)^m}{b_n(t)^s}\dot{b}_n(t)\ ,\ m,s \in N$ Stability: $2Ta\rho^s\left[\frac{a(1-m)}{1-s}\rho^{s-1} + c\right]^{\frac{1}{m-1}} > 1$ Flow: $q(\rho) = \rho\left[\frac{a(1-m)}{1-s}\rho^{s-1} + c\right]^{\frac{1}{1-m}}$
Newell model [70]: $v_n(t+T) = V_{max}\left[1 - \exp\left\{-\frac{a}{V_{max}}\left[b_n(t) - b_{min}\right]\right\}\right]$ Stability: $2TV' < 1$ Flow: $q(\rho) = \rho V(1/\rho)$
Bando model [8]: $\dot{v_n}(t) = a\left[V_B(b_n(t)) - v_n(t)\right]$ $V_B(b) = \tanh(b-2) + \tanh(2)$ Stability: $2V_B' < a$ Flow: $q(\rho) = \rho V_B(1/\rho)$
California model [16]: $\dot{v}_n(t+T) = a\left[b_n(t) + d - T_1 v_n\right]$ Stability: $aT_1^2 > 2$ Flow: $q(\rho) = \frac{1}{T_1}(1-\rho/\rho_{jam})$
Double look-ahead model [37]: $\dot{v}_n(t) = a_1\dot{b}_n(t-T_1) + a_2(\dot{b}_n + \dot{b}_{n+1})(t-T_2)$ Stability: $\frac{a_1+4a_2}{2(a_1+2a_2)^2} > \frac{a_1T_1+a_2T_2}{a_1+2a_2}$ Flow: $q(\rho) = a_1 + 2a_2 + c\rho$
Hayakawa model [26]: $\dot{v}_n = a\left[U(b_n)V(b_{n-1}) - v_n\right]$ $U(b) = V_B(b)\ ,\ V(b) = 1 + f_0\left[1 - \tanh(b-2)\right]$ Stability: $2(UV)'^2 > a(UV' - U'V)$ Flow: $q(\rho) = \rho U(1/\rho)V(1/\rho)$
Intelligent Driver Model [80]: $\dot{v}_n = a\left[1 - \left(\frac{v_n}{v_0}\right)^\delta - \left(\frac{s^*(v_n,\dot{b}_n)}{s_0}\right)^2\right]$ $s^*(v,\dot{b}) = s_0 + s_1\sqrt{\frac{v}{v_0}} + Tv + \frac{v\dot{b}}{2\sqrt{d}}$ Stability and Flow: no analytical expressions.

Table 2.1: An overview of car-following models, their stability criterion and equilibrium flow-density relation.

In fact, Holland [39] found that all car-following models obey a similar stability criterion. It states that a model is stable if the reaction time of the drivers is smaller than their *anticipation time*. The latter is basically given by the quotient of the equilibrium headway and the inter-vehicle wave speed of a disturbance. This yields the time in which a disturbance travels upstream from one vehicle to the following. Holland was able to show that this criterion holds for all the models summarized in Tab. 2.1 (apart from the intelligent driver model, which remains to be shown).
There is one crucial difference in the stability criterion between various car-following models. For a given set of parameters T and a, some are either stable or unstable for any initial equilibrium density, some are unstable for a sufficiently large density $\rho > \rho_c$, whereas more recent models are only unstable in an intermediate regime $\rho_{c1} < \rho < \rho_{c2}$, in which stop-and-go traffic forms[2]. Among the latter are the Bando, California and Hayakawa models. They are different from the earlier developed models, because they are based on a relaxation term, rather than on the change in headway.
It should be noted that instability can lead to a discontinuous flow-density curve, as shown in Fig. 2.7, which seems to agree with traffic data quite well. However, we assume stable flow throughout Tab. 2.1 with respect to the flow-density relations.

2.2.2.2 Flow-density Curves

In homogenous stationary flow, the speed and the headway are constants in time and among the cars, and the dynamical equations can be integrated because the time lag T is irrelevant. The car-following laws then reveal a speed-headway relation $v = v(b)$ [22, 72]. Since for these situations the headway is the inverse of the density $b = 1/\rho$, this also leads to flow-density curves $q = q(\rho)$, which can be compared with traffic data.
As an example, we consider the Bando model. In case of overall stability and homogenous flow ($\dot{v}_n \equiv 0$), the flow-density curve is continuous and is given by

$$v = V_B(b) = V_B(1/\rho) \quad \Rightarrow \quad q = \rho V_B(1/\rho). \tag{2.2.29}$$

V_B is again called the optimal-velocity function, since it gives the driver's desired speed for a traffic situation of a local headway b, which he adopts during $\bar{T} = 1/a$. This is similar to the relaxation term of the continuum models.
From Tab. 2.1 it can be seen that not all car-following models fulfill the requirements of flow-density curves, as stated in the previous subsection. The characteristics are violated by the following models:

[2] Note that the instability depends both on the density of the perturbed flow and the wavelength of the perturbation.

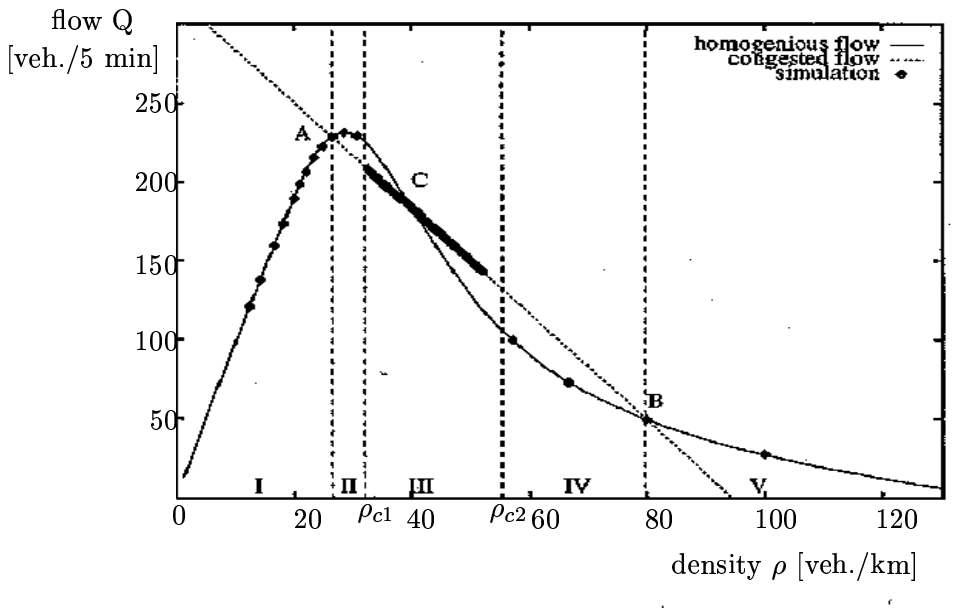

Figure 2.7: The fundamental diagram of the Bando model [4]. A discrete jump in flow appears when the model becomes unstable between critical densities ρ_{c1} and ρ_{c2}.

- $q(0) \neq 0$: Chandler, California, double-look ahead
- $q(\rho_{jam}) \neq 0$: Advanced Edie, Bando.

2.2.2.3 Nonlinear Features of Car-following Models

Even if some models appear simple, the reaction time introduces nonlinearity into the system and thereby leads to nonlinear phenomena. As shown in appendix C, for example, a linear system including damping might display oscillatory behaviour for a non-vanishing time lag, even though there is just a decaying oscillation when the time lag is zero. Hence, it is not surprising that new effects arise from the explicit introduction of a driver reaction time. However, **we will not consider** this factor in this dissertation, because we develop a link to the continuum models which, to date, do not contain **any time delay**.
In addition to the discrete jumps in the flow-density curves, the stop-and-go clusters, which form in some car-following models (Fig. 2.8) [15, 26], are of similar form to those of the Kerner-Konhäuser model [38, 48]. In chapter 3, it is revealed that there is a strong analytical relation between these models. Moreover, they produce similar results in the form of travelling wave solutions in which a specific nonlinear wave type occurs.
The characteristic parameters of these clusters, such as their speeds and densities,

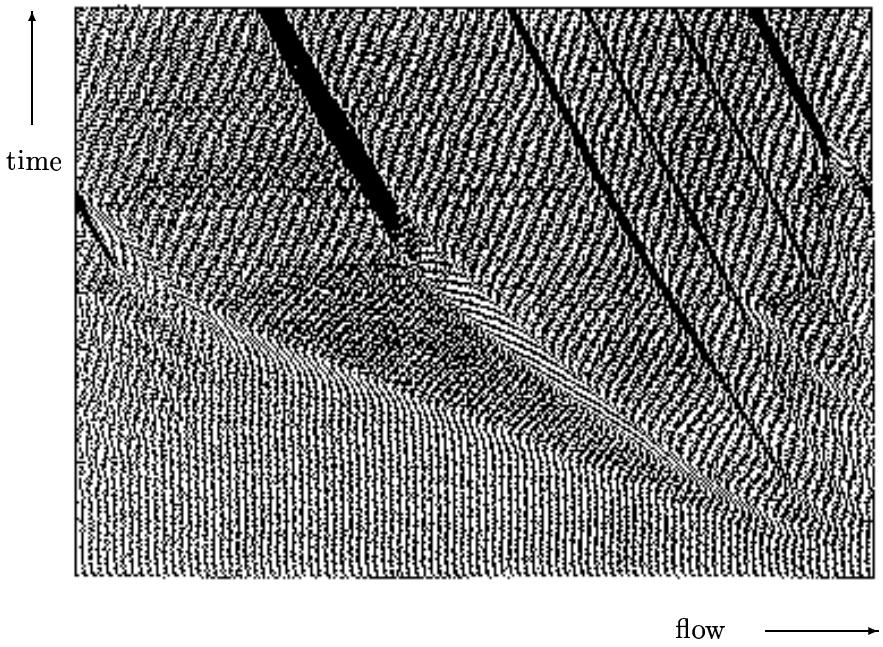

Figure 2.8: An initial disturbance in the Bando model causes the formation of stop-and-go jams on a ring road [39]: the darker the region, the higher the density.

and the free flow density between them, could be explained analytically for a Heaviside [78], as well as for a piecewise linear OV function [69]. We expect that this phenomenon also appears in other continuous OV functions.
Hayakawa and Nakanishi [26] derived kink solitons of their model using a weakly nonlinear analysis, which agrees very well with their numerical data, but the density in- and outside the cluster could not be obtained analytically, and one has to know them beforehand to calculate the kink solutions.
More nonlinear features are bound to appear if one considers multi-species traffic in a car-following model, as mentioned in chapter 5.

2.2.3 The Bando Model

As already mentioned, the calculations in this dissertation are mainly built on the Bando model,

$$\dot{v}_n(t) = a\left[V_B(b_n) - v_n\right], \tag{2.2.30}$$

first introduced in 1995 [8]. It represents the first car-following model to incorporate a relaxation term, and resembles earlier proposed continuum models such as Payne's, Kühne's and Kerner-Konhäuser's. Their solutions are similar to the predictions of the Bando model and supported by some numerical simulations, it is one major goal of this dissertation to show that the two types can be linked analytically.

Bando *et al* introduced the dimensionless optimal-velocity function

$$V_B(b) = \tanh(b-2) - \tanh(-2), \tag{2.2.31}$$

which corresponds to ideal vehicles of length zero, and this is what we will concentrate on in the following. This generic model was derived from real data, which originally led them to define

$$V_B(b) = \max\{0, 16.8\,[\tanh(0.086(b-25\text{m})) + 0.913]\}\,\text{m/s}. \tag{2.2.32}$$

The dimensionless version simplifies calculations and the extraction of analytical results, while still capturing the generic features of the flow.
Although successful at modelling some data, it is important to mention that this model has its limitations. Hooper [41] found out that it yields unrealistic accelerations, and he tried to set up a more realistic model by various means: limitation of the acceleration and deceleration which leads to crashes; the more successful approach of a double-look-ahead model in which a driver also reacts to cars further ahead; and last but not least, introduction of explicit time delay τ. In accordance with Bando *et al* [6], he concludes that a small delay does not affect the physics notably, whereas a larger delay leads to the unphysical state of backwards moving vehicles. Hence, the variables τ and a have to be chosen very carefully in order to make the model realistic.
The **Bando model** is, nevertheless, of great interest, since it is the only model that contains an OV function like the continuum models mentioned above. In addition, it reproduces more features of traffic flow than any other car-following model. It is, therefore, **the most suitable candidate to investigate the differences and similarities between the discrete and the continuum formulation**. This is what we will concentrate on in chapters 3 to 6, where several one-lane flow systems are considered using this model.[3]

2.2.4 Multi-lane, On- and Off-ramp Simulations

So far the discussion has treated the road as a single lane or averaged over the lanes. However, there are important effects which occur in multi-lane flow due to the diffusion of the flow between different lanes [40]. Another interesting example is the role of on- and off-ramps, and these are discussed in chapter 6. For completeness, we present a summary of the basic modelling of such systems.

[3] A final note on car-following models: there have been only a few attempts to describe traffic in terms of a mechanical system of particles whose interaction is given by a potential $\Phi_N(x_1, x_2, ..., x_N)$. The reason is that, "a car is an anisotropic particle that mostly responds to frontal stimuli"[17]. Therefore, the potential would be anisotropic, which means that the overall momentum is not a conserved quantity any longer, and the Lagrange formalism for non-dissipative systems does not apply.

The main problem of the modelling of multi-lane motorways is the lane-changing algorithm and the simulation of on- and off-ramps. They are both highly random and spontaneous processes, and difficult to integrate into any traffic model (continuum, car-following, CA, etc). On the other hand, the most important aspect of gaining high capacities is the distribution of traffic among the lanes. The European motorway code restricts overtaking to certain lanes which, according to recent simulations, seems to be a major disadvantage and results in inadequate lane usage compared to American highways [4].
Moreover, these processes are very similar, because an on-ramp can be regarded as a local lane-changing onto a lane, and correspondingly an off-ramp as the local departure from a lane. Since we will simulate an on-ramp in chapter 6, some remarks on multi-lane and ramp simulations to date are presented in the following.
Multi-lane simulations have been carried out mainly in continuum models. In 1971 Munjal and Pipes [63] published a paper on density perturbations between two- and three-lane highways. It was based on Lighthill and Whitham's continuum formulation, and considered small fluctuations around equilibrium solutions for non-uniform distributions along each lane, under the assumption of a linear lane-changing behaviour. This first-order analysis couples the lanes by adding a term to the right hand side of the equation of each lane,

$$K_{1t} + c_1 K_{1x} = a\,[K_2 - K_1]\,, \tag{2.2.33}$$

$$K_{2t} + c_2 K_{2x} = a\,[K_1 - K_2]\,. \tag{2.2.34}$$

Here, $K_1(x,t)$ and $K_2(x,t)$ are the deviations of the densities from their corresponding equilibrium values $K_1^{(0)}$ and $K_2^{(0)}$, which might well be different, and so the velocities of wave propagation are

$$c_i = \left.\frac{\partial q_i}{\partial k_i}\right|_{k_i = K_i^{(0)}} \quad , \quad i = 1, 2. \tag{2.2.35}$$

The authors derived analytical solutions for a uniform freeway ($K_1^{(0)} = K_2^{(0)}$, $c_1 = c_2$, $q_1 = q_2$), and simulated the spreading of an on-ramp flow across the lanes of the downstream highway for two and for three lanes.
This analysis was extended to a non-uniform highway of different equilibrium values of the corresponding lanes by Holland and Woods [39, 40]. However, the linear analysis is not sufficient if larger deviations of the densities from their equilibrium solutions are considered. In general, the wave speed is a function of the density $c_i = c_i(k_i)$, and the system of partial differential equations (2.2.33)-(2.2.34) is nonlinear.
Mason [60] studied travelling wave solutions of the full nonlinear system for arbitrary individual lane characteristics. Smooth travelling waves and shock waves appear in the system, as well as dispersive waves, depending on the initial conditions. The

first are a balance between nonlinear wave-steepening effects in a single lane and the dispersive "wave-spreading" of coupled lanes.
Recent models based on the Kerner-Konhäuser model are much more complicated. Lee *et al* [76] proposed that the lane-changing should be asymmetric with respect to the lanes, and moreover that the difference in speed between the two lanes should decrease with density. These assumptions seem to be very reasonable for European motorways, but do not apply to American highways.
It is rather surprising that to date, no continuum model contains an explicit dependency of the lane-changing terms on the velocities of both lanes. It is well known that drivers tend to change lane if the adjacent lane is as dense as their own one, but contains faster cars. This is obviously not possible in the Lighthill-Whitham formulation, which assumes that cars adjust their speed instantaneously to the corresponding density. On the other hand, this phenomenon is observed in real traffic, and it is another hint that inertia should be incorporated in the model.
This is naturally the case for car-following models. Helbing and Huberman have recently published a Bando-type model that simulates lane-changing [34]. The crucial difference from the continuum formulation is the discretization of the lane-changing algorithm. It is usually a highly nonlinear and random process that makes analytical approaches very difficult. A vehicle is supposed to change lanes if it can travel faster on the adjacent lane, and if several safety criteria such as the distance to the preceding and following car of the neighbouring lane, the difference in speed, etc, are fulfilled. This leads to various update steps, which make the numerical effort far bigger than in the case of a single lane. Nevertheless, different vehicles such as cars and lorries can be mixed, which might reveal new effects in multi-lane traffic flow. One example is that the authors discovered a coherent state of vehicle motion which they refer to as synchronized traffic.
There are also cellular automaton models for the simulation of multi-lane traffic flow, such as Wagner's [4]. According to the author, it is still unclear whether they describe the full range of density regimes properly.
So far, **on-ramp simulations** have been carried out mainly in continuum models. This process is rather easy to implement by adding a source term to the right hand side of the equation for the conservation of cars,

$$\rho_t + (\rho v)_x = q_{ramp}. \tag{2.2.36}$$

The evolution of the system is then determined by the initial conditions and the ramp flux $q_{ramp}(x,t)$.
The advantage of this approach is that the source term is continuous, both in space and time. Hence, no discrete process perturbs the continuity of the model, and huge gradients (section 3.2) in the density distribution near the on-ramp can be avoided. Moreover, q_{ramp} can be fitted to motorway data representing the time dependent

flux of on-ramps.
The occurrence of various traffic states near ramps is part of much current work. Lee *et al* [56] recently simulated on- and off-ramps on a single lane, and interpreted one traffic state as synchronized. Their results have consequences for traffic controlling: motorway flow might be kept stable by controlled on-ramps.
However, the literature provides very little information about on-ramp simulations in car-following models. One reason might be that entering a lane now becomes a discrete process both in space and time, which makes it very difficult to extract analytical results from the corresponding equation of motion.
Nevertheless, car-following as well as CA models are very suitable to incorporate stochasticity. Time series extracted from on-ramp data can be directly fed into the system. In addition, it is likely that entering a lane via an on-ramp has to be considered as a discrete process in order to explain phase transitions in their vicinity, since the critical amplitude of those transitions (Fig. 2.4) might well be different for car-following and continuum models.

As we can see, a vital question is how to incorporate lane-changing or on- and off-ramps on motorways. Continuum models tend to couple lanes by deterministic cross terms which depend on the density and the speed in the corresponding lanes. However, a stochastic, and hence more realistic, approach can only be realized in discrete models like the car-following or CA models. An algorithm in accordance with traffic data and driver behaviour is still not available and very little research on this topic has been done to date. We will come back to this problem in chapter 6.

Chapter 3

Continuum Approach to Car-following Models

In this chapter, a continuum version of the car-following Bando model [8] is developed using a series expansion of the headway in terms of density. This new continuum model obeys the same stability criterion as its discrete counterpart. To compare both types, it is shown that travelling wave solutions of the Bando model in the stable regime [11, 15] are very similar to those of the continuum counterpart in the limit of small changes of headway, and gradually diverge as the change of headway across the wave increases. The transformation relating headway to density enables predictions of the global impact and characteristics of any car-following model to be made by using the continuum analogue. However, chapter 4 shows that even simple differential delay equations, which describe various car-following models, lead to very complex equivalent continuum models and, thus, are easier to simulate in the original, discrete version.
After that, the inverse transformation, giving the density in terms of the headway, is derived, which allows us to obtain analogous discrete counterparts of various continuum models. Here, the problem lies in the interpretation of discrete spatial gradients, which occur in the corresponding car-following model.

3.1 The Need to relate Car-following and Continuum Models

The purpose of this chapter is to develop a systematic method for linking car-following and continuum models of road traffic. The relation between the two models is of interest since they provide different pictures of the flow, which should converge in the appropriate limit.

Continuum models give an overview of the global traffic flow, which is important for developing insight into traffic quantities such as throughput, density distributions or the onset of jams, without detailed regard to the properties of each car. They can illustrate the effects of speed control systems along the road and allow for analytical calculations. Continuum models also differ from car-following models with regard to numerical simulations, because one has to deal with two coupled partial differential equations, instead of a few hundred or even thousands of ordinary differential equations corresponding to the number of cars on the road. Which procedure is more costly depends on the problem.
However, car-following models represent the only class of models which describes each vehicle in a deterministic manner, including the response to local variables such as speed, headway and change of headway. Therefore, they seem to be of great importance when it comes to autonomous cruise control systems (ACCS), which should stabilize and maximize the flow.
In this chapter, we follow the Bando model [8] of road traffic

$$\dot{v_n} = a\,[V_B(b_n) - v_n] \tag{3.1.1}$$

with the optimal-velocity function

$$V_B(b_n) = \tanh(b_n - 2) + \tanh(2), \tag{3.1.2}$$

shown in Fig. 3.1. Since this model is able to reproduce various features of road traffic (see chapter 2), it is the subject of much current research [6, 26, 69].
By developing a formal asymptotic procedure, we derive the continuum approximation to the car-following model, which is valid when the spacing between cars is small, relative to the length scale of changes in speed and headway. We then compare this with the continuum model of Kerner and Konhäuser (K.-K.) [48] (subsection 2.2.1) which incorporates effects of inertia and dispersion, and is able to describe the formation of instabilities and traffic jams:

$$v_t + vv_x = \frac{V_{kk}(\rho) - v}{T} - c_0^2\frac{\rho_x}{\rho} + \mu\frac{v_{xx}}{\rho} \tag{3.1.3}$$

with an optimal-velocity function $V_{kk}(\rho)$ that is discussed in greater detail in section 3.5. Here, the coefficients c_0^2 of the *pressure* and μ of the *viscosity* (dissipative) term are considered to be constant. This is closed as usual by the conservation of cars

$$\rho_t + (\rho v)_x = 0. \tag{3.1.4}$$

In discussions [4] of the derivation of the higher order terms, it appears that the dissipative term was originally introduced as a means of stopping steepening waves from forming discontinuous shocks. Nagel [67] explained it as an averaging effect caused by implicit random fluctuations in ρ and v. It has been argued that these

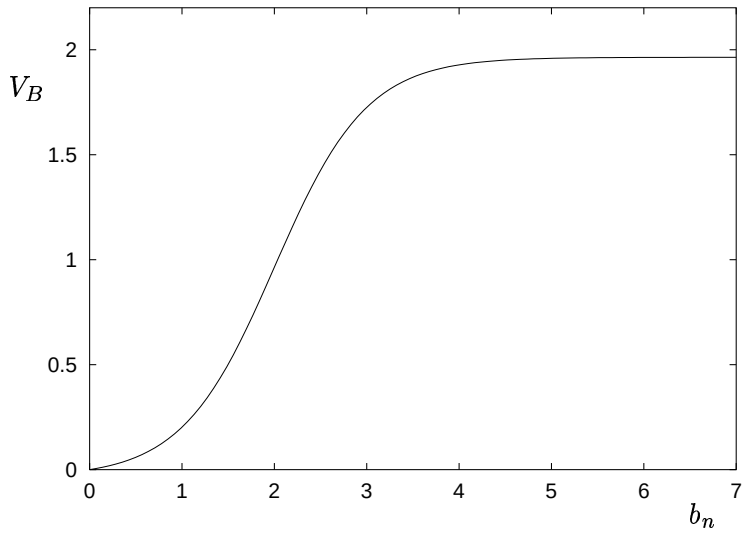

Figure 3.1: The monotonic increasing optimal-velocity function $V_B(b_n)$ of the Bando model with top speed $V_B(b_n \to \infty) \approx 1.964$.

noise terms are important, since they can have a profound effect on solutions of certain partial differential equations. For instance, Burger's equation

$$u_t + uu_x = \lambda u_{xx} \tag{3.1.5}$$

has well-known travelling N-wave solutions, which cease to exist if Gaussian noise is added to the right-hand side.

Here, rather than these heuristically motivated continuum models, we aim to derive an asymptotic equation analogous to Eq. (3.1.3) from the car-following model (3.1.1). We, thus, establish that such diffusive behaviour is an implicit part of the car-following model.

In the case of a homogenous stationary flow, all time and space derivatives vanish, and for the car-following model we then obtain the relation between speed v_0 and headway b_0 (section 2.1)

$$v_0 = V_B(b_0), \tag{3.1.6}$$

while from the continuum model we have

$$v_0 = V_{KK}(\rho_0). \tag{3.1.7}$$

For such uniform flow conditions, the density is simply given by the inverse of the headway

$$\rho = 1/b, \tag{3.1.8}$$

and one can compare the two types of models by drawing their fundamental diagrams

$$q_0(\rho_0) = \rho_0 v_0 = \rho_0 V_B(1/\rho_0) \tag{3.1.9}$$

and

$$q_0(\rho_0) = \rho_0 V_{KK}(\rho_0), \tag{3.1.10}$$

respectively. In non-homogenous non-stationary situations, however, the car-following and continuum models can only be compared by stability analysis and numerical simulations. It is hard to say which terms or effects are responsible for the difference in the simulations, but we can show that the relation between headway and density is of great importance. When there are long range fluctuations in the headway or the density along the road, Eq. (3.1.8) is only a first-order approximation. In the next section, we introduce a more accurate method to relate these variables.

3.2 The Transformation; Continuum Version of the Bando Model

[1] The difficulty of relating car-following and continuum models of road traffic is in part a result of the fact that the first are based on the headway, and the latter on the vehicle density. It is therefore important to relate these two quantities correctly. In the literature, the density ρ is usually defined as the inverse of the headway Eq. (3.1.8). However, there is a problem with this definition. For example, suppose we have a set of cars positioned at $x = 1, 2, 4, 8, \ldots$. The car at position x has headway $b = x$. Using the formula (3.1.8), we obtain $\rho = 1/x$, which is extended to the continuum domain by permitting x to take any positive real value. According to this, the number of cars on the open interval (1,y) is $\ln y$. However, the actual answer is $\log_2 y$ and, so, we are consistently wrong by a factor of $\ln 2$.
We deduce that for non-homogenous flow situations, we cannot transform the car-following model by simply using relation (3.1.8). We need a consistent way to set up a map

$$\{x_i\} \mapsto [\rho : \Re \mapsto \Re], \tag{3.2.1}$$

where the set $\{x_i\}$ represents the positions of the vehicles at a given instant in time, and $\rho(x)$ is the associated density function from which we should be able to find the positions of the vehicles. One approach is to require that

$$\int_{x_i}^{x_{i+1}} \rho(x)dx = 1 \tag{3.2.2}$$

for all i. Thus, in addition to our density function, we require the position of car one. Given only the condition Eq. (3.2.2), map (3.2.1) is not unique, but its inverse is. However, it is the inverse map that we require in constructing a continuum equation of motion from a car-following law. We use the definition of the headway $b = x_{i+1} - x_i$

[1] This section contains original work by Mason [60], which was also used in a publication by Berg, Mason and Woods [11].

to arrive at an equation involving the continuum variable ρ by extending Eq. (3.2.2) formally to all points along the road

$$\int_x^{x+b(x,t)} \rho(x',t)dx' = \int_0^{b(x,t)} \rho(x+y,t)dy \equiv 1. \tag{3.2.3}$$

Expanding the second integral in powers of y

$$\int_0^{b(x,t)} \left[\rho(x,t) + \rho_x(x,t)y + \frac{1}{2!}\rho_{xx}(x,t)y^2 + ...\right] dy, \tag{3.2.4}$$

we integrate to obtain the asymptotic series [60]

$$b\rho + \frac{1}{2!}b^2\rho_x + \frac{1}{3!}b^3\rho_{xx} + ... = 1, \tag{3.2.5}$$

where the first term corresponds to the common definition of the density Eq. (3.1.8). We expand the series to this order for two reasons. First, we would like to obtain a continuum model that is capable of describing some characteristic traffic parameters mentioned by Kerner and Konhäuser [48]. They showed that a dissipative term has to be incorporated to do so. Secondly, these higher order terms are needed to maintain the same stability criterion for the continuum model as for the car-following model, demonstrated in the next section.

When we truncate the series (3.2.5), it is assumed that each term is of smaller magnitude than the preceding one. This assumption is at the core of continuum approximations of many kinds, and can be summarized by the condition

$$\epsilon_\Lambda = \frac{\Lambda_x}{\rho\Lambda} \ll 1 \tag{3.2.6}$$

for all scalar quantities Λ associated with traffic. It amounts to saying that changes in the flow occur over a length scale of many vehicles.

If we consider the cubic term to be much smaller than the linear and quadratic term, we can first solve the quadratic equation for b

$$b\rho + \frac{1}{2}b^2\rho_x = 1, \tag{3.2.7}$$

obtaining

$$b \approx \frac{1}{\rho} - \frac{\rho_x}{2\rho^3}. \tag{3.2.8}$$

Regarding the cubic term as a perturbation, we expand b in a perturbation series

$$b = \frac{1}{\rho} - \frac{\rho_x}{2\rho^3} + \epsilon \quad , \quad \text{with} \quad |\epsilon| \ll \left|\frac{1}{\rho} - \frac{\rho_x}{2\rho^3}\right|, \tag{3.2.9}$$

and approximate the solution as

$$b \sim \frac{1}{\rho} - \frac{\rho_x}{2\rho^3} + \left(\frac{\rho_x^2}{2\rho^5} - \frac{\rho_{xx}}{6\rho^4}\right). \tag{3.2.10}$$

The first term represents the classic transformation for relating the headway and the density, and the second term is similar to a *pressure term* in gas kinetics and acts to destabilize the traffic flow. If we retain only this term, we end up with a continuum model similar to Payne's. The diffusive term ρ_{xx} smoothes variations in traffic density and has a stabilizing effect on traffic flow, which counteracts the pressure term. We therefore retain terms up to this order.
Equation (3.2.10) can be substituted into car-following models to yield equations for ρ instead of b.
So far, we have established a link between the continuum density and the headway. The other quantity relevant to both continuum and car-following models is the speed v. In order to link the two models consistently, we need to establish that v is now consistent with the quantity representing the speed of each vehicle in the car-following models.
Taking a total time derivative of each side of Eq. (3.2.3), we obtain

$$\int_x^{x+b} \rho_t(y)dy + (x_t + b_t)\,\rho(x+b) - x_t\rho(x) \tag{3.2.11}$$

$$= \int_x^{x+b} \rho_t(y)dy + v(x+b)\rho(x+b) - v(x)\rho(x) \tag{3.2.12}$$

$$= \int_x^{x+b} [\rho_t(y) + (\rho(y)v(y))_y]dy \tag{3.2.13}$$

$$= 0\ , \tag{3.2.14}$$

where $b(x)$ and all other quantities are evaluated at time t. Hence, the conservation equation (3.1.4) guarantees that the integral of density along the road from any vehicle to the one it is following is one. In this sense, the definition of velocity v is consistent.
Applying our analysis to the second-order model of Bando *et al* in Eq. (3.1.1), we obtain the expression for the conservation of cars Eq. (3.1.4), coupled with the approximation of the car-following model in terms of a Taylor expansion to first order

$$v_t + vv_x = a\left[V_B\left(\frac{1}{\rho} - \frac{\rho_x}{2\rho^3} + \frac{\rho_x^2}{2\rho^5} - \frac{\rho_{xx}}{6\rho^4}\right) - v\right] \tag{3.2.15}$$

$$\simeq a\left[\bar{V}(\rho) - v\right] + a\bar{V}'(\rho)\left[\frac{\rho_x}{2\rho} + \frac{\rho_{xx}}{6\rho^2} - \frac{\rho_x^2}{2\rho^3}\right]. \tag{3.2.16}$$

Here we set

$$\bar{V}(\rho) = V_B(1/\rho), \tag{3.2.17}$$

$$0 < \left.\frac{\partial V_B(b)}{\partial b}\right|_{b=1/\rho} = -\rho^2\frac{\partial \bar{V}(\rho)}{\partial \rho} = -\rho^2\bar{V}'(\rho). \tag{3.2.18}$$

Equation (3.2.16) is analogous to the Kerner-Konhäuser model Eq. (3.1.3). However, an important difference between their model and the new model lies in the coefficients of the higher order terms. In contrast to their heuristic model, in which the coefficients are assumed to be constant, Eq. (3.2.16) reveals a dependence on ρ: for example, c_0^2 is now analogous to the term $-\frac{a\bar{V}'(\rho)}{2}$. By comparison with the discrete Bando model, numerical simulations show that the dependence of these coefficients on the density ρ is necessary to match the length scale and qualitative behaviour of travelling wave solutions (sections 3.4 and 3.5). The accuracy increases with further terms of the asymptotic series Eq. (3.2.10).
As already mentioned, Nagel [67] argues that the dissipative term can be regarded in terms of stochasticity added as a high-frequency correction to density, which is supposed to vary slowly in space and time. However, our analysis reveals that the transformation from a car-following to a continuum model also produces a diffusive or smoothing effect, without the need to introduce any explicit stochasticity.

3.3 Stability Analysis

Before proceeding with numerical calculations, we first show that the continuum version of the Bando model Eq. (3.2.16) obeys the same stability criterion as its discrete counterpart. Bando *et al* [8] proved that an initial homogenous flow of headway b_0 is unstable if the inequality

$$\frac{2V_B'(b_0)}{a} > 1 \tag{3.3.1}$$

is satisfied. This relates the drivers' sensitivity a to the derivative of the OV function V_B' at $\rho_0 = 1/b_0$. The analogous criterion for the continuum model may be found by linearizing the model

$$\rho_t + (\rho v)_x = 0, \tag{3.3.2}$$

$$v_t + vv_x = a\left[\bar{V}(\rho) - v\right] + a\bar{V}'(\rho)\left[\frac{\rho_x}{2\rho} + \frac{\rho_{xx}}{6\rho^2} - \frac{\rho_x^2}{2\rho^3}\right] \tag{3.3.3}$$

around some initial values ρ_0 and $v_0 = \bar{V}(\rho_0)$

$$\rho = \rho_0 + \hat{\rho}, \tag{3.3.4}$$

$$v = v_0 + \hat{v}. \tag{3.3.5}$$

This leads to the perturbation equations

$$\hat{\rho}_t + \rho_0\hat{v}_x + v_0\hat{\rho}_x = 0, \tag{3.3.6}$$

$$\hat{v}_t + v_0\hat{v}_x = a\left[\bar{V}'(\rho_0)\hat{\rho} - \hat{v}\right] + a\bar{V}'(\rho_0)\left[\frac{\hat{\rho}_x}{2\rho_0} + \frac{\hat{\rho}_{xx}}{6\rho_0^2}\right]. \tag{3.3.7}$$

We now calculate the eigenvalues $\omega(k)$ of a harmonic disturbance of the form

$$\vec{f}(x,t) = \begin{pmatrix} \hat{\rho}(x,t) \\ \hat{v}(x,t) \end{pmatrix} = \begin{pmatrix} \hat{\rho}_0 \\ \hat{v}_0 \end{pmatrix} \exp\left\{i[kx - \omega(k)t]\right\}, \tag{3.3.8}$$

so that we can rewrite the equations as

$$\begin{pmatrix} i(kv_0 - \omega) & ik\rho_0 \\ -a\bar{V}' - \frac{ia\bar{V}'k}{2\rho_0} + \frac{a\bar{V}'k^2}{6\rho_0^2} & i(kv_0 - \omega) + a \end{pmatrix} \begin{pmatrix} \hat{\rho}_0 \\ \hat{v}_0 \end{pmatrix} \exp\left\{i\left[kx - \omega(k)t\right]\right\} = 0. \tag{3.3.9}$$

This equation has non-trivial solutions if the determinant vanishes,

$$\begin{vmatrix} i(kv_0 - \omega) & ik\rho_0 \\ -a\bar{V}' - \frac{ia\bar{V}'k}{2\rho_0} + \frac{a\bar{V}'k^2}{6\rho_0^2} & i(kv_0 - \omega) + a \end{vmatrix} = 0. \tag{3.3.10}$$

As long as the imaginary part of ω is negative, the system is stable. Solutions have the form

$$\omega_{1,2}(k) = kv_0 - i\frac{a}{2}\left[1 \pm \sqrt{1 + \frac{2\bar{V}'}{a}\left(k^2 - i2\rho_0 k + \frac{i}{3\rho_0}k^3\right)}\right], \tag{3.3.11}$$

and by defining

$$\Omega(k) := Re\left[1 + \frac{2\bar{V}'}{a}\left(k^2 - i2\rho_0 k + \frac{i}{3\rho_0}k^3\right)\right]^{1/2}, \tag{3.3.12}$$

the criterion is equivalent to $|\Omega(k)| < 1$. By writing

$$|\Omega(k)| = \left[\left(1 + \frac{2\bar{V}'}{a}k^2\right)^2 + \left(-\frac{4\bar{V}'\rho_0}{a}k + \frac{2\bar{V}'}{3a\rho_0}k^3\right)^2\right]^{1/4} |\cos(\phi/2)| \tag{3.3.13}$$

$$= [...]^{1/4}\,\frac{\sqrt{1+\cos\phi}}{\sqrt{2}}, \tag{3.3.14}$$

where [...] denotes the square bracket in Eq. (3.3.13) and

$$\phi = \arg\left[1 + \frac{2\bar{V}'}{a}\left(k^2 - i2\rho_0 k + \frac{i}{3\rho_0}k^3\right)\right], \tag{3.3.15}$$

it may be seen that the condition $\mathrm{Im}(\omega) < 0$ is equivalent to

$$[...]^{1/4}\,\frac{1}{\sqrt{2}}\sqrt{1 + \frac{1 + (2\hat{V}'/a)k^2}{[...]^{1/2}}} < 1. \tag{3.3.16}$$

In order to solve this inequality, we restrict k to be non-negative, since $|\Omega(k)|$ is symmetric. Solving $|\Omega(k)| = 1$ leads to three solutions,

$$k_0 = 0 \quad , \quad k_\pm = \sqrt{6\rho_0^2 \pm \frac{3a\rho_0}{\bar{V}'}\sqrt{-\frac{2\bar{V}'}{a}}}. \tag{3.3.17}$$

Recall $\bar{V}' < 0$ from Eq. (3.2.18). This implies that k_- is always real, whereas k_+ may be either real or complex. Since we know that $|k_+| < k_-$, $\Omega(0) = 1$ and

$$\Omega(k) \overset{k\to\infty}{\longrightarrow} -\infty, \tag{3.3.18}$$

we can deduce from the continuity of $\Omega(k)$ that $\Omega(k_-) = -1$. So for $k > k_-$ the model is unstable, but since this corresponds to disturbances which are smaller than the initial headway, we do not take this case into further consideration. However, if k_+ is real, there is a region $0 < k < k_+$ of instability $\Omega(k) > 1$ with respect to long wavelengths. In contrast, if $k_+ \notin \Re$, which means

$$6\rho_0^2 + \frac{3a\rho_0}{\bar{V}'}\sqrt{-\frac{2\bar{V}'}{a}} < 0, \tag{3.3.19}$$

the system is stable. Taking $V_B' = -\rho_0^2\bar{V}'$ into account, this reduces to

$$\frac{a}{2V_B'} > 1, \tag{3.3.20}$$

which is exactly the stability criterion found by Bando *et al* (cf. Eq. (3.3.1)). Accordingly, the continuum model is unstable in a regime $0 < \rho_{c_1}^B < \rho < \rho_{c_2}^B$ too, such that

$$\frac{a}{2\ V_B'(1/\rho)} < 1. \tag{3.3.21}$$

A stability analysis for the Kerner-Konhäuser model leads to a criterion similar to Eq. (3.3.13). Now, the system is stable if

$$|\Omega_{KK}(k)| = \left| Re\left[1 + \frac{i4\rho_0 a V_{KK}' k - 4\rho_o^2 c_0^2 k^2}{(a\rho_0 + \mu k^2)^2}\right]^{1/2}\right| < 1 \tag{3.3.22}$$

is satisfied. Taking the limits

$$k \to 0: \qquad |\Omega(k)_{KK}| \to 1 - \frac{2c_0^2}{a^2}k^2 \to 1_-, \tag{3.3.23}$$

$$k \to \infty: \qquad |\Omega(k)_{KK}| \to \sqrt{1 - \frac{4\rho_0^2 c_0^2}{\mu^2 k^2}} \to 1_-, \tag{3.3.24}$$

shows that the model is stable for any initial value ρ_0 of the density and arbitrary sensitivity $a = 1/T$ with respect to short and long range disturbances, unlike the continuum analogue of the Bando model. Moreover, for the set of parameters (3.5.10)-(3.5.16), the model is linearly unstable in a range $\rho > \rho_c^{KK}$, which is different from the intermediate range of the Bando model $\rho_{c_1}^B < \rho < \rho_{c_2}^B$. This reveals another basic difference between these two continuum models.

We have shown that the continuum version satisfies the same stability criterion as the original discrete model. However, one could argue that this is shear coincidence

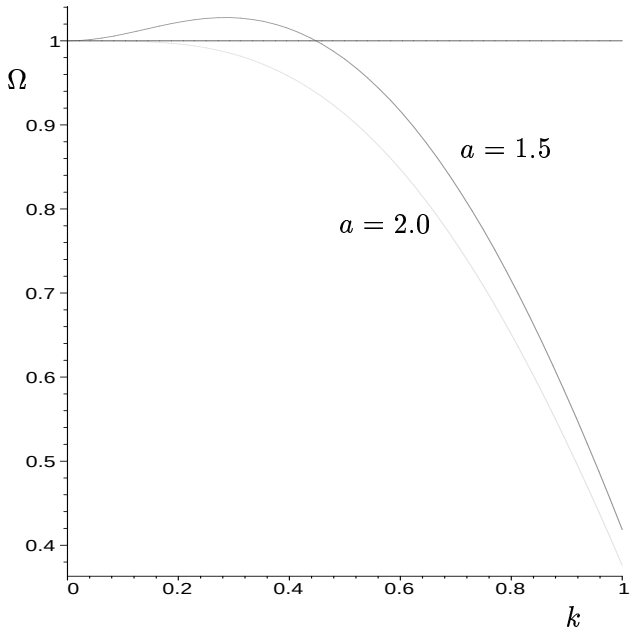

Figure 3.2: The function $\Omega(k)$ for two different values of the sensitivity a.

because we truncated the asymptotic series (3.2.5) after three terms, and that further terms in (3.2.10) might spoil the equivalence of the stability.
The answer lies in the prerequisite that we have used to derive our model. We have assumed that each term in the asymptotic series Eq. (3.2.5) is small compared to the preceding order. For the first two terms this is equivalent to

$$\left|\frac{\frac{b^2}{2}\rho_x}{b\rho}\right| = \left|\frac{\rho_x b}{2\rho}\right| = \left|\frac{b}{2}(\ln\rho)_x\right| \ll 1, \tag{3.3.25}$$

and likewise for the third and second terms

$$\left|\frac{b}{3}(\ln\rho_x)_x\right| \ll 1. \tag{3.3.26}$$

In general, the criterion for a sufficiently fast convergent series is

$$\left|\frac{b}{n}\left\{\ln\left[\left(\frac{\partial}{\partial x}\right)^{n-2}\rho\right]\right\}_x\right| \ll 1. \tag{3.3.27}$$

If we consider a Fourier component of the density

$$\rho(x,t) \sim \exp\left[i(kx-\omega t)\right], \tag{3.3.28}$$

(3.3.27) is equivalent to

$$\left|\frac{kb}{n}\right| \ll 1. \tag{3.3.29}$$

This means that the variation of the density should take place on a long wavelength of the order of several headways.
The car-following model is most unstable for $b = 2$, which leaves us in the case $n = 2$ with $|k| \ll 1$. Only in this regime can we expect the models to be equivalent. For large k, the prerequisite is not fulfilled and the models are no longer equivalent. They may therefore show different behaviour, which could be tested by a comparison between numerical simulations of the continuum and the discrete model: a short wavelength perturbation should only grow in the continuum model.
Figure 3.2 shows $\Omega(k)$ for two different sensitivities. It becomes clear that the instability $|\Omega(k)| > 1$ first occurs for $a = 2.0$ near $k = 0$. In this region, the lowest order terms in (3.3.12) dominate and, hence, further terms of higher order do not affect the stability. They only begin to play an important role for increasing values of k, where (3.3.29) is not fulfilled.

3.4 Comparison of Travelling Wave Solutions

So far, we only know that the models (3.1.1) and (3.2.16) have the same equilibrium flow-density curve and the same stability criterion. Here, linear terms have dominated the analysis since large gradients are neglected. Therefore, we have to look at the dynamics of the models in order to draw conclusions about their equivalence. One can only talk about analogous models if they produce similar results.
To further support our ideas, and to test the accuracy of our model, we compare some travelling wave solutions of the car-following Bando model in the stable regime [15] with those of the continuum version (see also chapter 5 for greater details of travelling wave solutions). By a travelling wave, we mean a density profile that travels up- or downstream on the highway without changing its shape. By choosing this wave type, the coupled partial differential equations of the continuum model reduce to one ordinary differential equation, which makes numerical simulations much easier.
If we move with a wave of speed c, we can transform the variables speed and density by a coordinate transformation

$$z = x - ct \tag{3.4.1}$$

into

$$v(x,t) = \quad v(x-ct) = \quad v(z), \tag{3.4.2}$$

$$\rho(x,t) = \quad \rho(x-ct) = \quad \rho(z). \tag{3.4.3}$$

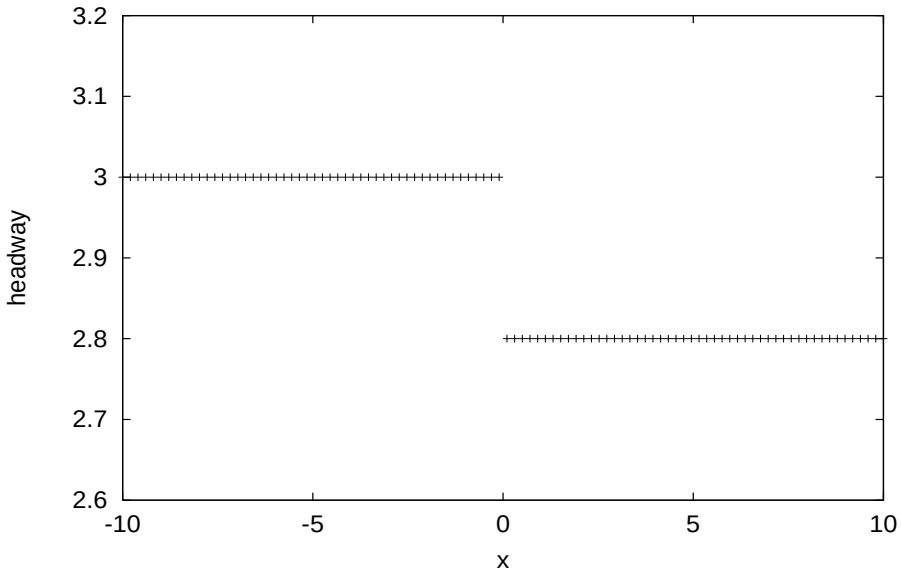

Figure 3.3: Initial change of headway in the Bando model, $t = 0$. The initial speed of the vehicles is given by $v_n(0) = V_B(b_n(0))$. Our special choice of Heaviside initial data is further discussed in chapter 5.

The equation (3.1.4) for the conservation of cars then reads

$$-c\rho_z + q_z = 0, \tag{3.4.4}$$

and can be integrated to yield

$$\rho(v - c) = q_0. \tag{3.4.5}$$

The parameter q_0 is some integration constant, which is determined by the boundary conditions $\rho_{-\infty} = \rho(x \to -\infty)$, $\rho_\infty = \rho(x \to \infty)$, $v_{-\infty} = v(x \to -\infty)$ and $v_\infty = v(x \to \infty)$ as follows

$$\begin{aligned} q_0 &= \rho_\infty(v_\infty - c) && (3.4.6)\\ &= \rho_\infty\left[\bar{V}(\rho_\infty) - c\right] && (3.4.7)\\ &= \rho_{-\infty}(v_{-\infty} - c) && (3.4.8)\\ &= \rho_{-\infty}\left[\bar{V}(\rho_{-\infty}) - c\right]. && (3.4.9) \end{aligned}$$

Eqs. (3.4.6) - (3.4.9) reveal that the wave speed c has the value

$$c = \frac{\rho_\infty \bar{V}(\rho_\infty) - \rho_{-\infty}\bar{V}(\rho_{-\infty})}{\rho_\infty - \rho_{-\infty}}, \tag{3.4.10}$$

and so both the variables q_0 and c are uniquely determined by the values of ρ at $\pm\infty$. Moreover, we can see that if a travelling wave between two uniform flows of

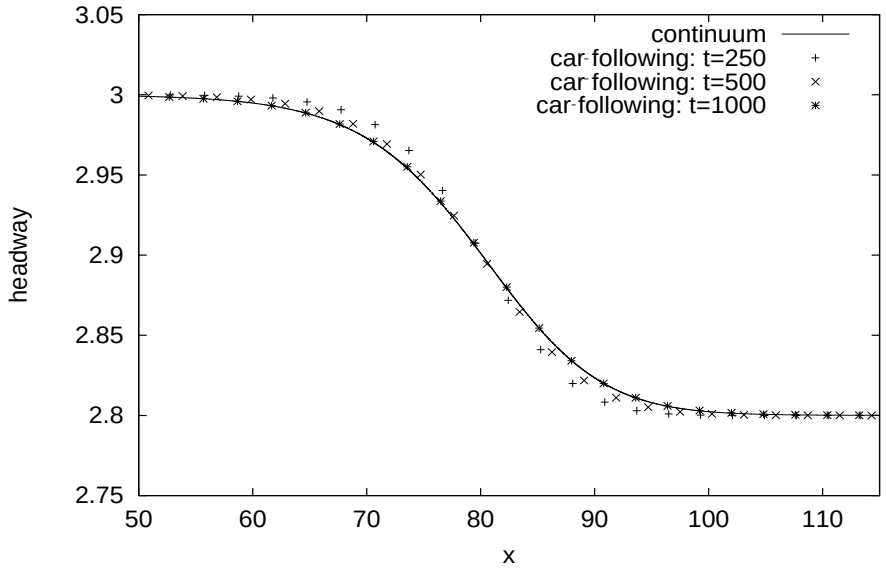

Figure 3.4: The wave profile of the Bando model approaching the travelling wave solution of the continuum model in the moving frame Eq. (3.4.1). Here as in what follows, we shift the origin of the solutions for reasons of comparison.

densitiy $\rho_{-\infty}$ and ρ_{∞} exists, then it moves with a speed that equals the gradient of the chord between these two densities in the fundamental diagram.
If we substitute these relations into our model equation (3.2.16) and make the transformation

$$u(z) = v(z) - c, \tag{3.4.11}$$

we obtain the equation for the speed of cars u in the frame moving with the wave

$$uu_z = a\left[\bar{V}(q_0/u) - u - c\right] - a\bar{V}'(q_0/u)\left(\frac{u_z}{2u} + \frac{u_{zz}}{6q_0} + \frac{2u_z^2}{3q_0 u}\right), \tag{3.4.12}$$

which can be integrated numerically using a shooting method (appendix D). **Unless stated otherwise**, throughout the remaining parts of this dissertation, **we assume** $a = 2.0$ in order to be in the linear stable regime, the results of which are discussed in the moving frame Eq. (3.4.11).
Figure 3.4 shows how the wave that develops from the initial condition Fig. 3.3 evolves towards the wave solution of the continuum model Eq. (3.4.12).[2] As the initial jump in headway increases, the wave develops an oscillatory tail (Fig. 3.5), and because of the increasing of headway gradients, the solution governed by the

[2]Where it appears more suitable, we present the figures of the car-following simulations with lines rather than with dots representing each car, in order to simplify the comparisons with travelling wave solutions.

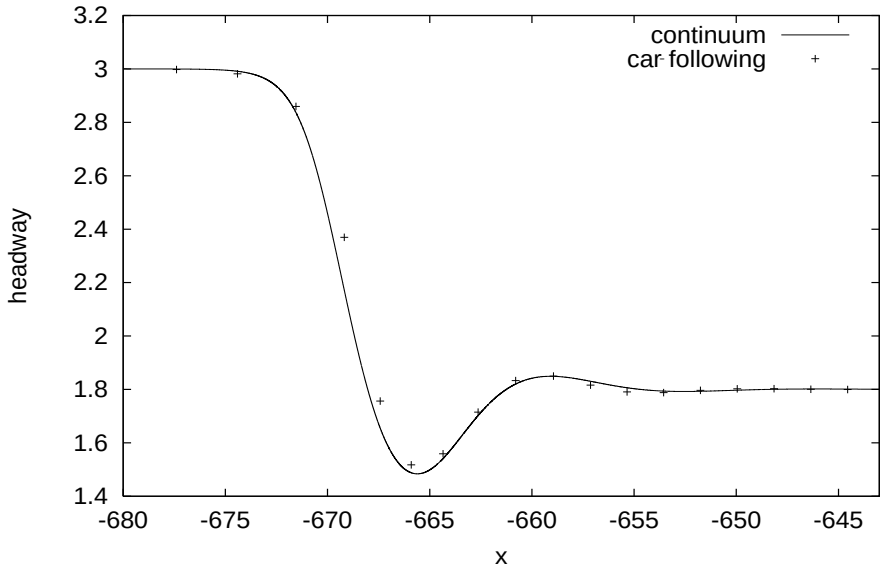

Figure 3.5: The change of headway at $t = 1000$ for an initial jump from $b_- = 3.0$ to $b_+ = 1.8$.

continuum model begins to diverge from its discrete car-following counterpart. However, the length scale and the oscillatory characteristic of the wave are still described properly.

If the downstream headway in the car-following model is decreased below some critical value b_{crit}, an unusual type of nonlinear wave solution develops [15]. It consists of two travelling waves of different speed (Fig. 3.6), separated by a growing region of congested traffic of density ρ_{bw}. We may call the upstream wave a **Bando wave**[3]: it also occurs in the numerical simulation of the continuum model when the integration breaks down. However, given ρ_{bw}, which can here only be determined numerically, we can calculate travelling wave solutions in the analogous continuum model for both up- and downstream waves. They may be matched to describe the new wave type, if one knows the long-time behaviour of the gap width. We assume that in this limit, the gap will increase at a constant rate v_{gap}, which can be calculated from the continuum model according to

$$v_{gap} = c_{down} - c_{up}. \tag{3.4.13}$$

Here c_{down} and c_{up} represent the downstream and the upstream wave velocity, respectively, and both parameters can be obtained following Eq. (3.4.10)

$$c_{up,down} = \frac{\rho_{\pm\infty}\bar{V}(\rho_{\pm\infty}) - \rho_{bw}\bar{V}(\rho_{bw})}{\rho_{\pm\infty} - \rho_{bw}}. \tag{3.4.14}$$

[3]More details of this wave type are presented in chapter 5.

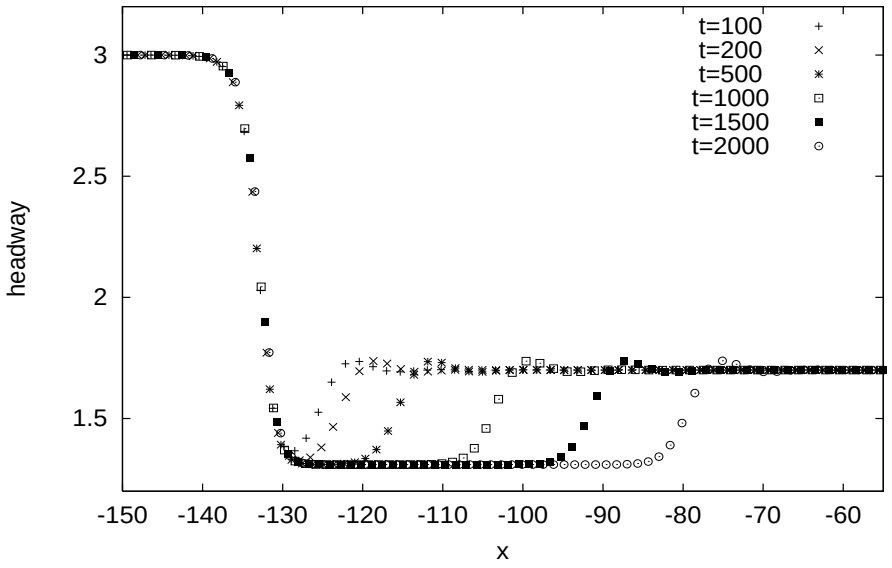

Figure 3.6: Formation of a Bando wave (upstream structure) and a second travelling wave (downstream structure) for initial conditions $b_{-\infty} = 3.0$ and $b_{\infty} = 1.7$. The waves move with different upstream speeds so that a growing region of congested traffic forms. Note that the wave profiles for different t have been shifted upstream for reasons of comparison.

Then the gap width d_{gap} has the long-time behaviour

$$d_{gap} = v_{gap}(t - t_{initial}) \quad , \quad t \gg t_{initial}, \tag{3.4.15}$$

where $t_{initial}$ is the time-offset associated with the development of the waves. Once more, it can only be estimated by numerical solutions of the car-following model, and comparison (Figs. 3.6 and 3.7) suggests that $t_{initial} \approx -189.78$. For the set of parameters

$$b_{-\infty} = 3.0, \tag{3.4.16}$$

$$b_{\infty} = 1.7, \tag{3.4.17}$$

we find the gap headway from the numerical data to be

$$b_{bw} = \frac{1}{\rho_{bw}} \approx 1.303 \tag{3.4.18}$$

and the gap speed from Eq. (3.4.13) as

$$v_{gap} = -0.6597 - (-6858) = 0.0261. \tag{3.4.19}$$

This corresponds very well to the slope of the curve in Fig. 3.7.
We are now able to compare the Bando wave and the two individual travelling wave

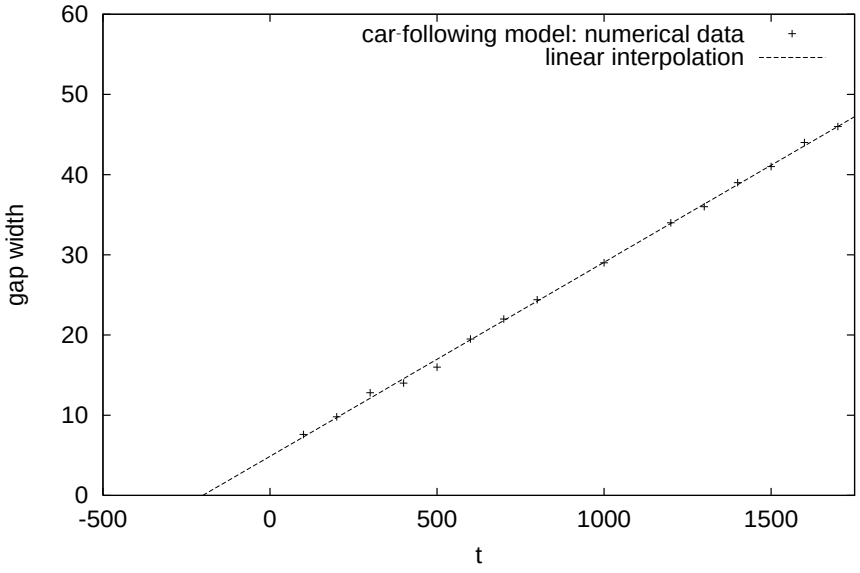

Figure 3.7: Determination of the time offset $t_{initial}$ of the Bando wave.

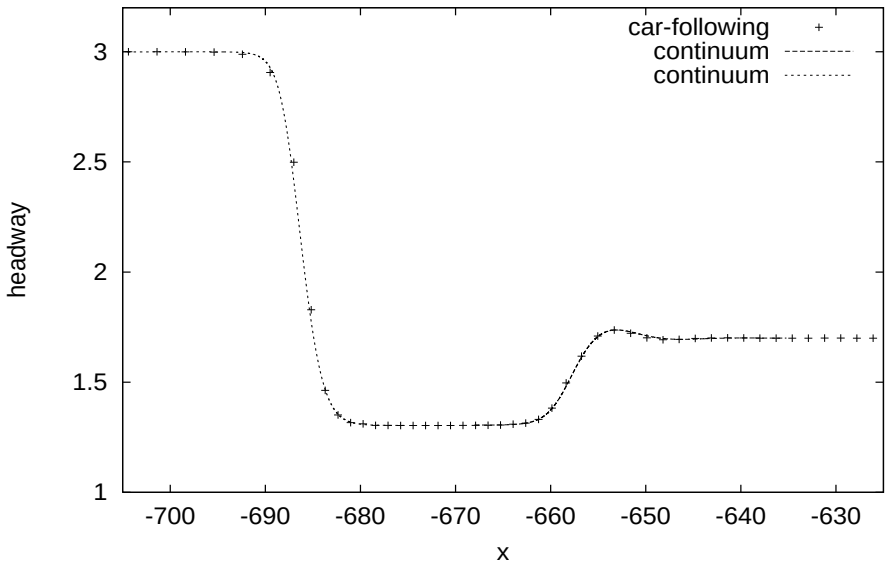

Figure 3.8: Comparison of the Bando wave and two individual travelling wave solutions of the continuum model.

solutions of the continuum model in the same graph (Fig. 3.8), which shows very good agreement. Even the oscillatory overshoot of the downstream front, before adopting the equilibrium headway, is matched accurately.
The Bando wave solution, including this oscillatory behaviour of the tail, was also found by Kerner and Konhäuser [48], but one needs the correct corresponding coefficients of the anticipation and dissipation term to reproduce the results of the car-following model accurately.

We conclude that our continuum model Eq. (3.2.16) is a very good approximation to the discrete car-following Bando model Eq. (3.1.1), and that the accuracy may increase with the number of terms retained in the asymptotic series (3.2.5).

3.5 Comparison with the Kerner-Konhäuser Model

Now, we further support the idea that the transformation (3.2.10) is crucial in order that the continuum model is qualitatively analogous to the underlying car-following model by using dimensional models. To this end we compare predictions of our new model with those of the Kerner-Konhäuser model Eq. (3.1.3) and the corresponding car-following model.
Herrmann and Kerner [38] investigated the similarities between their continuum model and a car-following model that is also based on a relaxation term. They considered cluster effects in greater detail in both models by examining traffic jams in a Bando type model

$$\dot{v}_n = \frac{1}{T}\left[\bar{V}_{kk}(b_n) - v_n\right], \tag{3.5.1}$$

and comparing the predictions with their own continuum model Eqs. (3.1.3) and (3.1.4). In both cases they chose the same OV function

$$V_{kk}(\rho) = v_0\left[\left(1+\exp\frac{(\rho-\rho_i)/\hat{\rho}}{\sigma}\right)^{-1} - d\right] \tag{3.5.2}$$

with

$$d = \left(1+\exp\frac{1-\rho_i/\hat{\rho}}{\sigma}\right)^{-1} \tag{3.5.3}$$

and

$$\bar{V}_{kk}(b) = V_{kk}(1/b). \tag{3.5.4}$$

The top speed of cars is defined as $v_f := V_{kk}(0)$, and they come to a standstill in a jam of density $\hat{\rho} = 180$veh./km. The parameters of the car-following model are fitted so that in their simulations, both models show the same stationary stop-and-go jams moving on a circular road, which gives the following parameters for the

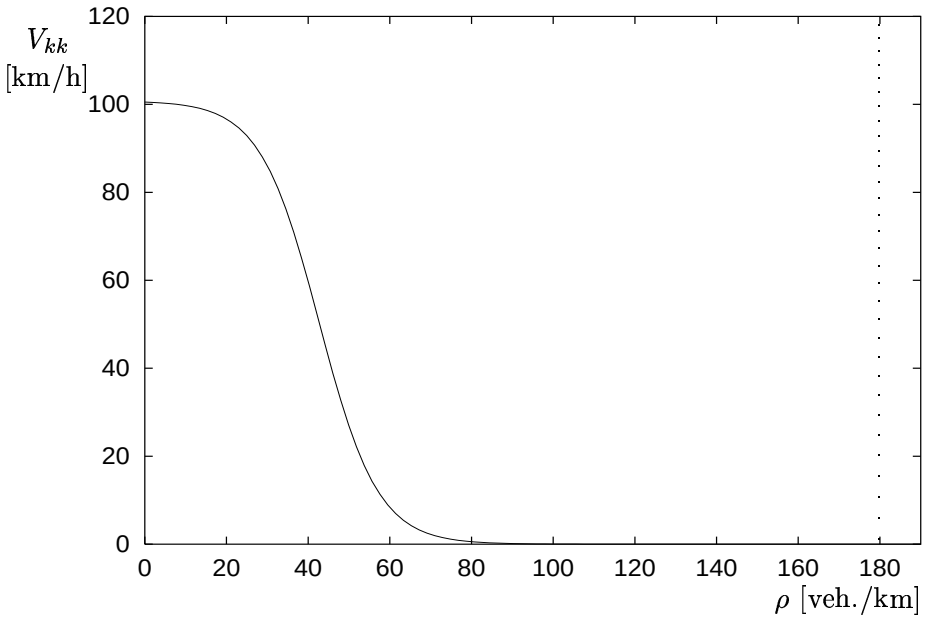

Figure 3.9: The monotonic decreasing optimal-velocity function of the Kerner-Konhäuser model.

discrete model

$$T = 0.985\text{s} \tag{3.5.5}$$
$$\hat{\rho} = 180\text{veh./km} \tag{3.5.6}$$
$$v_f = 100.8\text{km/h} \tag{3.5.7}$$
$$\rho_i = 36.5\text{veh./km} \tag{3.5.8}$$
$$\sigma = 0.02875, \tag{3.5.9}$$

whereas the parameters of the continuum model are based on traffic data

$$T = 5\text{s} \tag{3.5.10}$$
$$c_0 = 39.88\text{km/h} \tag{3.5.11}$$
$$\mu = 210\text{veh.km/h} \tag{3.5.12}$$
$$\hat{\rho} = 180\text{veh./km} \tag{3.5.13}$$
$$v_f = 100.8\text{km/h} \tag{3.5.14}$$
$$\rho_i = 42.7\text{veh./km} \tag{3.5.15}$$
$$\sigma = 0.04. \tag{3.5.16}$$

For unstable flow, these two models may seem to describe the same qualitative type of moving structures, as such. However, if we examine the stable regime, we find that these models are actually not equivalent.

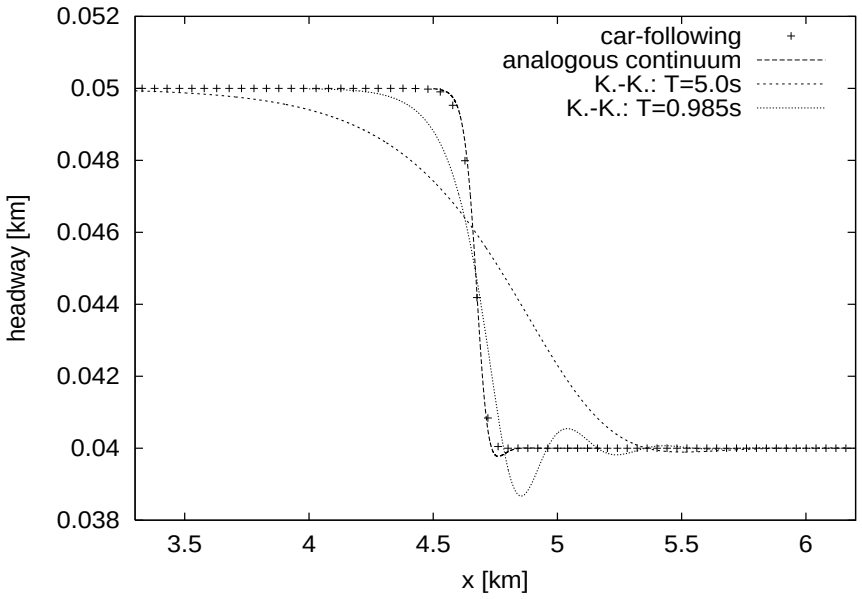

Figure 3.10: Comparison of travelling waves in the Bando model Eq. (3.5.1), the analogous continuum model Eq. (3.4.12), and the Kerner-Konhäuser (K.-K.) model Eq. (3.5.17) in the stable region for the same optimal-velocity (OV) function.

The calculations are carried out by substituting Eqs. (3.4.4) and (3.4.5) into Eq. (3.1.3) to obtain the travelling wave equation analogous to Eq. (3.4.12)

$$uu_z = \frac{1}{T}\left(V_{kk}(q_0/u) - u - c\right) + c_0^2\frac{u_z}{u} + \frac{\mu}{q_0}uu_{zz}. \tag{3.5.17}$$

For comparison, Fig. 3.10 shows that the Kerner-Konhäuser model fails to match the length scale of a jump in headway of a travelling wave predicted by the car-following model Eq. (3.5.1). Even for the same driver reaction time $T = 0.985s$, the model predicts a much more extensive region of adjustment in order for the headway to decrease to $b = 40$m.

We now compare solutions of the ordinary differential equation (3.5.17), and the car-following model (3.5.1) to those of our continuum model (3.4.12), with an OV function (3.5.4) and parameters as in Eqs. (3.5.5) - (3.5.9). Our model predicts oscillatory behaviour, in contrast to the car-following model, but significantly it predicts the same length scale (Figs. 3.10 and 3.11). This arises from the dependency of the coefficients of the higher order terms on the density Eq. (3.2.16) or the velocity, respectively. If higher order terms are retained in the transformation, it will show the same qualitative behaviour as the numerical solution with no oscillations, but a monotonic rapid transition from the upstream to the downstream headway. It is, therefore, the appropriate continuum analogue. We expect that the car-following analogue of the K.-K. model must contain additional terms, apart from the relaxation

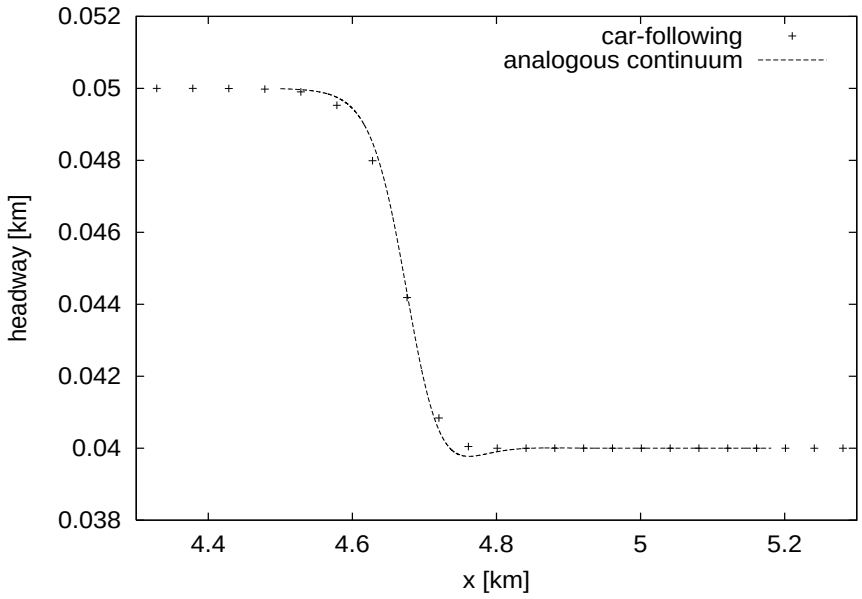

Figure 3.11: Comparison of travelling waves in the Bando model Eq. (3.5.1), and the analogous continuum model Eq. (3.4.12).

term, to match its different length scale behaviour (section 4.2).

The dependency of the coefficients on the density does not occur in conventional continuum models, but it could well be an intrinsic feature of a differential delay equation as recently proposed by Nagatani [64, 65]. In order to derive a modified Kortweg-de Vries equation (MKdV) for the jamming transition in a continuum model, he used a simplified version of the Kerner-Konhäuser model

$$(\rho v)_t = a\left[\rho_0 V_N(\rho(x+1)) - \rho v\right] \tag{3.5.18}$$

with the OV function $V_N(\rho) = V_B(1/\rho)$ of the Bando model Eq. (3.1.2). He simplifies it in the sense that he drops the pressure, convective and dissipative terms of the original model. On the other hand, the anticipation is now incorporated in a non-local term $\rho(x+1)$. In this dimensionless model, the average headway b_0 is supposed to be of order one ($b_0 = 1/\rho_0 = 1$), and the idea is that a driver adjusts his velocity according to the observed headway $b(x) = 1/\rho(x+1)$. Even though this is not the correct relation between headway and density as shown above, we proceed to derive the corresponding ordinary differential equation for the travelling waves.
Nagatani couples the dynamic equation to a continuity equation of the form

$$\rho_t + \rho_0(\rho v)_x = 0. \tag{3.5.19}$$

In case of a travelling wave, the transformations Eqs. (3.4.2) - (3.4.4) enable Eq. (3.5.19)

to be integrated to give

$$\rho(\rho_0 v - c) = q_0. \tag{3.5.20}$$

Substituting this relation into Eq. (3.5.18) yields

$$ww_z = \frac{a\rho_0^2}{q_0 c^2} V_N\left(\frac{q_0}{w(z+1)}\right) w^3 - \frac{a}{c^2}w^3 - \frac{a}{c}w^2 \tag{3.5.21}$$

with

$$w = \rho_0 v - c. \tag{3.5.22}$$

Since this is a differential delay equation it is not straightforward to compare it to our model Eq. (3.4.12). In general, a differential delay equation cannot be solved by a Taylor expansion and its truncation after a certain amount of terms (appendix C). Nevertheless, if the equations are similar the first terms of the Taylor expansion should be similar too. If we retain terms up to first order in V_N'

$$\begin{aligned} V_N\left(\frac{q_0}{w(z+1)}\right) &\sim V_N\left(\frac{q_0}{w(z)}\right) - q_0 V_N'\left(\frac{q_0}{w(z)}\right)\frac{w_z(z)}{w(z)^2} \\ &- \frac{1}{2}q_0 V_N'\left(\frac{q_0}{w(z)}\right)\left[\frac{w_{zz}(z)}{w(z)^2} - 2\frac{w_z^2(z)}{w(z)^3}\right], \end{aligned} \tag{3.5.23}$$

we obtain a corresponding second order model

$$\begin{aligned} ww_z &= \frac{a\rho_0^2}{q_0 c^2}\left[V_N\left(\frac{q_0}{w}\right) - q_0 V_N'\left(\frac{q_0}{w}\right) * \left(\frac{w_z}{w^2} + \frac{w_{zz}}{2w^2} - \frac{w_z^2}{w^3}\right)\right] w^3 \\ &- \frac{a}{c^2}w^3 - \frac{a}{c}w^2 \end{aligned} \tag{3.5.24}$$

that differs from our model not only by its expansion terms but, also, by the nonlinear terms aw^3/c^2 and aw^2/c. Hence, the class of solutions differs too. Nevertheless, the expansion Eq. (3.5.24) shows that a dependency of the coefficients of the pressure and diffusive terms on the density is an intrinsic feature of this model, but it is not analogous to the Bando model.

3.6 Travelling Waves of the Unstable Regime

The correspondence of the travelling wave solutions of both the continuum and the car-following model cannot be generalized to all values of the sensitivity parameter a due to instability. The line

$$sb(b) = 2V_B'(b) = 2\left[1 - \tanh^2(b-2)\right] \tag{3.6.1}$$

defines a region SB in the headway-sensitivity diagram, in which the model is linearly unstable (Fig. 3.12). For $a \geq 2$, the model is linearly stable and the travelling wave solutions with the specific initial condition $b_- = 3.0$ and $b_+ < b_-$ can be divided into

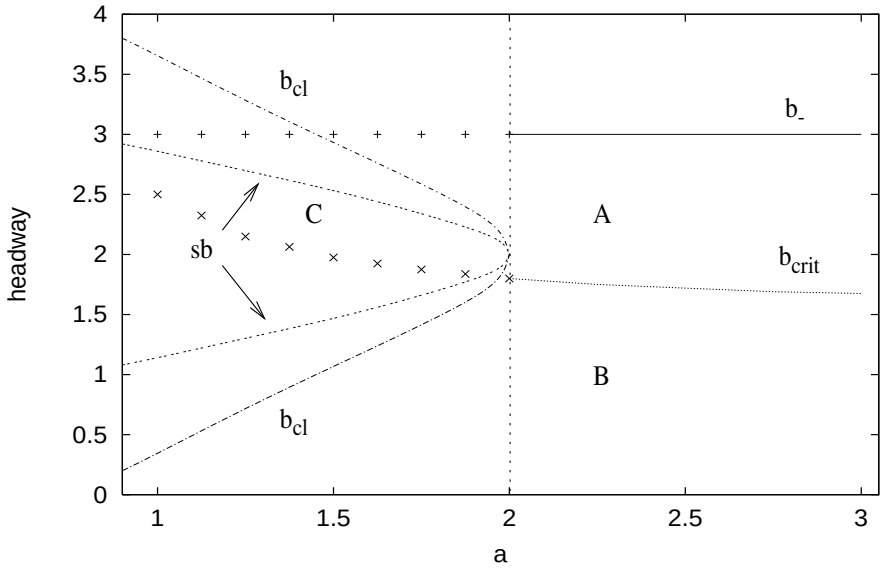

Figure 3.12: Travelling waves with upstream $b_- = 3$ and downstream headway $b_+ = b_{crit}$ become unstable for $a < 2$ and form clusters with headways given by the curve b_{cl}.

two regions. In region A, they are linearly stable, unless the downstream value b_+ hits the critical value b_{crit} when Bando waves form. This type of wave as described above occurs in region B. The two travelling waves with a growing region of a specific headway b_{bw} in between are stable.

Keeping the upstream and downstream headway fixed and varying a, the travelling wave solutions eventually become unstable for sufficiently small values of a. However, formally we can still obtain solutions from the ODE (3.4.12). b_{crit} can still be derived by investigating the downstream headway for which the integration breaks down, but whether a particular solution is stable or unstable depends on the values of the headways which are involved. If the upstream and downstream headways are not part of the region SB and the adjustment does not consist of an oscillatory overshoot that intersects sb, the solution Eq. (3.4.12) is linearly stable and can be reproduced by the car-following model with corresponding initial conditions as presented above. On the other hand, the solution is unstable if these conditions are not fulfilled. Figure (3.13) shows how an initial jump in headway evolves with time in the car-following model. After $t = 50$, the solution is very similar to those of the continuous counterpart Eq. (3.4.12), but eventually it becomes unstable and the typical cluster forms. For given a, the solution eventually jumps between two headways whose values can be read from the graph b_{cl} in Fig. 3.12 [39].

Whether travelling waves of the region C, the part of the unstable regime which corresponds to A, are stable or not, has to be investigated in every single case. If either the upstream or downstream headway is part of the region SB, the solution is

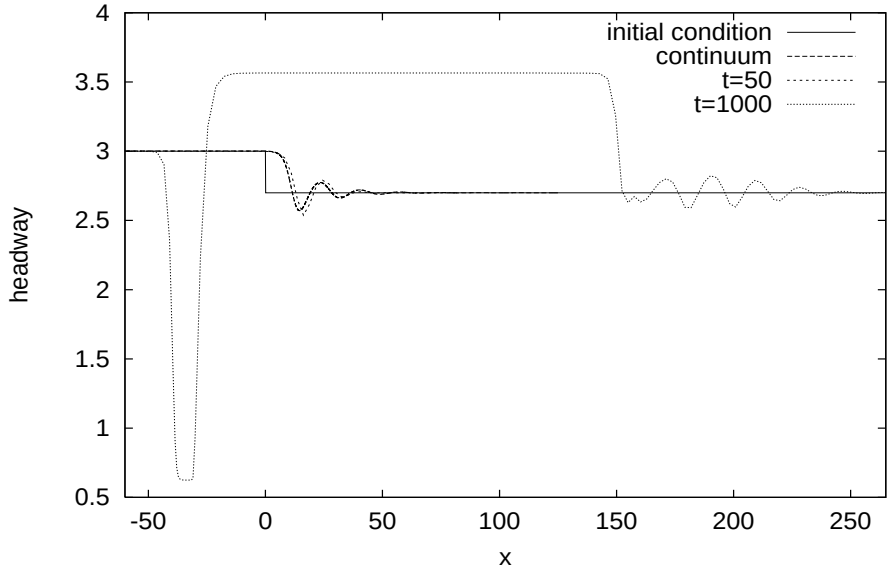

Figure 3.13: The travelling wave solution of a modest jump in headway from $b_- = 3$ to $b_+ = 2.7$ in the unstable regime ($a = 1.0$) cannot be reproduced by the car-following model. Clusters form.

clearly unstable and develops towards the corresponding cluster solutions of a traffic jam. For $b_- = 3$ and $b_+ \gtrsim b_{crit}$, the solutions turn out to be unstable for all $a < 2$. The rich structure of travelling wave solutions is discussed in greater detail in chapter 5.

3.7 Asymptotic Solutions

So far, we have considered travelling wave solutions of the Bando model, its continuous counterpart and the Kerner-Konhäuser model. The first two showed a very good agreement between a number of different steady traffic situations. However, it is also of interest to examine the dynamic case of a non-stationary wave solution. This can be done in certain regimes, because in some special cases the higher order terms of dynamic equations of the form

$$v_t + vv_x = a\left[\bar{V}(\rho) - v\right] + O(\rho_x, \rho_{xx}, \rho_x^2) \tag{3.7.1}$$

do not play an important role and can be neglected. The traffic flow is then uniquely determined by the driver's sensitivity a and the optimal-velocity function $\bar{V}(\rho)$, combined with the equation for the conservation of cars Eq. (3.1.4).
As an example, one might consider an initial disturbance in the car-following Bando model Eq. (3.1.1), as in Fig. 3.14. Here, a region of slightly more congested traffic is inserted in a homogenous flow. As time increases, one ends up with a wave solution

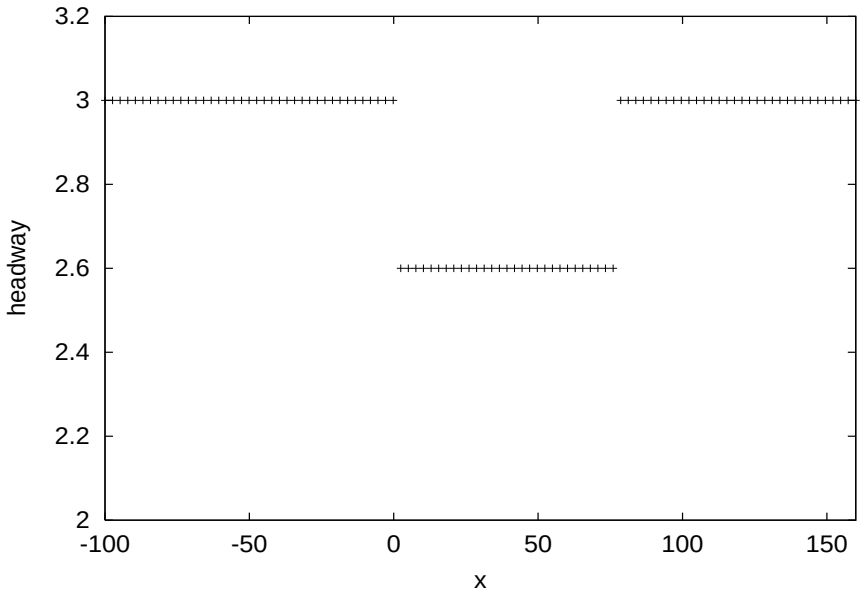

Figure 3.14: Initial condition: region of slightly higher congested traffic. Again the initial speed of the vehicles is given by $v_n(0) = V_B(b_n(0))$.

shown in Fig. 3.15 (10 solutions for $t = 250, 500, ..., 2500$): the headway overshoots the initial disturbance by a shock and eventually readjusts to the original headway; the jump in headway decreases with time, and a dispersive tail forms. As can be seen from the graph, there is a *stationary point* K_0 along the road, where all solutions intersect until the downstream propagating, nonlinear shock front passes this point. This effect can be explained using a very simple continuum model proposed by Lighthill and Whitham [58] (subsection 2.2.1), which is based on the conservation of cars Eq. (3.1.4). By substituting the stationary relation

$$q(\rho) = \bar{V}(\rho)\rho \tag{3.7.2}$$

between the flow and the density for q, we obtain

$$\rho_t + q(\rho)_x = 0 \tag{3.7.3}$$

$$\Rightarrow \rho_t + \left[\bar{V}(\rho)\rho\right]_x = 0. \tag{3.7.4}$$

This model does not incorporate inertia and describes flow that adjusts rapidly to its surrounding traffic situation. Using the method of characteristics, it can be shown that regions of density ρ travel with speed

$$c(\rho) = \frac{\partial q(\rho)}{\partial \rho} = \bar{V}(\rho) + \rho\frac{\partial \bar{V}(\rho)}{\partial \rho}, \tag{3.7.5}$$

which is equivalent to the slope of the tangent in the fundamental diagram Fig. 3.16 (see subsection 2.2.1 for greater detail). K_0, therefore, simply corresponds to the

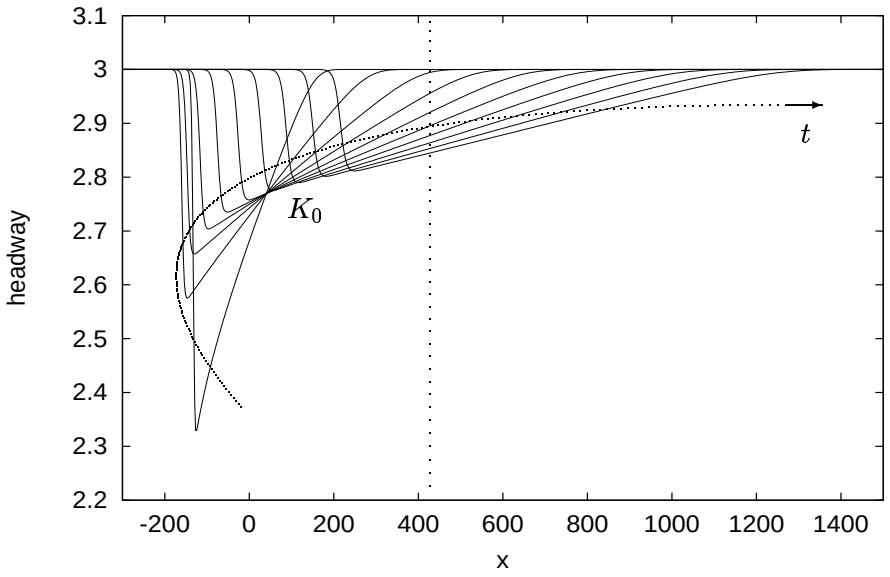

Figure 3.15: The evolution of the pulse Fig. 3.14; $t = 250, 500, ..., 2500$.

maximum of this curve ($\rho_0 = 0.36 \Rightarrow b_0 = 2.78$), where the speed of the density wave vanishes.

To explain the other features, we start with the higher order continuum model Eq. (3.2.16). First, we approximate the wave profile by piecewise linear solutions, which model a triangle evolving in space and time, as shown by Fig. 3.17 (cf. Whitham 1974, [84]). For the dispersive tail, one can formally write an asymptotic solution ($t \to \infty$) as

$$\rho(x,t) = \rho_0 + \hat{\rho}(x,t) = \rho_0 + \rho_1 \frac{x^\alpha}{t^\beta} \quad , \quad \frac{\hat{\rho}}{\rho_0} \ll 1 \tag{3.7.6}$$

$$v(x,t) = v_0 + \hat{v}(x,t) = v_0 + v_1 \frac{x^\gamma}{t^\delta} \quad , \quad \frac{\hat{v}}{v_0} \ll 1. \tag{3.7.7}$$

Two equations have to be balanced: the conservation of cars and the dynamic equation

$$v_t + v v_x = a\left[\bar{V}(\rho) - v\right] + a\bar{V}'(\rho)\left[\frac{\rho_x}{2\rho} + \frac{\rho_{xx}}{6\rho^2} - \frac{\rho_x^2}{2\rho^3}\right]. \tag{3.7.8}$$

By substituting Eqs. (3.7.6) and (3.7.7) into (3.7.8), it is seen that the relaxation term $a\left[\bar{V}(\rho) - v\right]$ dominates all the other terms as $t \to \infty$ and $x \to \infty$, because they incorporate time and space derivatives. Therefore, this term has to vanish exactly,

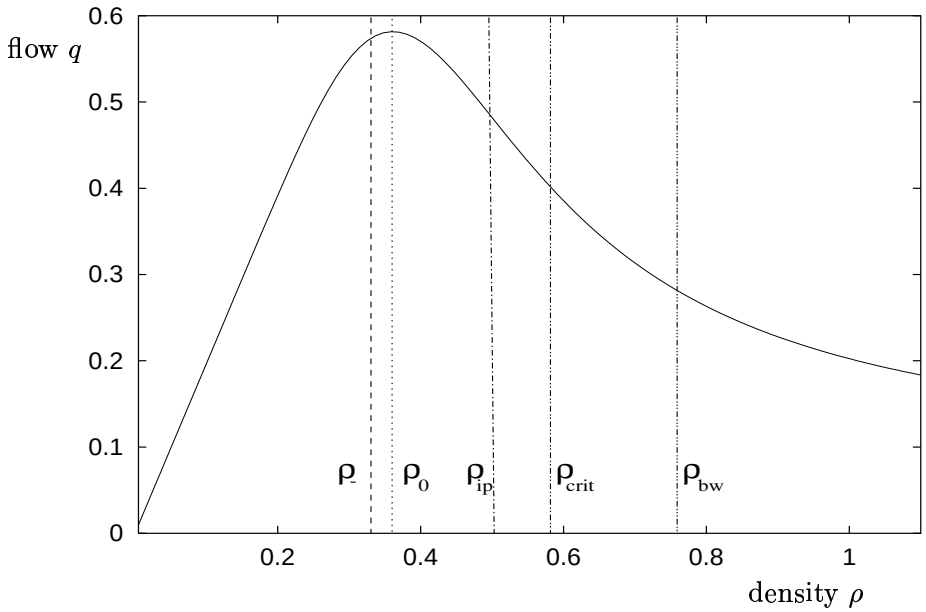

Figure 3.16: Fundamental diagram of the Bando model with significant densities: background density $\rho_- = 1/b_- = 1/3$, maximum of the flow $\rho_0 = 0.36$, inflection point $\rho_{ip} = 0.5$, onset of the Bando wave $\rho_{crit} = 0.58$, and the Bando wave $\rho_{bw} = 0.77$.

leading to

$$v = \bar{V}(\rho), \tag{3.7.9}$$

$$\alpha = \gamma, \tag{3.7.10}$$

$$\beta = \delta. \tag{3.7.11}$$

Equation (3.7.9) can be substituted into the conservation of cars Eq. (3.7.3), which leads to Eq. (3.7.4). A Taylor expansion of $\bar{V}(\rho)\rho$ around the maximum ρ_0

$$\bar{V}(\rho)\rho = \left(\bar{V}\rho\right)_0 + \left(\bar{V}\rho\right)_0' \hat{\rho} + \frac{1}{2}\left(\bar{V}\rho\right)_0'' \hat{\rho}^2 + ... \tag{3.7.12}$$

(dash equals derivative with respect to ρ), analogous to the asymptotic expansion Eq. (3.7.6), turns (3.7.4) into

$$\hat{\rho}_t + \left(\bar{V}\rho\right)_0' \hat{\rho}_x + \left(\bar{V}\rho\right)_0'' \hat{\rho}\hat{\rho}_x = 0. \tag{3.7.13}$$

Near the maximum of the flow, the first derivative vanishes, and a possible balance can be extracted from

$$-\rho_1 \beta \frac{x^\alpha}{t^{\beta+1}} + \left(\bar{V}\rho\right)_0'' \rho_1^2 \alpha \frac{x^{2\alpha-1}}{t^{2\beta}} = 0 \tag{3.7.14}$$

as

$$\alpha = 1 \ , \ \beta = 1 \ \text{ and } \ \rho_1 = \frac{1}{(\bar{V}\rho)_0''} < 0. \tag{3.7.15}$$

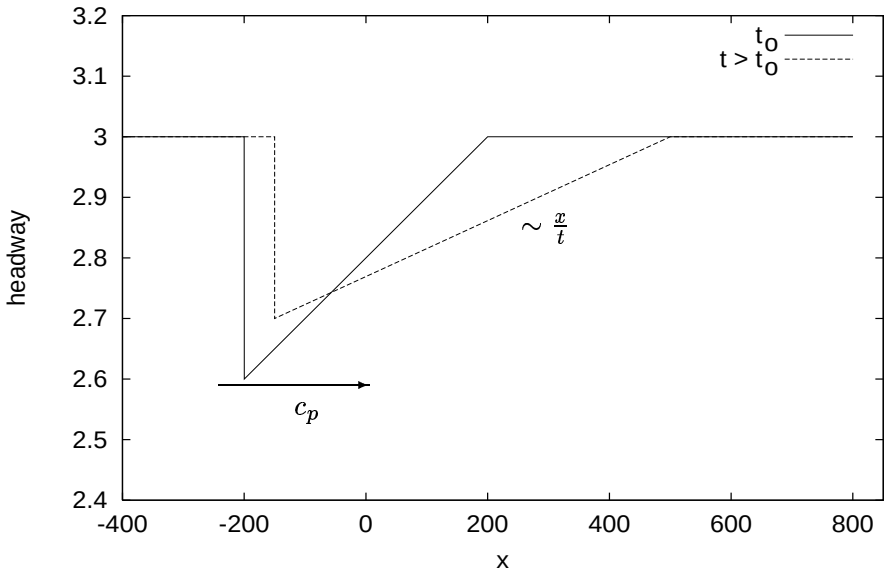

Figure 3.17: A model for the pulses.

Now the density around the flow maximum becomes

$$\rho(x,t) = \rho_0 + \rho_1 \frac{x}{t} \tag{3.7.16}$$

$$= 0.36 - 0.062\ \frac{x}{t} \tag{3.7.17}$$

and the velocity

$$v = \bar{V}(\rho) \approx \frac{\bar{V}\rho}{\rho} = \frac{\left(\bar{V}\rho\right)_0 + \frac{1}{2}\left(\bar{V}\rho\right)_0'' \hat{\rho}^2}{\rho_0 + \hat{\rho}} \tag{3.7.18}$$

$$\Rightarrow v(x,t) = \frac{\left(\bar{V}\rho\right)_0}{\rho_0} - \frac{\left(\bar{V}\rho\right)_0}{\rho_0^2 \left(\bar{V}\rho\right)_0''}\ \frac{x}{t} \tag{3.7.19}$$

$$= 1.61 + 0.28\ \frac{x}{t}. \tag{3.7.20}$$

The headway is given by

$$b(x,t) = b_0 + \hat{b}(x,t) \tag{3.7.21}$$

$$\simeq \frac{1}{\rho_0} - \frac{\rho_1}{\rho_0^2}\frac{x}{t} \tag{3.7.22}$$

$$= 2.78 + 0.48\ \frac{x}{t}. \tag{3.7.23}$$

This corresponds to an increasing velocity and headway, respectively, which is consistent with the graph 3.15. To compare the asymptotic solution Eq. (3.7.23) with

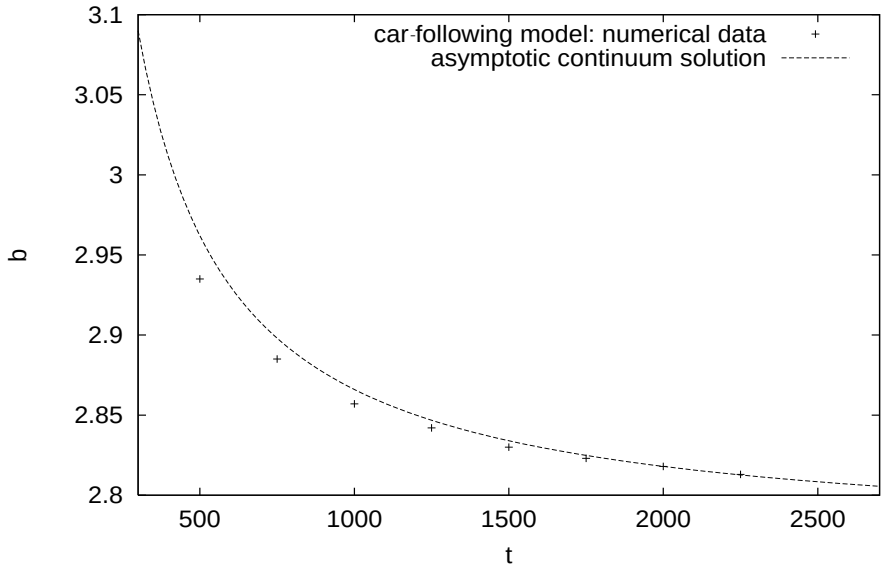

Figure 3.18: Comparison of the numerical data and the asymptotic solution Eq. (3.7.23).

the numerical data from the car-following model, we place the origin in Fig. 3.15 at the stationary point K_0, where the pulses intersect and take the data from $x = 200$. The dependence on x is obviously linear, but the inverse time relation, as well as the coefficient ρ_1, have to be checked. Fig. 3.18 shows a very good agreement between these data sets, so that we can regard the tail as being understood.
What remains is the movement of the shock but, here again, the fundamental diagram gives a qualitative explanation. Two successive jumps in headway are drawn in Fig. 3.17. The shock moves with a velocity

$$\dot{x} = c_p(\rho_s) = \frac{q_{-\infty} - q(\rho_s)}{\rho_{-\infty} - \rho_s} \tag{3.7.24}$$

(cf. Eq. (3.4.10)) along the road where ρ_s denotes the highest density of the pulse. The jump in headway is given by the intersection of the asymptotic solution Eq. (3.7.17) and the shock front

$$\dot{\rho}_s = \underbrace{\dot{\hat{\rho}}}_{\text{change of tail}} + \underbrace{\frac{\partial \hat{\rho}}{\partial x}\, c_p(\rho_s)}_{\text{change of shock front}} \tag{3.7.25}$$

$$= -\frac{x}{\left(\bar{V}\rho\right)_0'' t^2} + \frac{1}{\left(\bar{V}\rho\right)_0'' t}\, c_p(\rho_s). \tag{3.7.26}$$

The system of coupled differential equations (3.7.24) and (3.7.26) describes the motion of the shock along the road. It is easy to see that it must turn around at a

point when

$$\dot{x} = c(\rho) = q_{-\infty} - q(\rho) = 0, \tag{3.7.27}$$

and eventually it passes by the stationary point K_0. For a background headway $b_- = 3.0$ ($\Rightarrow \rho_- = 1/3$), as in Fig. 3.15, one finds from the fundamental diagram Fig. 3.16 a corresponding headway $b \approx 2.5$ ($\rho \approx 0.4$) for which $\dot{x} = 0$. This agrees quite well with the pulses in Fig. 3.15.

The final asymptotic behaviour is in analogy with Whitham's [84] theory of asymptotic shock wave forming that contains equations similar to Eq. (3.7.3) with a convex function $q(\rho)$. Instead of the asymptotic solution Eq. (3.7.6), he writes

$$\rho(x,t) = \rho_\infty - \frac{c_\infty}{c'_\infty} + \frac{x}{c'_\infty t} \quad , \quad c'_\infty = \left.\frac{\partial^2 q}{\partial \rho^2}\right|_{\rho=\rho_\infty} < 0 \tag{3.7.28}$$

for a region

$$c_\infty t - x_s(t) < x < c_\infty t. \tag{3.7.29}$$

Recall $c_\infty = c_{-\infty}$ and $\rho_\infty = \rho_{-\infty}$. To determine the position of the shock $c_\infty t - x_s(t)$, one has to take the conservation of cars into account. The additional number of cars relative to the background density $\rho_{-\infty}$

$$N = \int_{-\infty}^{\infty} (\rho - \rho_{-\infty}) dx \tag{3.7.30}$$

has to be conserved. By definition, this is equivalent to

$$N = \int_{c_\infty t - x_s(t)}^{c_\infty t} (\rho - \rho_{-\infty}) dx \tag{3.7.31}$$

and, hence,

$$\int_{c_\infty t - x_s(t)}^{c_\infty t} (x - c_\infty t) dx = c'_\infty t N. \tag{3.7.32}$$

Solving this quadratic equation in $x(t)$ leads to two solutions

$$x_s(t) = \pm\sqrt{2t\,|c'_\infty N|}, \tag{3.7.33}$$

which corresponds to a shortage ($+$) and an overshoot ($-$) of density, relative to the background density ρ_∞. In this particular example, the latter case is considered. The shock is at

$$x_s = c_\infty t - \sqrt{2\,|c'_\infty N|\,t}. \tag{3.7.34}$$

Inserting this relation into Eq. (3.7.28) gives an asymptotic expression for the time dependency of the jump in density at the shock front (ρ_s: maximum density at the shock)

$$\Delta\rho = \rho_s - \rho_\infty = \sqrt{\frac{2}{t}\left|\frac{N}{c'_\infty}\right|}. \tag{3.7.35}$$

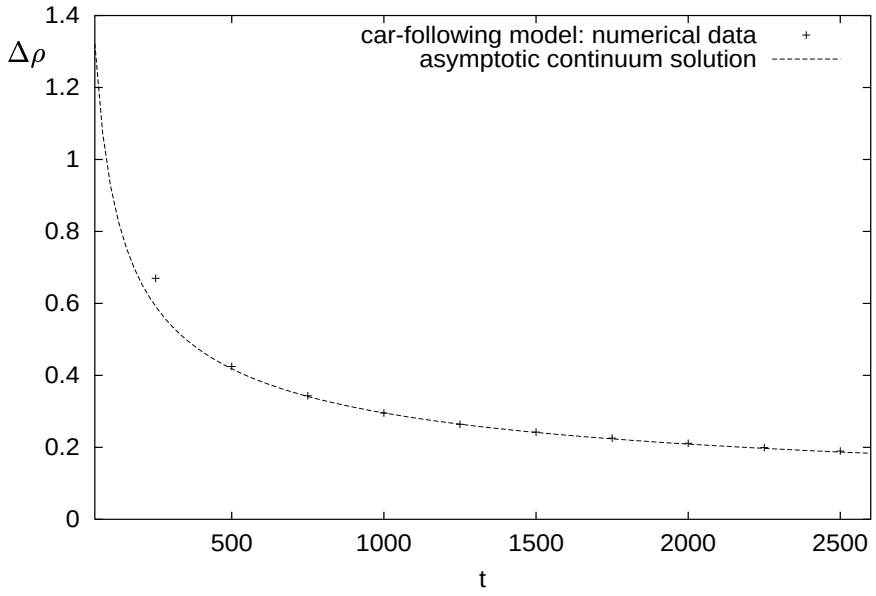

Figure 3.19: The asymptotic height of the pulse $\Delta\rho$ decays like $t^{-1/2}$.

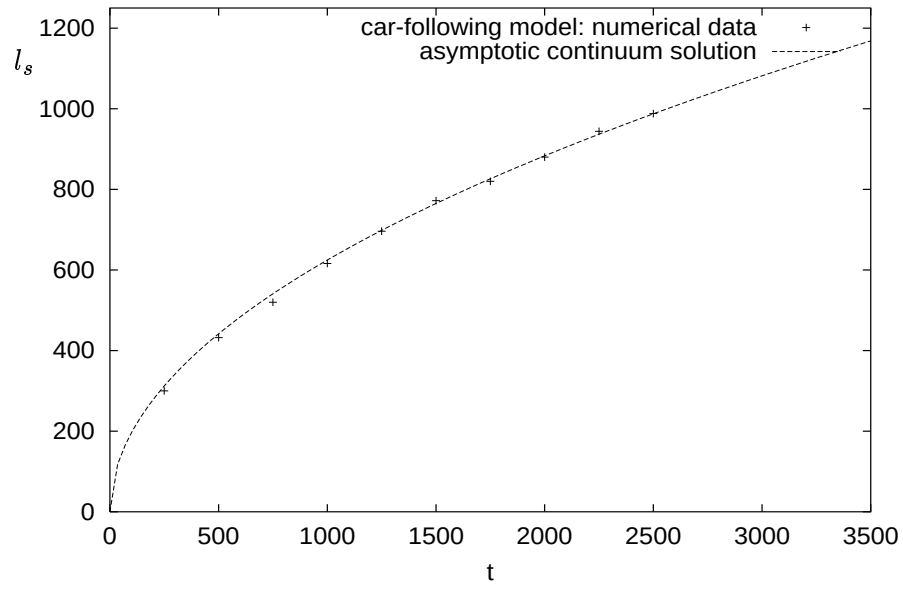

Figure 3.20: The pulse spreads out along the road like $t^{1/2}$.

This means that the length l_s of the wave increases like $t^{1/2}$ and the jump in density $\Delta\rho$ decays like $t^{-1/2}$.
To check both results, the long time behaviour of these two quantities is plotted in Figs. 3.19 and 3.20. The asymptotic expressions agree very well with the numerical data extracted from Fig. 3.15. Since the speed of the shock front changes its direction between $t = 250$ and $t = 500$ where $\rho_s = 1/b_s \approx 0.4$, the point at $t = 250$ in Fig. 3.19 differs remarkably little from the asymptotic solution, with the data eventually approaching the curve with high accuracy.

In this section, the features of traffic flow described by a car-following model were analysed by a simple continuum model without inertia in which the length scale of evolution of the flow is long compared to $1/a$, the relaxation required by traffic to adjust to the optimal velocity. Hence, the flow is accurately modelled by assuming that it has the optimal velocity.

3.8 The Inverse Transformation

It is also of interest to find the inverse transformation, a relation between the density ρ of cars in the continuum picture in terms of the analogous parameter, the headway b, in the car-following picture. This enables one to derive an equivalent car-following model for every continuum model.
We expect ρ to be a function of b and its spatial derivatives

$$\rho = \rho(b, b_x, b_{xx}). \tag{3.8.1}$$

As discussed in the next chapter, the derivatives with respect to x are not easy to interpret in a discrete model. However, if we regard b formally as a continuous variable, the inverse transformation can be found by solving equation (3.2.5) for ρ. This time it has to be treated as a non-homogenous linear ordinary differential equation with variable coefficients

$$b\rho + \frac{b^2}{2}\rho_x + \frac{b^3}{6}\rho_{xx} = 1. \tag{3.8.2}$$

If we again suppose that each term is sufficiently smaller than the preceding order, it is possible to solve for ρ successively.
However, a trivial way to find the solution is to argue that only certain terms in b, b_x and b_{xx} have the right dimensions. To leading order, ρ is once again the inverse of the headway

$$\rho = \frac{1}{b}. \tag{3.8.3}$$

To find the whole solution up to second order (b_{xx}) and linear in b_x and b_{xx}, the only possible ansatz is

$$\rho = \frac{1}{b} + a_1 \frac{b_x}{b} + a_2 b_{xx} \tag{3.8.4}$$

with coefficients a_1 and a_2 to be determined. Inserting this into Eq. (3.8.2) leads to

$$(1 + a_1 b_x + a_2 b b_{xx}) + (-\frac{b_x}{2} + a_1 \frac{b b_{xx}}{2}) + (-\frac{b b_{xx}}{6}) = 1, \tag{3.8.5}$$

since the derivatives to relevant order are

$$\rho_x = -\frac{b_x}{b^2} + a_1 \frac{b_{xx}}{b}, \tag{3.8.6}$$

$$\rho_{xx} = -\frac{b_{xx}}{b^2}. \tag{3.8.7}$$

Equation (3.8.5) may be simplified to

$$(a_1 - \frac{1}{2}) b_x + (a_2 + \frac{a_1}{2} - \frac{1}{6}) b b_{xx} = 0. \tag{3.8.8}$$

This equation must hold for arbitrary functions $b(x)$ and, hence,

$$a_1 = \frac{1}{2} \quad , \quad a_2 = -\frac{1}{12} \tag{3.8.9}$$

yielding the transformation

$$\rho = \frac{1}{b} + \frac{b_x}{2b} - \frac{b_{xx}}{12}. \tag{3.8.10}$$

This is consistent with a straightforward, but more detailed derivation of the solution (see Eqs. (3.8.23) - (3.8.39)).
To support this somewhat heuristic ansatz, the inverse transformation of the continuous Bando model Eq. (3.2.16) is carried out, which must lead to the original discrete Bando model Eq. (3.1.1). By inserting Eq. (3.8.10) into

$$v_t + v v_x = a\left(\bar{V}(\rho) - v\right) + a\bar{V}'(\rho)\left[\frac{\rho_x}{2\rho} + \frac{\rho_{xx}}{6\rho^2} - \frac{\rho_x^2}{2\rho^3}\right], \tag{3.8.11}$$

we obtain formally

$$\begin{aligned} v_t + v v_x &= a\left[\bar{V}\left(\frac{1}{b} + \frac{b_x}{2b} - \frac{b_{xx}}{12}\right) - v\right] \\ &+ a\bar{V}'\left(\frac{1}{b} + \frac{b_x}{2b} - \frac{b_{xx}}{12}\right)\left[\frac{\rho_x}{2\rho} + \frac{\rho_{xx}}{6\rho^2} - \frac{\rho_x^2}{2\rho^3}\right]. \end{aligned} \tag{3.8.12}$$

Once again a Taylor expansion of the optimal-velocity function $\bar{V}$ around $\rho = \frac{1}{b}$ is carried out, whereas only the leading term $\frac{1}{b}$ in $\bar{V}'$ is kept. Moreover, ρ_x and ρ_{xx} are expressed by Eqs. (3.8.6) and (3.8.7), and the nonlinear term ρ_x^2 is neglected since

the inverse transformation Eq. (3.8.10) was only derived linearly. Equation (3.8.12) then turns into

$$\begin{aligned} v_t + vv_x &= a\left[\bar{V}\left(\frac{1}{b}\right) - v\right] \\ &+ a\bar{V}'\left(\frac{1}{b}\right)\left[\frac{b_x}{2b} - \frac{b_{xx}}{12}\right] \\ &+ a\bar{V}'\left(\frac{1}{b}\right)\left[\frac{1}{2}\left(-\frac{b_x}{b^2} + \frac{b_{xx}}{2b}\right)\left(\frac{1}{b} + \frac{b_x}{2b} - \frac{b_{xx}}{12}\right)^{-1}\right. \\ &\qquad \left. + \frac{1}{6}\left(-\frac{b_{xx}}{b^2}\right)\left(\frac{1}{b} + \frac{b_x}{2b} - \frac{b_{xx}}{12}\right)^{-2}\right]. \end{aligned} \tag{3.8.13}$$

The last square bracket may be simplified to give

$$[...] = \left[-\frac{b_x}{2b} + \frac{b_{xx}}{12} + ...\right] \tag{3.8.14}$$

and cancels the preceding term. If b is now interpreted as a discrete variable, the terms transform as

$$v(x,t) \longrightarrow v(x_n,t) = v_n \tag{3.8.15}$$

$$b(x,t) \longrightarrow b(x_n,t) = b_n \tag{3.8.16}$$

$$v_t(x,t) + v(x,t)v_x(x,t) = \frac{d}{dt}v(x,t) \longrightarrow \dot{v}(x_n,t) = \dot{v}_n \tag{3.8.17}$$

and Eq. (3.8.13) is equivalent to the Bando model Eq. (3.1.1) as required.
This analysis shows that even though the continuum version incorporates higher order terms like a *pressure* and a diffusive term, they vanish under the inverse transformation. This may appear surprising, since spatial derivatives contain non-local information about the traffic flow ahead or even behind the car, and we would expect those terms to occur in both models at first sight. However, since the transformation from the discrete model to its continuous counterpart, inevitably, brings along higher order terms and, therefore, incorporates such non-local information, it must already be contained somehow in the car-following model.
A look at the dynamics tells us, firstly, that the acceleration of each car $\dot{v}_n$ depends on the headway b_n to the preceding car. Secondly, the change of this headway $\dot{b}_n$ does not only depend on the velocity of the nth car, but also on that of the car in front

$$\dot{b}_n = v_{n+1} - v_n \tag{3.8.18}$$

$$= V(b_{n+1}) - \frac{\dot{v}_{n+1}}{a} - v_n \tag{3.8.19}$$

$$= V(x_{n+2} - x_{n+1}) - \frac{\dot{v}_{n+1}}{a} - v_n \tag{3.8.20}$$

and is, therefore, a function of the parameters of the cars in front. If we express the speed of the n-th car by a Taylor series, we obtain

$$v_n(t+\Delta t) = v_n(t) + \sum_{m=1}^{\infty} \frac{(\Delta t)^m}{m!} \frac{d^m}{dt^m} v_n(t) \tag{3.8.21}$$

$$= v_n(t) + \sum_{m=1}^{\infty} \frac{(\Delta t)^m}{m!} \frac{d^m}{dt^m} \left[V(b_n(t)) - \frac{\dot{v}_n(t)}{a} \right]. \tag{3.8.22}$$

The differentiation of the second term in the square bracket is straightforward, but the mth derivative of the first term $V(b_n(t))$ includes the $(n+m)$th headway and velocity, as can be seen from Eq. (3.8.19). This way non-local information enters the model. Hence, the car-following model already obeys dispersive effects, which are explicitly revealed by the transformation into a continuum model as well as by numerical simulations: small disturbances in the stable regime decay and spread along the road as presented in section 3.7.

For completeness, we now carry out a stricter derivation of the inverse transformation. The problem of integrating the differential equation (3.8.2) lies in the variable coefficients, but once again it can be solved successively. By taking only the first two terms

$$b\rho + \frac{b^2}{2}\rho_x = 1, \tag{3.8.23}$$

and using the ansatz

$$\rho(x) = A(x) \exp\left(- \int_0^x \frac{2}{b(x')} dx' \right), \tag{3.8.24}$$

we find

$$A' = \frac{2}{b^2} \exp\left(\int \frac{2}{b} \right). \tag{3.8.25}$$

This can be written as

$$A(x) = \int_0^x \frac{1}{b} \left[\frac{2}{b} \exp\left(\int \frac{2}{b} \right) \right] dx' + A_0. \tag{3.8.26}$$

As one repeats partial integration, it becomes

$$A = \frac{1}{b} \exp\left(\int \frac{2}{b} \right) + \int_0^x \frac{b_x}{2b} \left[\frac{2}{b} \exp\left(\int \frac{2}{b} \right) \right] dx' + A_0 \tag{3.8.27}$$

$$= \left(\frac{1}{b} + \frac{b_x}{2b} \right) \exp\left(\int \frac{2}{b} \right) - \int_0^x \frac{b_{xx}}{4} \left[\frac{2}{b} \exp\left(\int \frac{2}{b} \right) \right] dx' + A_0 \tag{3.8.28}$$

$$= \left(\frac{1}{b} + \frac{b_x}{2b} - \frac{b_{xx}}{4} \right) \exp\left(\int \frac{2}{b} \right) + \int \frac{b_{xxx}}{4} \exp\left(\int \frac{2}{b} \right) dx + A_0 \tag{3.8.29}$$

So to second order the solution of Eq. (3.8.23) is

$$\rho = \frac{1}{b} + \frac{b_x}{2b} - \frac{b_{xx}}{4}, \tag{3.8.30}$$

and the full solution of Eq. (3.8.2) may be expressed by a perturbation

$$\rho = \frac{1}{b} + \frac{b_x}{2b} - \frac{b_{xx}}{4} + \delta. \tag{3.8.31}$$

Substituting this expression into Eq. (3.8.2) leads to a differential equation for δ

$$b\delta + \frac{b^2}{2}\delta_x + \frac{b^3}{6}\delta_{xx} = \frac{bb_{xx}}{6}. \tag{3.8.32}$$

For our purpose it is sufficient to solve this equation by neglecting the second-order term δ_{xx}, since it contributes only higher order terms in which we are not interested. Therefore, we solve only

$$\delta_x + \frac{2}{b}\delta = \frac{b_{xx}}{3b} \tag{3.8.33}$$

by taking δ to be

$$\delta(x) = B(x) \exp\left(-\int \frac{2}{b}\right). \tag{3.8.34}$$

Hence, $B(x)$ has to fulfill the integral equation

$$B = \int \frac{b_{xx}}{3b} \exp\left(\int \frac{2}{b}\right) dx' + B_0 \tag{3.8.35}$$

$$= \frac{b_{xx}}{6} \exp\left(\int \frac{2}{b}\right) - \int \frac{b_{xxx}}{6} \exp\left(\int \frac{2}{b}\right) dx' + B_0. \tag{3.8.36}$$

Likewise δ has the form

$$\delta = \frac{b_{xx}}{6} + \text{higher order terms} \tag{3.8.37}$$

giving

$$\rho = \frac{1}{b} + \frac{b_x}{2b} - \frac{b_{xx}}{4} + \frac{b_{xx}}{6} + ... \tag{3.8.38}$$

$$= \frac{1}{b} + \frac{b_x}{2b} - \frac{b_{xx}}{12} + ... \tag{3.8.39}$$

which is consistent with Eq. (3.8.10).

The inverse transformation can also be extended to the first nonlinear term b_x^2, similar to ρ_x^2 in Eq. (3.2.10). Either one adds $a_3 b_x^2/b$ to the right hand side of Eq. (3.8.4) and determines a_3 by a similar method, or the equation (3.8.32) is solved including the second order term, which gives an extra term in Eqs. (3.8.36) and (3.8.39). Both methods are again equivalent and lead to a higher order approximation of the inverse transformation

$$\rho = \frac{1}{b} + \frac{b_x}{2b} - \frac{b_{xx}}{12} - \frac{b_x^2}{12} + ... \ . \tag{3.8.40}$$

Hence, if $\rho(x,t)$ obeys the relation (3.3.29), both the transformation (3.2.10) and its inverse (3.8.40) deliver proper analogous models for which the basic properties and features of the traffic flow are maintained, and also qualitatively similar. Some examples of car-following counterparts of continuum models and vice versa are given in the next chapter. In addition, appendix B further comments on the inverse transformation.

3.9 Conclusion

We have derived a continuum model from a second-order car-following model by using an integral representation of the headway. This enables us to transform the headway and the velocity consistently by using an asymptotic approximation for the former in terms of the density. For car-following models of the Bando type, including an optimal-velocity function V, we have given a general expression of the equivalent continuum model. In fact, the transformation allows for any model to be transformed into its continuous counterpart. In the case of the Bando model [8], the continuum version obeys the same stability criterion as the discrete counterpart. Numerical simulations predict the formation and evolution of wave profiles, which are well modelled by travelling waves using our continuum model, provided the gradients are moderate.

One benefit of the transformation to the continuum analogue is that it creates a powerful tool for traffic simulations. To calculate the travelling wave solutions on a straight road, the programs for the Bando version require up to 1h (2000 cars, step-size $\Delta t = 0.005$, simulation time 2000; Pentium 233MHz) and involve integrating 2000 coupled differential equations, whereas the solution of the ordinary differential equations (3.4.12) and (3.5.17) takes about 5 seconds. In addition, the continuum type allows for simple estimations of overall traffic quantities. This way, some features of autonomous cruise control systems, whose algorithms for the regulation of headway are often based on dynamic equations similar to the Bando type Eq. (3.1.1), may be investigated in a continuum manner.

In a similar fashion, the inverse transformation relating density to headway enables one to derive car-following analogues of any macroscopic traffic flow model that depends on the density ρ and the velocity v. It is characteristic that they lead to microscopic models, which consist of spatial derivatives of the headway and, hence, include information of the traffic events further down- and/or upstream. The next chapter will look more closely at this phenomenon.

Chapter 4

Analogous Models

Using the transformation (3.2.10) and its inverse (3.8.10) which relate continuum to car-following models, it is now possible to derive the continuum analogues of various car-following models, and vice versa. This forms the subject of the present chapter in which we develop analogous descriptions for a range of discrete car-following and continuum models. We state the conditions and situations for which the corresponding version is a good first-order approach.
Tables 4.1 and 4.2 give an overview of some models and their counterparts. For the interested reader, this is followed by a more detailed discussion of their derivations, containing some subtleties that arise throughout the transformations.[1]
One is that the analogous model is usually of higher complexity than the original one, and it might not seem to be useful at first sight to transform it. However, the advantage in doing so is to investigate what new terms arise. This gives an insight into how different terms describe traffic features, and it might help to model traffic flow more accurately. Future traffic flow models will have to take this into account, and for autonomous cruise control systems this understanding is useful to set up appropriate algorithms.

4.1 Continuum Counterparts of Various Car-following Models

There is a great variety of different car-following models (subsection 2.2.2). As early as in the 1950s the first ideas came up of how to model the individual *interaction* between a vehicle and its preceding cars. (Interaction is a misleading word in the sense that it is not Newtonian interaction that one deals with in traffic flow mod-

[1]Since the remainder of this chapter does not provide any background for the remaining dissertation, it may be omitted and the reader may proceed with chapter 5.

	Car-following models and their continuum analogues
1.	**Chandler model (4.1.a)**
o:	$\dot{v}_n(t+T) = a\dot{b}_n(t)$
t:	$\frac{d}{dt}v(x+\Delta x, t+T) = a\left[-\frac{\rho_t}{\rho^2} - \frac{\rho_{xt}}{2\rho^3} + \frac{3\rho_x\rho_t}{2\rho^4}\right]$
2.	**Gazis model (4.1.b)**
o:	$\dot{v}_n(t+T) = \frac{a}{b_n(t)}\dot{b}_n(t)$
t:	$\frac{d}{dt}v(x+\Delta x, t+T) = a\left[-\frac{\rho_t}{\rho} - \frac{\rho_{xt}}{2\rho^2} + \frac{3\rho_x\rho_t}{2\rho^3}\right]$
3.	**Advanced Edie model (4.1.c)**
o:	$\dot{v}_n(t+T) = \frac{a v_n(t+T)^m}{b_n(t)^l}\dot{b}_n(t)$
t:	$\frac{1}{1-m}\frac{d}{dt}\left[v^{(1-m)}(x+\Delta x, t+T)\right] = a\rho^{l-1}\left[-\frac{\rho_t}{\rho} - \frac{\rho_{xt}}{2\rho^2} + \frac{3\rho_x\rho_t}{2\rho^3}\right]$
4.	**Newell model (4.1.d)**
o:	$v_n(t+T) = V_{max}\left[1 - \exp\left\{-\frac{a}{V_{max}}\left[b_n(t) - b_{min}\right]\right\}\right]$
t:	$v(x+\Delta x, t+T) = V_{max}\left[1 - \exp\left\{-\frac{a}{V_{max}}\left[b(x,t) - b_{min}\right]\right\}\right]$
5.	**Bando model (4.1.e)**
o:	$\dot{v_n}(t) = a\left[V_B(b_n(t)) - v_n(t)\right]$
t:	$v_t + vv_x = a\left[\bar{V}(\rho) - v\right] + a\bar{V}'(\rho)\left[\frac{\rho_x}{2\rho} + \frac{\rho_{xx}}{6\rho^2} - \frac{\rho_x^2}{2\rho^3}\right]$
	with $\bar{V}(\rho) = V_B(1/\rho)$
6.	**California model (4.1.f)**
o:	$\dot{v}_n(t+T) = a\left[b_n(t) + c - T_1 v_n\right]$
t:	$\frac{d}{dt}v(x+\Delta x, t+T) = a\left[\frac{1}{\rho} - \frac{\rho_x}{2\rho^3} - \frac{\rho_{xx}}{6\rho^4} + \frac{\rho_x^2}{2\rho^5} + c - T_1 v\right]$
7.	**Double Look-ahead model (4.1.g)**
o:	$\dot{v}_n(t) = a_1\dot{b}_n(t-T_1) + a_2(\dot{b}_n + \dot{b}_{n+1})(t-T_2)$
t:	$v_t + vv_x = a_1 b_t(x-\Delta x_1, t-T_1) + 2a_2 b_t(x-\Delta x_2, t-T_2)$
	$+ a_2\left[b_x(x-\Delta x_2, t-T_2)b(x-\Delta x_2, t-T_2)\right]_t$
8.	**Hayakawa model (4.1.g)**
o:	$\dot{v}_n = a\left[U(b_n)V(b_{n-1}) - v_n\right]$
t:	$v_t + vv_x = a\left[U(b)V(b - bb_x) - v\right]$

Table 4.1: An overview of some (original) car-following models (o) and their (transformed) macroscopic counterparts (t). The variables Δx, Δx_1, Δx_2 are determined by integrating Eq. (4.1.7), the right hand sides are to be taken at (x,t) except from model 7, and the headway b in the models 4, 7 and 8 has to be substituted by Eq. (3.2.10).

elling.)
However, a crucial difference from the continuum models lies in the application of differential delay equations to simulate the driver's response time T. The equations are usually of the form

$$\dot{v}_n(t+T) = F(b_n, \dot{b}_n, v_n), \tag{4.1.1}$$

where F is some function of the headway b_n (the distance of the nth car to its preceding vehicle), the rate of change of the headway $\dot{b}_n$, and the car's velocity v_n.
The time delay intensifies the expenditure of numerical calculations, since one has to retain the values of each variable over a period T. By taking small time steps Δt for the simulation, one ends up with $T/\Delta t$ different values for each parameter and each car. These have to be kept in the memory throughout the numerical run.
The time delay also causes trouble when applying the transformation (3.2.10) to obtain the continuum analogue. As further explained in Appendix C, we cannot represent this delay using a Taylor expansion of $v_n(t+T)$ around $v(t)$ that is truncated after a certain order. This method simply does not reveal an equivalent model. Therefore, these models cannot be transformed easily and, instead, they lead to a system of partial differential delay equations (PDDE)[2].
However, since car-following models may deliver a future algorithm to apply autonomous cruise control systems, the reaction time T will drop immensely and might be neglected. A first-order approach might then be sufficient to derive a macroscopic traffic flow model, similar to Eq. (3.2.16), but its validity would have to be checked in every single case.
However, new terms arise under the transformation, which can be interpreted one by one. This gives an insight into the macroscopic dynamics of the microscopic car-following models.

a) The Chandler Model

A suitable example to show the problems involved in transforming a differential delay equation is the simple Chandler model [16]

$$\dot{v}_n(t+T) = a\dot{b}_n(t). \tag{4.1.2}$$

Due to its simplicity, it is regarded as the beginning of car-following modelling. Here, a is equivalent to the inverse of inertia or, equivalently, the inverse of mass, since Eq. (4.1.2) can be written as $M\dot{v}_n(t+T) := \frac{1}{a}\dot{v}_n(t+T) = \dot{b}_n(t)$.
The model is stable for

$$2Ta < 1, \tag{4.1.3}$$

[2]Some may also refer to this as a delay partial differential equation

which seems quite plausible because instability should increase with rising reaction time T and with extremely harsh braking, which is proportional to a.
To find the continuous analogue, we change formally to continuum variables, bearing in mind that the reaction time T also affects the spatial coordinate x

$$\frac{d}{dt}v(x+\Delta x, t+T) = a\dot{b}(x,t). \tag{4.1.4}$$

Applying Eq. (3.2.10) yields

$$\begin{aligned} v_t(x+\Delta x, t+T) + v(x+\Delta x, t+T)v_x(x+\Delta x, t+T) \quad &= \\ a\left[\frac{1}{\rho(x,t)} - \frac{\rho_x(x,t)}{2\rho^3(x,t)} - \frac{\rho_{xx}(x,t)}{6\rho^4(x,t)} + \frac{\rho_x^2(x,t)}{2\rho^5(x,t)}\right]_t, & \end{aligned} \tag{4.1.5}$$

which is coupled with the conservation of cars

$$\rho_t + (v\rho)_x = 0. \tag{4.1.6}$$

To solve this system of PDDE, both $v(x,t)$ and $\rho(x,t)$ must be given on an initial interval $[t_0; t_0+T]$ (appendix C). These initial conditions differ from those of common partial differential equations, and we can, therefore, expect the phase space of the solutions of a PDDE to be much richer than that of the corresponding partial differential equation ($T \to 0$, $\Delta x \to 0$).
When v and ρ are both determined on $[t_0; t_0+T]$, the system (4.1.5) and (4.1.6) can be integrated by the usual tools for solving partial differential equations. The only problem that remains is how to interpret $x+\Delta x$, which is the position that a car at (x,t) will have at $t+T$. $x_i + \Delta x_i$ at $t_i + T$ is obtained by integrating

$$\dot{x}(t) = v(x,t)\ ,\ x(t_i) = x_i, \tag{4.1.7}$$

from $t_i \to t_i + T$.
This is why the whole integration procedure becomes very complex: first of all, v and ρ must be known on some initial interval $[t_0; t_0+T]$. Secondly, the coordinates $(x_i+\Delta x, t_i+T)$ must be determined after every time step of integration by solving Eq. (4.1.7). This is what makes PDDE so difficult to solve.
Therefore, one might attempt to approximate the continuum analogue by a first-order Taylor approximation. Even though this is not correct in the first place (appendix C), we carry out this expression to see what terms arise and in what way they are intrinsic features of the full PDDE-problem.
By writing

$$\dot{v}_n(t) = a\dot{b}_n(t-T) \tag{4.1.8}$$

and taking formally continuous variables, the governing equation becomes

$$v_t(x,t) + v(x,t)v_x(x,t) = ab_t(x-\Delta x, t-T). \tag{4.1.9}$$

As a first-order approach, the distance Δx that the vehicle has travelled during T can be estimated as

$$\Delta x \sim v(x,t)T. \tag{4.1.10}$$

Substituting this expression into Eq. (4.1.9) and carrying out a Taylor expansion to first order leads to

$$v_t + vv_x = a\left(b - b_x vT - b_t T\right)_t. \tag{4.1.11}$$

The application of the transformation is straightforward, and if one neglects non-linear terms $O(\rho_x^2, ...)$ and terms of higher order than second, the dynamic equation reads

$$v_t + vv_x = \underbrace{a\left[-\frac{\rho_t}{\rho^2}\right.}_{\text{1st order}} \left. -\frac{\rho_{xt}}{2\rho^3} + T\frac{\rho_{tt}}{\rho^2} + Tv\frac{\rho_{xt}}{\rho^2} + Tv_t\frac{\rho\rho_x + \rho_{xx}}{\rho^3}\right]. \tag{4.1.12}$$

The first-order equation combined with the conservation of cars Eq. (4.1.6) does not incorporate the driver's reaction time T and, hence, the stability criterion must differ from the car-following case Eq. (4.1.3). However, as $T \to 0$ Eq. (4.1.12) might well be a suitable approach to the PDDE (4.1.5).

The transformation of most car-following models is similar to this example and straightforward, but for completeness, the continuum analogues of some popular car-following models are given.

b) The Gazis Model

Most car-following models are based on the Chandler model. The parameter a is often replaced by a function that also depends on the headway b_n and/or the speed v_n of the car. Obviously, a driver tends to brake more harshly if he is closer to the preceding car. Gazis [22] first tried to incorporate this effect by modifying the Chandler model to obtain

$$\dot{v}_n(t+T) = \frac{a}{b_n(t)}\dot{b}_n(t). \tag{4.1.13}$$

The stability criterion is also similar,

$$\frac{1}{2T} > \frac{a}{b_0} \tag{4.1.14}$$

as well as the continuum counterparts of both models. Since it differs only by the division by headway, the continuum model to leading order is the same as the Chandler model multiplied by the density ρ

$$\frac{d}{dt}v(x+\Delta x, t+T) = a\left[-\frac{\rho_t}{\rho} - \frac{\rho_{xt}}{2\rho^2} + \frac{3\rho_x\rho_t}{2\rho^3}\right]. \tag{4.1.15}$$

Here as well as in the following, we retain the delay terms on the left hand side for reasons of simplicity.

c) The Advanced Edie Model

A more advanced ansatz is to let the constant of proportionality depend on the speed as well. It is a reasonable assumption, since for the same headway and change of headway a driver tends to brake more harshly the faster he is travelling.
Gazis *et al* [23] assumed that the headway and the velocity depend on integer exponents, and that the latter has an immediate impact on the driver's reaction

$$\dot{v}_n(t+T) = \frac{a v_n(t+T)^m}{b_n(t)^l} \dot{b}_n(t). \tag{4.1.16}$$

This means that the reaction time T towards the traffic situation is much bigger than the time, say T_S, to realize someone's speed: $T_S/T \ll 1$. It can be argued that the driver knows his car's "speed history" and that he is familiar with his speed situation. On the other hand, T refers to the surrounding cars, especially the one in front, and their behaviour is not predictable to the individual driver.
The transformation is rather straightforward and we obtain

$$\frac{\frac{d}{dt} v(x+\Delta x, t+T)}{v(x+\Delta x, t+T)^m} = a\rho^{l-1}\left[-\frac{\rho_t}{\rho} - \frac{\rho_{xt}}{2\rho^2} + \frac{3\rho_x\rho_t}{2\rho^3}\right]. \tag{4.1.17}$$

d) The Newell Model

A car-following model does not necessarily incorporate inertia explicitly. As long as the governing equation is of second order in time, like Newton's equation of motion, inertia is certainly included. However, there are a few first-order models, such as that of Newell [70],

$$v_n(t+T) = V_{max}\left[1 - \exp\left\{-\frac{a}{V_{max}}\left[b_n(t) - b_{min}\right]\right\}\right] \tag{4.1.18}$$

with some constants a, top speed V_{max} and minimum headway b_{min}. No matter what the car's current speed is, it is given for a time T later on by the current headway b. This clearly shows the lack of explicit inertia.
Even though this is too naive a model, it is worth carrying out the transformation because it possesses an interesting mathematical feature. Either the transformation is applied in the usual way as described so far, or Eq. (4.1.18) is turned into a partial differential equation for the density ρ. Formally, the continuum analogue is

$$v(x,t) = V_{max}\left[1 - \exp\left\{-\frac{a}{V_{max}}\left[b(x-\Delta, t-T) - b_{min}\right]\right\}\right], \tag{4.1.19}$$

and this can be substituted into the equation for the conservation of cars

$$\rho_t(x,t) + \left[v(x,t)\rho(x,t)\right]_x = 0. \tag{4.1.20}$$

Then the headway $b(x-\Delta, x-T)$ may be expressed in the usual fashion by the transformation Eq. (3.2.10), which defines a new PDDE for ρ. However, we still require the function $v(x,t)$, because Δ can only be derived by integrating Eq. (4.1.7) backwards in time.

e) The Bando Model

The Bando model [8] has already been discussed in great detail in chapter 3. This model does not explicitly incorporate any reaction time T in the form of a differential delay equation. However, it contains a driver's sensitivity a, which is proportional to the inverse of the relaxation time of adjustments to the flow conditions, and is similar to most of the advanced continuum models. Due to this fact, it is able to describe various features of real traffic flow.
The transformation of the car-following model

$$\dot{v_n}(t) = a\left[V_B(b_n(t)) - v_n(t)\right] \tag{4.1.21}$$

is straightforward. As it was already shown, it obeys the same stability criterion

$$\frac{a}{2V_B'} > 1 \tag{4.1.22}$$

for long wavelengths, if the approximation of the continuum model is carried out to first order,

$$v_t + vv_x = \underbrace{a\left(\bar{V}(\rho) - v\right)}_{\text{lowest order}} + a\bar{V}'(\rho)\left[\frac{\rho_x}{2\rho} + \frac{\rho_{xx}}{6\rho^2} - \frac{\rho_x^2}{6\rho^3}\right]. \tag{4.1.23}$$

The lowest order approximation yields a model that is always unstable and, hence, unrealistic.
It was proved that both the continuum and the car-following model predict qualitatively the same traffic behaviour in terms of travelling waves, asymptotic evolution of pulses and instability. It should, therefore, be regarded as an equivalent continuum model, when only modest spatial variations of traffic parameters such as density or speed are involved.

f) The California Model

A model that is similar to the Bando type, but explicitly contains the reaction time T, is the California model [16]. By taking the optimal-velocity function of the Bando model to be $V_B(b_n) = (b_n + c)/T_1$, one ends up with

$$\dot{v}_n(t+T) = a\left[b_n(t) + c - T_1 v_n\right], \tag{4.1.24}$$

where a is given by "a/T_1" from the Bando model. It is slightly unrealistic, because the desired speed V_B tends to infinity when the headway tends to infinity.
Chandler showed in his paper that the time delay is not important for a stability analysis and that the system is stable for

$$aT_1^2 > 2, \tag{4.1.25}$$

which is, as expected, the same as Bando's criterion. The continuum counterpart is given by

$$\frac{d}{dt}v(x+\Delta x, t+T) = a\left[\frac{1}{\rho} - \frac{\rho_x}{2\rho^3} - \frac{\rho_{xx}}{6\rho^4} + \frac{\rho_x^2}{2\rho^5} + c - T_1 v\right]. \tag{4.1.26}$$

Once again, it should be emphasized that the continuum analogues of differential delay equations are much tougher to handle than those of ordinary differential equations, like the Bando model. Since the latter succeeds in reproducing numerous characteristic traffic features, it is not clear, yet, whether differential delay equations are necessary to describe car-following models.

g) The Double Look-ahead and the Hayakawa Model

There are a few car-following models which account for the traffic behaviour further up- or downstream, and not only for the driver's own speed, headway and change of headway.

The **Double Look-ahead model** [37] assumes that the driver's reaction does not only depend on the distance to the car in front. Instead, he will also pay attention to the events further downstream. Assuming the same headway, change of headway and speed, a driver will brake harsher if he approaches a region of increasing rather than decreasing congestion. One possible way to model this behaviour is to add another term depending on the headway to the car in front of the preceding car. Different reaction times and sensitivities of these processes are represented by different parameters a_1, a_2, T_1 and T_2,

$$\begin{aligned} \dot{v}_n(t) &= a_1\dot{b}_n(t-T_1) + a_2(\dot{b}_n + \dot{b}_{n+1})(t-T_2) && (4.1.27)\\ &= a_1\dot{b}_n(t-T_1) + a_2\dot{b}_n(t-T_2) + a_2\dot{b}_{n+1}(t-T_2). && (4.1.28)\end{aligned}$$

A change to continuous variables formally yields

$$\begin{aligned} &v_t(x,t) + v(x,t)v_x(x,t) = \\ &a_1 b_t(x-\Delta x_1, t-T_1) + a_2 b_t(x-\Delta x_2, t-T_2) + a_2 b_t(x+b-\Delta x_2, t-T_2). \end{aligned} \tag{4.1.29}$$

To apply the transformation relating headway to density, Eq. (3.2.10), we have to estimate the headway b_{n+1} in the continuous formulation by

$$b_{n+1}(X) = b_n(x_n + b_n) \to b(x + b(x)) \sim b(x) + b_x(x)b + \frac{1}{2}b_{xx}(x)b(x)^2 + \dots \,. \quad (4.1.30)$$

This gives to lowest order

$$\begin{aligned} &v_t(x,t) + v(x,t)v_x(x,t) = \\ &a_1 b_t(x - \Delta x_1, t - T_1) + a_2 b_t(x - \Delta x_2, t - T_2) \\ &+ a_2 \left[b(x - \Delta x_2, t - T_2) + b_x(x - \Delta x_2, t - T_2)b(x - \Delta x_2, t - T_2)\right]_t , \end{aligned} \quad (4.1.31)$$

and the substitution $b = 1/\rho - \rho_x/(2\rho^3) - \rho_{xx}/(6\rho^4)$ reveals a continuum approach to the Double Look-ahead model. This time, it is no surprise that diffusive terms arise, because their discrete analogue contains parameters of cars that are two ahead, which reveals information further downstream.

Finally, a recent model by **Hayakawa** *et al* [26] is presented. It is based on the Bando model, but also depends on the headway to the following car

$$\dot{v}_n = a\left[U(b_n)V(b_{n-1}) - v_n\right] \quad (4.1.32)$$

without proposing any explicit time delay. If it can be once more assumed that the headway is only slowly varying, b_{n-1} can be approximated in continuous variables similar to Eq. (4.1.30)

$$\begin{aligned} b_{n-1}(X) &= b_n(x_n - b_{n-1}) && (4.1.33)\\ &\simeq b_n(x_n) - b_n'(x_n)b_{n-1}(X) + \dots && (4.1.34)\\ &\overset{\text{(iteration)}}{\simeq} b_n(x_n) - b_n'(x_n)b_n(x_n) + \dots , && (4.1.35) \end{aligned}$$

where the dash denotes derivation with respect to x. The continuum version to lowest order is then given by

$$v_t + vv_x = a\left[U(b)V(b - bb_x) - v\right] \quad (4.1.36)$$

with b being replaced by the transformation Eq. (3.2.10). A Taylor expansion of the optimal-velocity function $\hat{V} = UV$, which now depends on ρ, ρ_x and ρ_{xx}, yields cross terms like VU' and $V'U$, respectively. It is a very lengthy formula and for this reason not included here.

However, it is significant that higher order terms of the density are involved. In the same way as the asymptotic series (3.2.10) is truncated after a particular order to be applied to the continuous formulation, it is also justified to truncate the series Eqs. (4.1.30) and (4.1.35) after the same order. The accuracy of these approximations depends crucially on the gradients of the traffic variables. As shown above, terms of rising order have to be included to reproduce increasing gradients accurately.

	Continuum models and their car-following counterparts
1.	**Ross model (4.2.a)**
o:	$v_t + vv_x = \frac{1}{T}\left(V_f - v\right)$
t:	$\dot{v}_n = \frac{1}{T}\left(V_f - v_n\right)$
2.	**Payne model (4.2.b)**
o:	$v_t + vv_x = \frac{1}{T}\left[V(\rho) - v\right] - \nu\frac{\rho_x}{\rho}$
t:	$\dot{v}_n = \frac{1}{T}\left[\hat{V}(b_n) - v\right] + \nu\left(\frac{b_n'}{b_n} - \frac{b_n''}{2}\right) - \frac{\hat{V}'(b_n)}{T}\left(\frac{b_n b_n'}{2} - \frac{b_n^2 b_n''}{12}\right)$
3.	**Kühne model (4.2.c)**
o:	$v_t + vv_x = \frac{1}{T}\left[V(\rho) - v\right] - c_0^2\frac{\rho_x}{\rho} - \mu v_{xx}$
t:	$\dot{v}_n = \frac{1}{T}\left[\hat{V}(b_n) - v\right] + c_0^2\left(\frac{b_n'}{b_n} - \frac{b_n''}{2}\right)$ $- \frac{\hat{V}'(b_n)}{T}\left(\frac{b_n b_n'}{2} - \frac{b_n^2 b_n''}{12}\right) - \mu v_n\frac{b_n''}{b}\left(1 + \frac{b_{n_t}}{2v_n}\right)$
4.	**Kerner-Konhäuser model (4.2.d)**
o:	$v_t + vv_x = \frac{1}{T}\left[V(\rho) - v\right] - c_0^2\frac{\rho_x}{\rho} - \mu\frac{v_{xx}}{\rho}$
t:	$\dot{v}_n = \frac{1}{T}\left[\hat{V}(b_n) - v\right] + c_0^2\left(\frac{b_n'}{b_n} - \frac{b_n''}{2}\right)$ $- \frac{\hat{V}'(b_n)}{T}\left(\frac{b_n b_n'}{2} - \frac{b_n^2 b_n''}{12}\right) - \mu v_n b_n''\left(1 + \frac{b_{n_t}}{2v_n}\right)$

Table 4.2: An overview of some continuum (o) models and their microscopic counterparts (t).

4.2 Car-following Counterparts of Various Continuum Models

There are a few continuum models which contain inertia, but only a handful are still of interest. In principle, each model is based on another, giving successively more advanced approaches to describe traffic flow by continuous variables.
The way Lighthill and Whitham [58] (subsection 2.2.1) tried to describe traffic flow turned out to be useful for specific traffic situations, but it is in general of no great use in dynamic situations where inertia gives rise to instability. One setback is that their model does not incorporate stop-start waves, which are a well known phenomenon in real traffic events. Therefore, we restrict our attention to types which include inertia, represented by a relaxation term of the form

$$\frac{1}{T}\left[V(\rho(x,t)) - v(x,t)\right] \tag{4.2.1}$$

with an optimal-velocity function V. This expression is similar to various relaxation terms in physics, for example, friction or bringing density gradients into line.
So far, none of the continuum models include an explicit time delay, which in turn simplifies the transformation into the corresponding car-following model. Nevertheless, it is doubtful whether traffic flow can be described in a continuum model which incorporates neither the driver's reaction time explicitly, nor the varying composi-

tion of vehicles along the road.
We see in what follows that terms depending on the headway of following cars are involved in the dynamic equation when continuum models are transformed into their car-following counterparts. This reminds one of the Hayakawa model of the last section.

a) The Ross Model

The simplest model that includes a relaxation term, and hence inertia, was suggested by Ross [75],

$$v_t + vv_x = \frac{1}{T}(V_f - v) \tag{4.2.2}$$

with a top speed V_f. It does not address the anticipation and "dissipative" effects of traffic flow and should be regarded as a very basic approach. In addition, the conservation of cars

$$\rho_t + (v\rho)_x = 0 \tag{4.2.3}$$

must be fulfilled as for any of the following models. This model is special with regard to the independence of the dynamic equation Eq. (4.2.2) on the density ρ. The velocity evolves according to its own autonomous partial differential equation, whereas the density is given by the coupled partial differential equation (4.2.3). It means that it is necessary to know v to calculate ρ once the initial conditions are given, but not vice versa.
The car-following analogue is similarly simple,

$$\dot{v}_n = \frac{1}{T}(V_f - v_n), \tag{4.2.4}$$

which is a Bando model with an OV function

$$V_B(b) = V_f = const. \tag{4.2.5}$$

For equilibrium flow situations, we have $\dot{v}_n \equiv 0$ and in turn $v = V_f$, which is independent of the density ρ. Accordingly, the equilibrium flow $q = v\rho = V_f\rho$ has no upper limit and corresponds to a uniform wave speed. Hence, this OV function is too simple an approach to the driver's behaviour and is not of greater interest in the literature.

b) The Payne Model

The Payne model [71] of road traffic incorporates an anticipation term $\frac{\rho_x}{\rho}$ that reflects the driver's reaction to a preceding traffic situation of increasing density, but still with no dissipation. To transform the model

$$v_t + vv_x = \frac{1}{T}[V(\rho) - v] - \nu\frac{\rho_x}{\rho}, \tag{4.2.6}$$

we restrict the consideration to the orders b_x and b_{xx}, and neglect higher order terms $O(b_x^2, ...)$. The inverse transformation Eq. (3.8.10) and its derivatives then become

$$\rho = \frac{1}{b} + \frac{b_x}{2b} - \frac{b_{xx}}{12}, \tag{4.2.7}$$

$$\rho_x = -\frac{b_x}{b^2} + \frac{b_{xx}}{2b}, \tag{4.2.8}$$

$$\rho_{xx} = -\frac{b_{xx}}{b^2}. \tag{4.2.9}$$

We first carry out the derivation formally by substituting these expressions into the Payne model (4.2.6) and by discretizing these parameters. A Taylor expansion of the OV function to first order similar to (3.2.16) then reveals

$$\dot{v}_n = \frac{1}{T}\left[\hat{V}(b_n) - v\right] + \nu\left(\frac{b_n'}{b_n} - \frac{b_n''}{2}\right) - \frac{\hat{V}'(b_n)}{T}\left(\frac{b_n b_n'}{2} - \frac{b_n^2 b_n''}{12}\right), \tag{4.2.10}$$

where we have introduced the abbreviations

$$\hat{V}(b_n) = V(1/b_n), \tag{4.2.11}$$

$$b_n' = \frac{\partial}{\partial x} b(x_n, t), \tag{4.2.12}$$

$$\hat{V}'(b_n) = \frac{\partial}{\partial b_n}\hat{V}(b_n). \tag{4.2.13}$$

The terms (4.2.11) and (4.2.13) cause no problems, whereas the discrete derivative (4.2.12) needs more explanation. It has to be expressed by traffic quantities of the system, since the continuous variable x is no longer involved in the car-following model. Hence, when one discretizes a system, derivatives have to be expressed by local variables that are known. For example, the first derivative of the headway with respect to space becomes

$$\frac{\partial}{\partial x} b(x_n) \sim \left.\frac{\Delta b}{\Delta x}\right|_{x_n} \tag{4.2.14}$$

$$= \frac{b(x_{n+1}) - b(x_{n-1})}{b(x_n) + b(x_{n-1})} \tag{4.2.15}$$

$$= \frac{b_{n+1} - b_{n-1}}{b_n + b_{n-1}} \tag{4.2.16}$$

and similarly the second derivative

$$\frac{\partial^2}{\partial x^2} b(x_n) \sim \left.\frac{\Delta b'}{\Delta x}\right|_{x_n} \tag{4.2.17}$$

$$= \left(\frac{b_{n+2} - b_n}{b_{n+1} + b_n} - \frac{b_n - b_{n-2}}{b_{n-1} + b_{n-2}}\right) / (b_{n-1} + b_n). \tag{4.2.18}$$

We can see that when the model is discretized, headways of cars in front of and behind the particular vehicle are involved. This is a bit surprising, since all car-following theories but Hayakawa's [26] neglect the impact of the following vehicles

on the driver's reaction.
To lowest order, the discrete model is obviously equivalent to the Bando model, but the derivatives make it more complicated. It includes a second spatial derivative b'', even though the original model does not explicitly incorporate diffusion in the form of a term ρ_{xx}. Therefore, this term represents one reason for the spreading of an initial disturbance in the stable regime

$$|V_\rho| < \frac{\sqrt{\nu}}{\rho_0} \tag{4.2.19}$$

of the continuum model Eq. (4.2.6). On the other hand, the involvement of the second car (b_{n+1}) ahead was already given in the Double Look-ahead model by the term $\dot{b}_{n+1}$ in Eq. (4.1.27). However, even the third car ahead now has an explicit impact on the nth car via b_{n+2} in Eq. (4.2.18).
One might try to avoid the dependence on headways of following vehicles by writing

$$\left.\frac{\Delta b}{\Delta x}\right|_{x_n} = \frac{b_{n+1} - b_n}{b_n}, \tag{4.2.20}$$

but in fact this is not the local derivative at $x = x_n$. Moreover, the second derivative b'' would still involve headways of following cars. This shows that terms of the continuum formulation might have a physical and sensible explanation, but fail to do so in the corresponding car-following model. It is, therefore, an interesting question, whether Nagatani's idea of a non-local term $\rho(x + \Delta, t)$ in the continuum model (section 3.5) is a more useful approach.

c) The Kühne Model

The first approach to consider dissipation explicitly in traffic flow theory was that of Kühne [53]. He added a dissipative term to the right hand side of Payne's model Eq. (4.2.6), which gives the dynamic equation a Navier-Stokes-like nature

$$v_t + v v_x = \frac{1}{T}\left[V(\rho) - v\right] - c_0^2 \frac{\rho_x}{\rho} + \mu v_{xx}. \tag{4.2.21}$$

The additional term can be interpreted as representing viscosity. Energy is clearly not conserved in the system due to the braking and accelerating of individual cars. This can be explained by the non-Newtonian nature of the interaction of vehicles. Defining the mean momentum P of the car convoy in the usual fashion by the sum of the individual momenta p_n

$$P := \sum_{n=1}^{N} p_n, \tag{4.2.22}$$

the change of the mean momentum is given by

$$\dot{P} = \sum_{n=1}^{N} \dot{p}_n = \sum_{n=1}^{N} F_n \tag{4.2.23}$$

$$= \sum_{n=1}^{N} \left(F_n^{(p)} + F_n^{(f)} \right) (\neq 0). \tag{4.2.24}$$

In most models apart from Hayakawa's, the force $F_n^{(f)}$ vanishes and the force $F_n^{(p)}$ of a preceding car and $F_n^{(f)}$ of a following car do not cancel each other. Hence, the mean momentum is not conserved and dissipation is always present.
The problem that arises when one tries to apply the inverse transformation to this model is the second derivative of speed. It has to be expressed by the speed of cars surrounding the nth car analogous to the discrete derivatives of the headway Eq. (4.2.18), if it is retained during the transformation. This can be avoided because it may also be expressed by the velocity v and spatial and temporal derivatives of the density ρ by making use of the conservation of cars Eq. (4.2.3). Writing the latter as

$$v_x = -\frac{\rho_t + v\rho_x}{\rho} \tag{4.2.25}$$

yields the required equation

$$v_{xx} = \frac{1}{\rho^2} \left(v\rho_x^2 + \rho_t\rho_x - v\rho\rho_{xx} - v_x\rho\rho_x - \rho\rho_{xt} \right) \tag{4.2.26}$$

$$\overset{(4.2.25)}{=} \frac{1}{\rho^2} \left(2v\rho_x^2 + 2\rho_t\rho_x - v\rho\rho_{xx} - \rho\rho_{xt} \right). \tag{4.2.27}$$

The occurrence of ρ_{xx} shows that the dissipative term of the Kühne and the Kerner-Konhäuser model is somehow related to the diffusive term of the Bando model. However, Eq. (4.2.27) can be substituted into Eq. (4.2.21) to replace v_{xx} by variables that are well known under the transformation

$$\rho = \frac{1}{b} + \frac{b_x}{2b} - \frac{b_{xx}}{12}. \tag{4.2.28}$$

It is straightforward algebra to determine the derivatives ρ_x, ρ_{xx} and ρ_t from Eq. (4.2.28). We obtain

$$\mu v_{xx} = \mu v \frac{b_{xx}}{b} \left(1 + \frac{b_t}{2v} \right) \tag{4.2.29}$$

for the additional dissipation term up to order $O(b_{xx})$ by neglecting nonlinear terms $O(b_x^2)$. The analogous car-following model is similar to that of the Payne model. Adding Eq. (4.2.29) to the right hand side of Eq. (4.2.10) yields

$$\dot{v}_n = \frac{1}{T} \left[\hat{V}(b_n) - v \right] + c_0^2 \left(\frac{b_n'}{b_n} - \frac{b_n''}{2} \right) - \frac{\hat{V}'(b_n)}{T} \left(\frac{b_n b_n'}{2} - \frac{b_n^2 b_n''}{12} \right) - \mu v_n \frac{b_n''}{b} \left(1 + \frac{b_{n_t}}{2v_n} \right), \tag{4.2.30}$$

which again includes headways of the following cars. This time it is less surprising, since the original continuum model already contains a dissipative term. Moreover, it also incorporates the temporal change of headway b_{n_t} of the n-th car

$$b_{n_t} = v_{n+1} - v_n. \tag{4.2.31}$$

This term also appears in the Chandler, Gazis, Pipes, (Advanced) Edie and the Double Look-ahead models. It reveals that a term which represents the headway change in the car-following model is somehow related to a dissipative term in the continuum formulation.

d) The Kerner-Konhäuser Model

Finally, we consider the Kerner-Konhäuser model which is one of the most recent and most discussed types. It is basically a slight modification of the Kühne model Eq. (4.2.21). The dissipation term is divided by the density ρ to account for diffusion relative to the overall density

$$v_t + vv_x = \frac{1}{T}\left[V(\rho) - v\right] - c_0^2\frac{\rho_x}{\rho} + \mu\frac{v_{xx}}{\rho}. \tag{4.2.32}$$

The car-following analogue is easily derived from the Kühne model by taking the division by ρ into consideration

$$\begin{aligned} \dot{v}_n &= \frac{1}{T}\left[\hat{V}(b_n) - v\right] + c_0^2\left(\frac{b_n'}{b_n} - \frac{b_n''}{2}\right) \\ &\quad -\frac{\hat{V}'(b_n)}{T}\left(\frac{b_n b_n'}{2} - \frac{b_n^2 b_n''}{12}\right) - \mu v_n b_n''\left(1 + \frac{b_{n_t}}{2v_n}\right). \end{aligned} \tag{4.2.33}$$

It has a richer structure than the Bando model Eq. (3.1.1), which is just a lowest order approximation to this dynamic equation. It is, therefore, not surprising that Herrmann and Kerner [38] discovered different numerical results when comparing their model to a Bando model with almost the same optimal-velocity function (section 3.5). To obtain as similar results for both models as possible, they fitted the parameters of the OV function of their Bando model. The derivation Eq. (4.2.33) suggests that it would be more accurate to use exactly the same OV function and to incorporate the additional terms on the right hand side. It remains an interesting question, as to what sense this model is an approximation to the original one (4.2.32). This analysis is not carried out here due to the complicated numerical modelling of Eq. (4.2.33).

4.3 Conclusion

In this chapter, we have presented continuum counterparts of some car-following models, and vice versa. For this purpose, the transformation of chapter 3 is applied

to various traffic flow models.

Most car-following models include an explicit reaction time T in the form of a differential delay equation, so that the continuum counterpart consists of a partial differential delay equation. It turns out that this is harder to solve than the original ordinary differential delay equation. However, a Taylor expansion of the analogous model reveals new terms which are an intrinsic feature of the original discrete car-following model.

The derivation of car-following analogues from continuum models yields spatial derivatives of the headway, which are difficult to interpret. It seems that even traffic events behind a vehicle now determine its dynamics. Hence, it appears more sensible to start from a car-following model which might even contain events further downstream and to transform this into a continuum version, as presented in chapter 3 for the Bando model.

This analysis shows the disadvantage of continuum models when it comes to modelling time delay, as well as different vehicles and driver behaviour. However, it also reveals that discrete models contain diffusive behaviour, which is made explicit when they are transformed into their continuum counterparts.

Chapter 5

Wave Types in the Bando Model

One advantage of car-following models is that they both simulate traffic flow and have practical applications in the form of autonomous cruise control systems (ACCS). These systems link each car to the preceding car via a follow-the-leader algorithm similar to the governing equation of a car-following model, and the target is to enable high flux driving in stable and safe convoys. Hence, insight into the phenomena associated with car-following models gives insight into ACCS.

One common and fundamental process is the merging of a platoon of moving cars at one headway into a platoon moving with a different headway. This situation appears at bottlenecks and lane merging, for example. In order to prevent instabilities and dangerous traffic situations it is important to know what transitions can possibly occur in the system.

Therefore, in order to deepen our understanding of car-following models, in this chapter, we examine the transition from a linearly stable stream of cars of one headway into a linearly stable stream of a second headway, using the Bando model as a popular representative of the car-following class.

Numerical results of the governing equations identify a range of transition phenomena including monotonic and oscillating travelling waves, and a time dependent dispersive adjustment wave. However, for certain conditions, we find that the adjustment takes the form of a nonlinear travelling wave from the upstream headway, to a third intermediate headway, followed by either another travelling wave, or a dispersive wave further downstream matching the downstream headway. This intermediate value of the headway is selected such that the nonlinear travelling wave is the fastest stable travelling wave which is observed to develop in the numerical calculations.

The development of these nonlinear waves, connecting linearly stable flows of two

different headways, is somewhat reminiscent of stop-start waves in congested flow on freeways.
The different types of adjustments are classified in a phase diagram, which shows their dependence on the upstream and downstream headway and on the response time of the model. These plots have profound consequences for ACCS, since for an autocade of both identical and different vehicles, the control system itself may trigger formations of nonlinear steep wave transitions.
Finally, we demonstrate that the phase diagram of different transition types, which has been determined by extensive numerical simulations, may also be derived using the continuum analogue. This approach could be far less time consuming, since it considers an analysis of the phase space of the travelling wave solutions rather than comprehensive simulations.

5.1 The Linear Stable Case

We examine flows in the linearly stable regime of the Bando model [8]

$$\dot{v}_n = a\left[V_B(b_n) - v_n\right], \tag{5.1.1}$$

with the usual optimal-velocity (OV) function

$$V_B(b) = \tanh(b-2) + \tanh(2). \tag{5.1.2}$$

As mentioned in chapter 3, Bando *et al* showed that the model is unstable in a headway range

$$b_{c_1} < b < b_{c_2} \tag{5.1.3}$$

for which

$$\frac{2V_B'(b)}{a} > 1. \tag{5.1.4}$$

Under these conditions, an initial uniform flow breaks down under the slightest perturbation and turns into stop-and-go traffic. This is characterized by stable regions of high speed merging into regions of low speed so as to conserve total flux, and the high and low speed flows are both in the stable regime [78].
However, the dynamics of transitions in the two stable ranges

$$b < b_{c_1} \tag{5.1.5}$$

and

$$b > b_{c_2}, \tag{5.1.6}$$

have received less attention. Here, we examine the richness of behaviour which may develop when one stream merges into a second. This is a generalization of the

transition waves found in chapter 3, and provides new insight into the selection of nonlinear stop-and-go waves. In the next section, we identify different transition phenomena as the size of headway jump across the transition varies, and section 5.3 relates a nonlinear wave type of the stable regime to the stop-and-go jam fronts of unstable flow.
Although the main part of our study uses the Bando car-following model, we include some calculations using another OV function suggested by Herrmann and Kerner [38]. This is in order to consider a dimensional model, and to investigate whether the range of wave types found in the next section is an intrinsic feature of car-following models based on a relaxation term.

5.2 Travelling Waves of the Stable Regime

The transition between traffic flows of different throughput is a well observed phenomenon. Bottlenecks, speed limits, cars entering a jam or emerging from it, are typical situations. Here, we study transitions which occur in freely moving traffic without local speed limits or any other artificial hindrance caused by the road layout. We expect the transitions that evolve to travel along the road, either up- or downstream. Their direction and shape depend on the OV function and on the sensitivity, which is related to the inverse of inertia.
From the instability criterion (5.1.4), it is clear that a platoon of cars is more stable the smaller the inertia is. Heavier vehicles of higher inertia, which cannot react sufficiently fast to changing traffic situations, are more likely to cause flow breakdown. We therefore study travelling waves with large sensitivity a corresponding to more stable flow. At $a = 2.0$, the flow is just on the verge of instability.
In our analysis, we consider transitions which evolve from initial conditions, similar to Fig. 5.1, where the jump of headway is determined by the boundary conditions $b_- = b(x \to -\infty)$ and $b_+ = b(x \to \infty)$. Again, we prefer to present the figures with lines rather than with dots representing each car, in order to simplify the comparisons of travelling wave solutions.

5.2.1 Transition Involving a Decrease in Headway: Decelerating Traffic

Once the optimal-velocity function V_B is given, the only remaining parameter in the system is the sensitivity a. For given a, the analysis of the wave fronts in terms of upstream and downstream headways can be summarized in a diagram, as shown in Fig. 5.2. On the verge of instability ($a = 2.0$), decelerating traffic can be classified into six categories. Among these are two broad classes of travelling waves

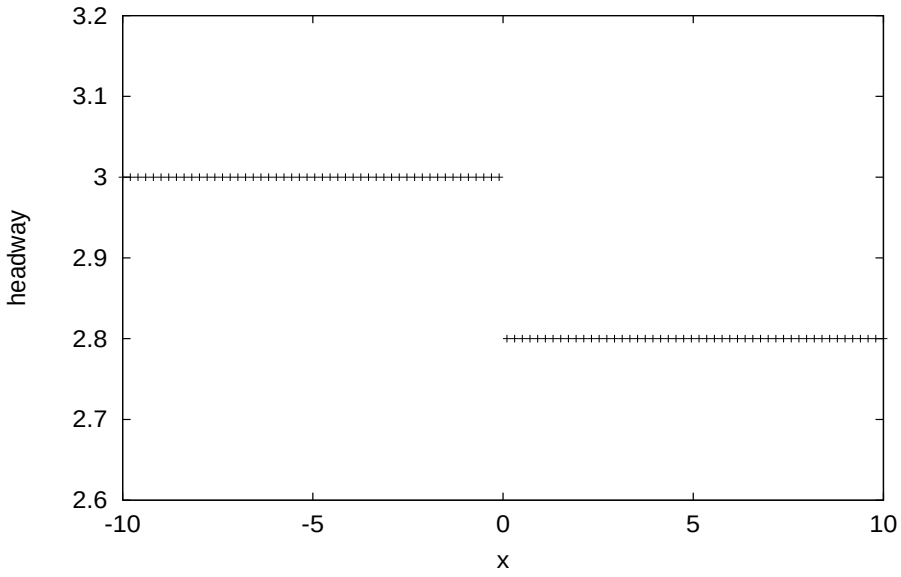

Figure 5.1: Initial change of headway in the Bando model, $t = 0$. The initial speed of the vehicles is given by $v_n(0) = V_B(b_n(0))$.

of permament form. Firstly, those which we call the *Bando waves* that lie on a line in the (b_+, b_-) plane separating regions III and IV and are in that sense non-generic waves. They are always monotonic and will be analyzed later on. Secondly, there is a class disjoint from the Bando wave which occurs for a whole area of the (b_+, b_-) plane. This has two sub-types: I which is monotonic; II which is oscillating.
We start with the interpretation of monotonic (region I), oscillatory (region II) and dispersive transitions (region VI). These can be explained by looking at the fundamental diagram of this stable model (Fig. 5.3), which describes stationary and homogenous flow situations

$$q(\rho) = \rho v(\rho) = \rho V_B(1/\rho). \tag{5.2.1}$$

In the case of a **monotonic travelling wave** solution (region I), both up- and downstream headways are greater than the point of inflexion $b_{tp} = 2.0$, and occur at a density ρ that is smaller than the point of inflexion $\rho_{tp} = 1/b_{tp} = 0.5$ (Fig. 5.3).
We can interpret this result in the limit $a \gg 1$, where the Bando model corresponds to the continuum model of Lighthill and Whitham [58]

$$\rho_t + q_x = \rho_t + [\rho V_B(1/\rho)]_x = 0. \tag{5.2.2}$$

In this model, the method of characteristics shows that the local wave speed $c(\rho)$ is given by the slope of the tangent of the fundamental diagram at its corresponding

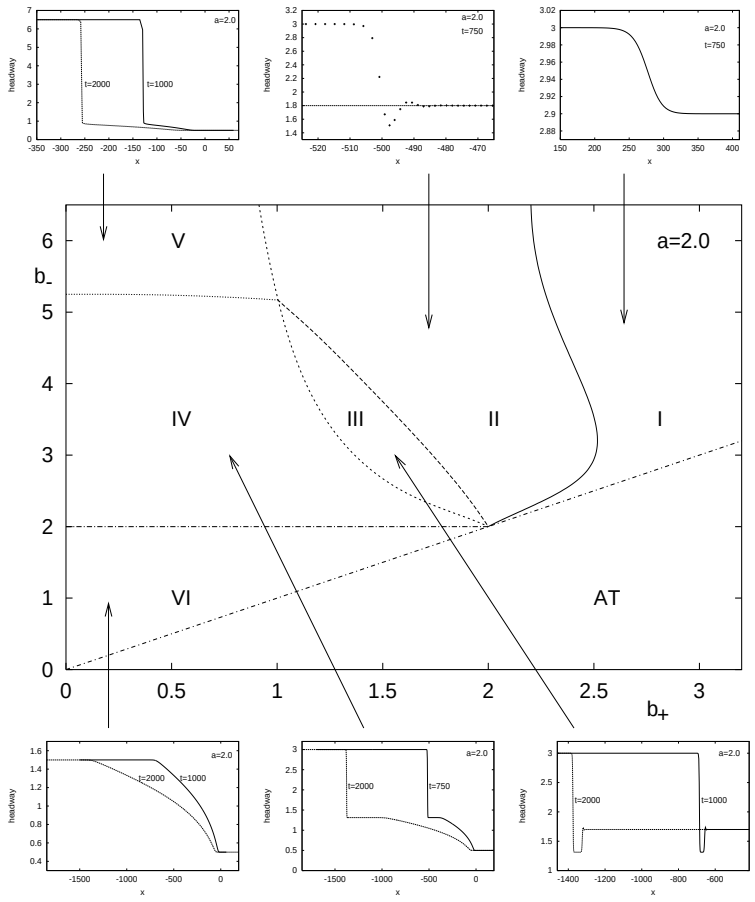

Figure 5.2: Transitions of decelerating traffic ($a = 2.0$): I: monotonic, II: oscillatory, III: solution locks on to Bando wave plus a downstream travelling wave, IV: Bando wave, plateau and dispersive tail, V: jump and dispersive tail for large jumps in headway, VI: purely dispersive; AT: region of accelerating traffic (Fig. 5.5).

density

$$c(\rho) = q_\rho(\rho). \tag{5.2.3}$$

For densities greater than $\rho_0 = 0.36$ of the maximum flow, the slopes are negative and the information travels upstream. For waves of region I, the local upstream wave speed as a function of position in the wave increases down the road. This leads to a shock wave solution, where the wave speed is determined by its upstream (ρ_-) and downstream (ρ_+) densities

$$c = \frac{q(\rho_+) - q(\rho_-)}{\rho_+ - \rho_-}. \tag{5.2.4}$$

Strictly speaking, waves of region I are monotonic travelling waves rather than shock waves, since they do not include any discontinuous jump in headway. However, in

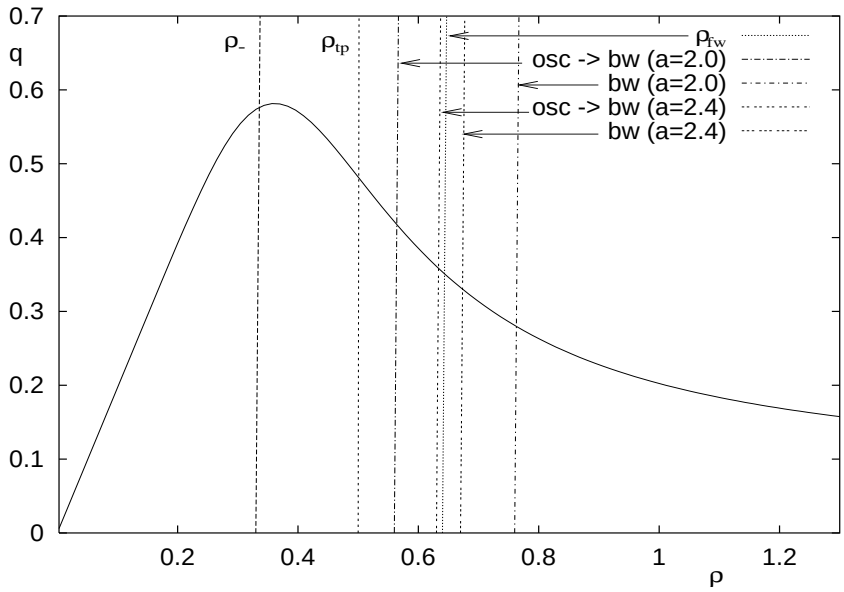

Figure 5.3: Fundamental diagram: the transitions oscillatory $\rightarrow$ Bando wave (osc $\rightarrow$ bw) and the Bando wave itself (bw) approach the fastest wave (ρ_{fw}) with increasing a.

what follows we will also refer to monotonic travelling waves as shock waves to underline their structure and steep gradients.

For **purely dispersive, time-dependent waves** (region VI), both up- and downstream densities are larger than the point of inflexion and the magnitude of the wave speed across the profile now decreases. This means that the speed of information decreases as one moves downstream. Hence, drivers entering the transition react faster to the traffic situation than drivers further downstream and, therefore, the number of drivers who are part of the decelerating manoeuvre grows, and a dispersive tail forms. A travelling wave solution does not exist in this regime.

The **oscillatory waves** (region II) always have an upstream density smaller than the point of inflexion, whereas their downstream density can be either smaller or bigger than the point of inflexion. It is, therefore, not as straightforward to interpret the results. One has to be aware that the fundamental diagram shows the flow as a function of the density only for a steady flow. Generally, for non-stationary situations, the flow is not a function of the density any more. A given ρ might correspond to various flows depending on the traffic situation, and the wave speed is not a function of the density. One example is the travelling wave solution of region I, where every point along the profile has the same wave speed, even though the density varies.

However, in the limits of transitions involving small changes of headway and $a \rightarrow \infty$, we expect a monotonic transition, since cars assume their desired speed immediately

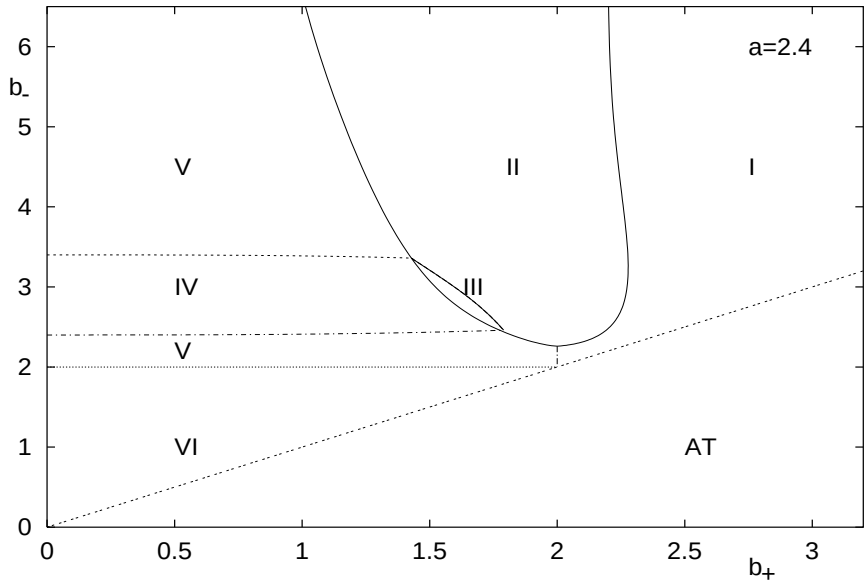

Figure 5.4: Transitions of decelerating traffic ($a = 2.4$): with increasing sensitivity regions III and IV shrink until they vanish. Region V spreads out between region IV and VI. The region II of oscillatory waves shrinks too, since the traffic flow reacts faster to changes in headway due to lower inertia (which is proportional to $1/a$).

and react sufficiently fast to the surrounding traffic situation. For greater jumps in headway and smaller values of the sensitivity, deviations from the monotonic adjustment occur as oscillatory waves in a similar fashion to the transition from over- to underdamping of a spring. With these larger changes in headway, the inertia of cars is too large to allow for simple monotonic transitions in flow. We will present a more mathematical argument in section 5.9.

However, when the jump in headway increases to a certain value, the oscillations become so large that the wave jumps on to another solution (region III). It consists of **two monotonic travelling waves of different speeds**, with a growing region of slow moving traffic in between. This solution first jumps from the upstream headway b_- to an intermediate headway b_{bw}, represented by the dotted line between region III and IV in Fig. 5.2 before it eventually matches the downstream headway through another travelling wave. The parameter b_{bw} is a function of b_- and the sensitivity a and is here only determined numerically [11]. We refer to this nonlinear wave between the upstream headway b_-, and the intermediate headway b_{bw}, as a **Bando wave**.

For lower downstream headways than b_{bw}, the transition involves a **Bando wave followed by a plateau of increasing length with a dispersive tail** (region IV). Transforming the headways of this graph, $b_- = 3$ and $b_+ = 0.5$, into the fun-

damental diagram Fig. 5.3, the corresponding densities are rather far apart from each other, with the point of inflexion in between. Therefore, the magnitude of the local wave speed across a monotonic profile between these two headways firstly increases, leading to a travelling wave, and then decreases, leading to a dispersive wave. The wave profile we obtain consists of these two types of waves, as expected, with a plateau $b_{bw} \approx 1.3$, overshooting the point of inflexion $b_{tp} = 2$, due to the inertia of cars. The plateau forms because the upstream speed of the Bando wave is higher than the local speed of the dispersive tail at its onset. In terms of fluxes, the Bando wave provides more cars per unit time (outflow of the Bando wave) than cars beginning to brake at the onset of the dispersive tail (inflow of the dispersive tail).
If the upstream headway is too big (region V), the difference of speed between the Bando wave and the onset of the dispersive tail is negligible. The wave profile assumes a solution in which the **dispersive tail and the Bando wave** have the same speed and no plateau forms.
For higher sensitivities, equivalent to smaller inertia (Fig. 5.4), the cars react faster to the traffic situation. Therefore, the regions of oscillatory waves and Bando waves shrink until the latter eventually disappears. Monotonic and purely dispersive waves (I and VI) still exist, and waves of type V take the place of plateau waves (type IV). For large a, $a \gg 2.0$, four different wave types remain: monotonic (I), oscillatory (II), purely dispersive (VI), and Bando wave plus an adjoining dispersive tail (V).

There are at least two criticisms of our method. The first might be the very specific initial conditions that we have chosen. In general, a different initial wave structure might trigger another wave type. However, we could not find in any of our simulations, including the on-ramp case of the next chapter, a further transition type. These findings are supported by the interpretation of the transition types with the help of the fundamental diagram.
Futhermore, the phase diagrams have been derived from numerical data only. It presents qualitative rather than quantitative results. In particular, it was difficult to reveal if waves of region V are really distinct from those of region IV. Moreover, region III could as well become very narrow for $b_- \to \infty$ rather than being cut off at a certain headway. Accordingly, region III might as well become very small for $a \to \infty$ rather than vanishing.

5.2.2 Transition Involving an Increase in Headway: Accelerating Traffic

Once the diagrams for the wave types of decelerating traffic (Figs. 5.2 and 5.4) are worked out, those of accelerating traffic can be obtained by a mathematical

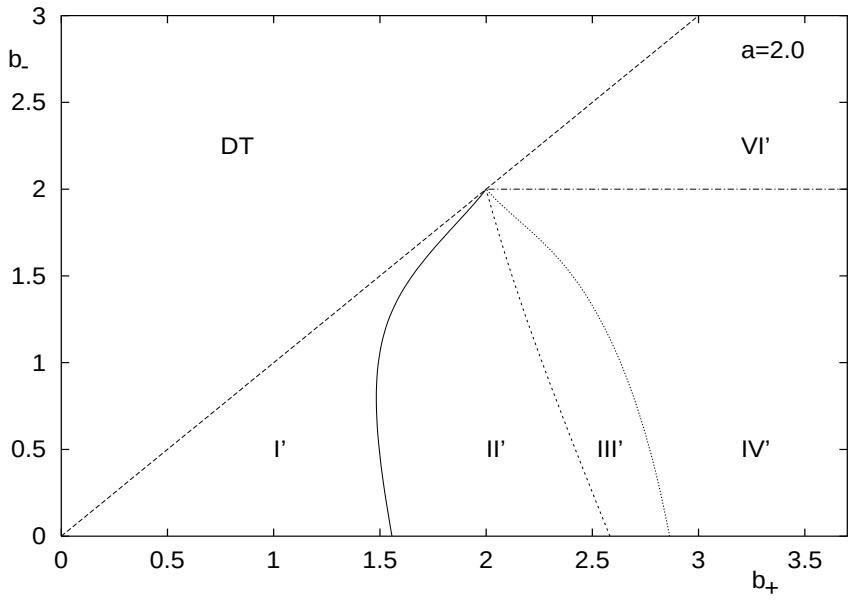

Figure 5.5: Transitions of accelerating traffic ($a = 2.0$): I′: monotonic, II′: oscillatory, III′: Bando wave and second shock wave, IV′: Bando wave, plateau and dispersive tail, VI′: purely dispersive; DT: decelerating traffic (Fig. 5.2); the wave phenomena are equivalent to decelerating traffic apart from a missing region V′ analogous to region V in Figs. 5.2 and 5.4.

transformation. By subtracting the governing equations (5.1.1) for two adjacent cars $n+1$ and n, say, we obtain the equation for the n-th headway

$$\ddot{b}_n = a\left[V_B(b_{n+1}) - V_B(b_n) - \dot{b}_n\right]. \tag{5.2.5}$$

For the OV function Eq. (5.1.2), this equation is invariant under the transformation

$$b' = 4 - b. \tag{5.2.6}$$

As a consequence, the wave profiles are symmetric about $b = 2$, and this relates accelerating and decelerating traffic. The Figs. 5.5 and 5.6 showing the variety of the wave types associated with accelerating traffic, are simply derived by reflecting the diagrams Figs. 5.2 and 5.4 at the point (2.0/2.0). Here, the dispersive region V' only appears for higher values of a (Fig. 5.6), because its upstream headway would be negative and, hence, meaningless (Fig. 5.5). Similarly, we discover the same types of transitions, and the disappearance of Bando waves and plateaus for sufficiently high a.

For any given OV function, there is not necessarily a transformation similar to (5.2.6) that correlates accelerating and decelerating traffic. Accordingly, the phase diagram for accelerating traffic may not be determined by easy means as in this section.

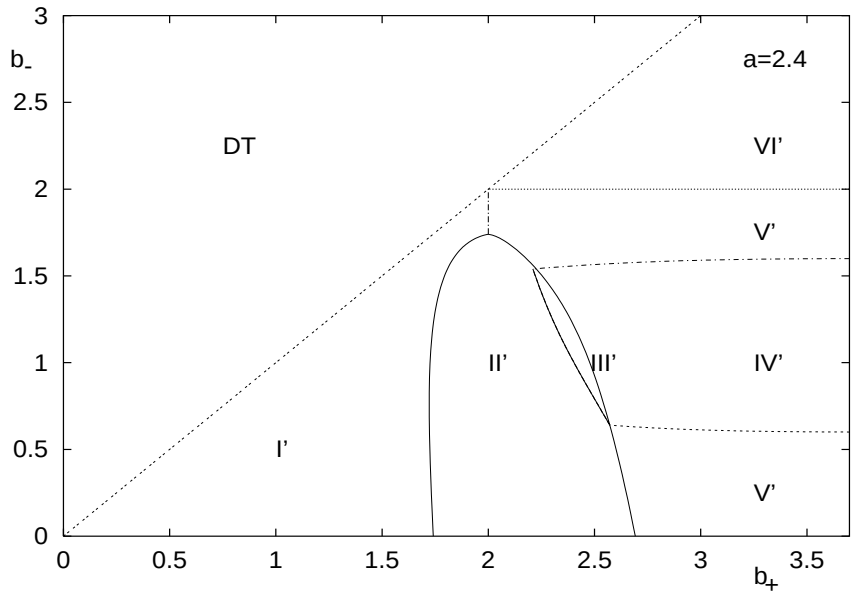

Figure 5.6: Transitions for accelerating traffic ($a = 2.4$): again, with increasing sensitivity, regions III$'$ and IV$'$ shrink until they vanish. Similarly, region V$'$ spreads out between region IV$'$ and VI$'$, and eventually takes the place of region IV$'$.

However, we can still expect it to be qualitatively similar to the reflected image of the phase portrait of decelerating traffic as shown here, even though it might have quantitative deviations.

5.2.3 Fastest Wave and Bando Wave

For any given upstream headway b_-, the model predicts a fastest travelling wave; this can be identified from the fundamental diagram.
For a headway b_-, equivalent to a density $\rho_- = 1/b_-$, the downstream density of the fastest wave is given by the extremum of the wave speed Eq. (5.2.4). Setting the first derivative to zero $c'(\rho_+) = 0$, and excluding $\rho_- = \rho_+$ leads to

$$q'(\rho_+) = \frac{q(\rho_+) - q(\rho_-)}{\rho_+ - \rho_-}, \tag{5.2.7}$$

which can be solved numerically for any OV function V_B. Equation (5.2.7) defines the maximum speed as the point where the chord $\rho_- \to \rho_+$ and the tangent at ρ_+ are identical. It does not necessarily mean that this travelling wave exists, since the transition can also occur as a dispersive wave, for example.
In Fig. 5.3, we choose $b_- = 3.0$ and find the fastest wave possible as the tangent of this point onto the flow curve. The downstream headway $b_+ = 1.54$ of the fastest wave corresponds to a density $\rho_+ = 0.65$. We can see now that, as a increases, the

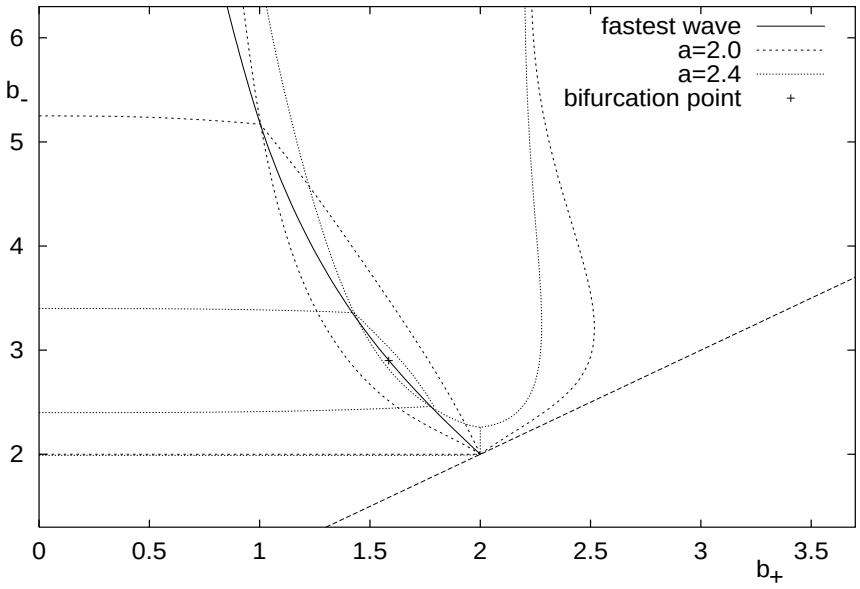

Figure 5.7: For a given upstream headway b_-, the fastest wave theoretically possible is either not accessible or just for two cases, Bando waves. Otherwise it is either part of region III (Bando wave) or of the dispersive domains V and VI.

headway jump, at which the oscillatory travelling wave (region II) is replaced by the Bando wave (region III), approaches the headway jump associated with the fastest wave. Similarly, the headway jump, at which the Bando wave (region III) is replaced by region IV, also approaches the headway jump associated with the fastest wave. This is consistent with the shrinkage of region III.

The curve of maximum speed Eq. (5.2.7) can now be added to the diagrams Figs. 5.2 and 5.4, which yields Fig. 5.7. It shows that for values $2.0 \leq a \leq 2.43$, there are only two points where the fastest wave exists, and these are the vertices of region III. Otherwise, they are either part of the dispersive regimes V and VI or of the Bando wave regime III. In the latter case, the solution jumps on to the slower Bando wave. However, for values of a greater than the bifurcation point $a = 2.43$, region III disappears and there are no Bando waves in the system. Then, the fastest waves predicted by the fundamental diagram lie entirely in the dispersive regions V and VI.

We conclude that in the stable regime $a \geq 2.0$, the fastest wave predicted by the fundamental diagram can only be found for two cases, which correspond to the vertices of region III, the Bando wave regime. Since this region disappears for large a, no fastest wave which is theoretically possible can be found for highly stable traffic, $a > 2.43$.

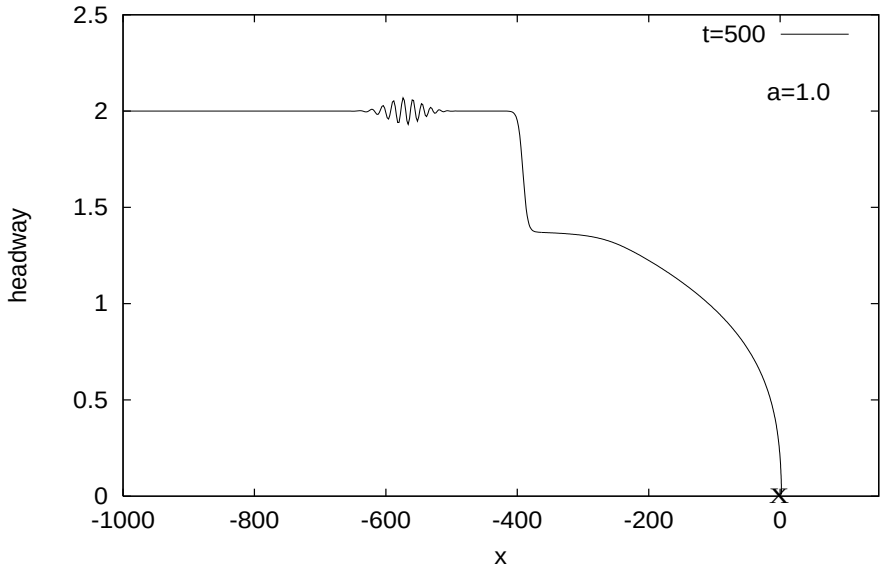

Figure 5.8: Onset of instability: wave profile after $t = 500$ and $a = 1.0$ for an initial ($t = 0$) jump at $x = 0$ from $b_- = 2.0$ to $b_+ = 0$.

5.3 Stable and Unstable Flow Patterns

In this section, we show that the jam fronts of stop-and-go traffic correspond to two specific Bando wave solutions in the unstable regime.

Holland [39] investigated the plateau effect for unstable flow $a < 2.0$. This can be discovered by setting up special road conditions, as illustrated in Figs. 5.8 and 5.9. The first figure exhibits how an initial steady flow of uniform headway, $b_n \equiv 2.0$ at $t = 0$, evolves if the leading car approaches red traffic lights (X), and decelerates until it comes to a standstill at $x = 0$. The wave profile of Fig. 5.9 evolves from the same initial conditions, but now the leading car accelerates at $t = 0$ and $x = 0$, from $v_{n=1}(t = 0) = V_B(b = 2)$ to maximum speed $v_{n=1}(t \to \infty) = V_B(b \to \infty) = 1.96$. This simulates the end of a temporal speed limit along a motorway. At $a = 1.0$, the model is unstable for $b = 2.0$ and after $t = 500$, the oscillations in the platoon mark the onset of traffic breakdown. However, we can already observe the plateau effect. Now one can set up a map $b_{bw}(b_-)$, say, which specifies the plateau headway as a function of the upstream headway, for both accelerating and decelerating traffic. It turns out that the qualitative difference between the maps of the stable ($a \geq 2.0$) and unstable ($a < 2.0$) regimes is significant, as shown in Fig. 5.10. The line $4 - b_+$ that represents the invariance of Eq. (5.2.5) under the transformation (5.2.6), cuts the curve of the Bando waves only for $a < 2.0$. The intersections tell us how to fit Bando waves for accelerating and

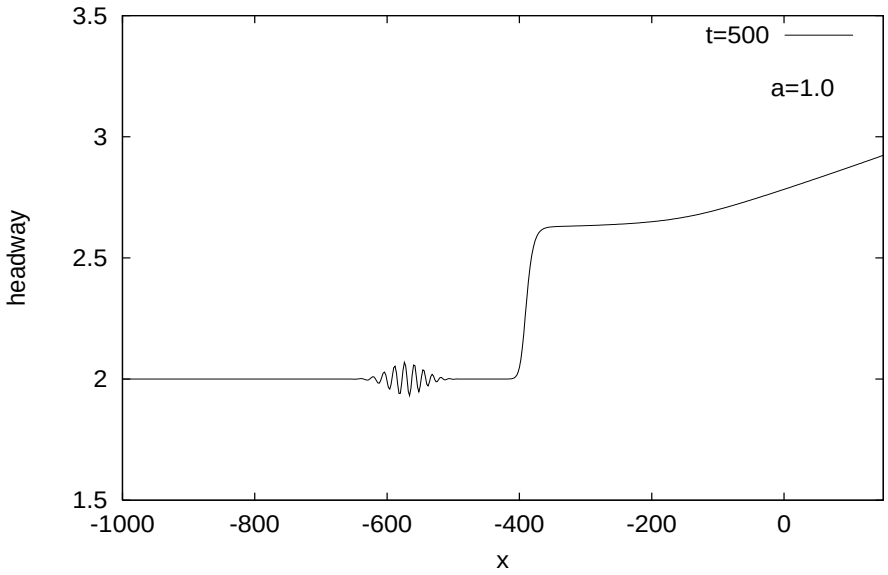

Figure 5.9: Onset of instability: wave profile after $t = 500$ and $a = 1.0$ for a freely accelerating vehicle at $x = 0$ and $t = 0$ from $b_- = 2.0$.

decelerating traffic together, to obtain the travelling jam fronts of stop-and-go traffic. Starting with an arbitrary headway b_-, of decelerating traffic for $a = 1.0$, the map gives the corresponding headway b_+ of the plateau and hence the Bando wave. Now using this as the new headway b_- for accelerating traffic, we obtain the corresponding headway for the next Bando wave. Therefore, the curve defines recursive maps $b_+ = f(b_-)$ and $b_- = \bar{f}(b_+)$, say, for decelerating and accelerating traffic, respectively. Iteration leads to two fixed points, which correspond to the intersections with $4 - b_+$, and this gives the stop-and-go pattern for $a < 2.0$. For $a \geq 2.0$, there are no fixed points and hence no jam front pattern. This may be understood, because the flow is stable and no flow breakdown appears.
Moreover, the asymptotic behaviour of the curve $a = 2.0$ suggests that the fixed points are a linear function for $a \lesssim 2.0$. In fact, for an OV function Eq. (5.1.2), Komatsu's [52] results reveal that the jump Δb of headway across the wave front near $a = 2$ can be approximated by [39]

$$\Delta b = 1.581\sqrt{1 - 0.5a}. \tag{5.3.1}$$

This analysis shows that Bando waves define one class of solutions for the stable and the unstable regime, in which plateau effects can also be found for various upstream headways. However, when the instability sets in, eventually only two specific solutions of this class are picked out and evolve: the stable, nonlinear stop-and-go waves. This establishes a link between Bando waves and the work of Bando

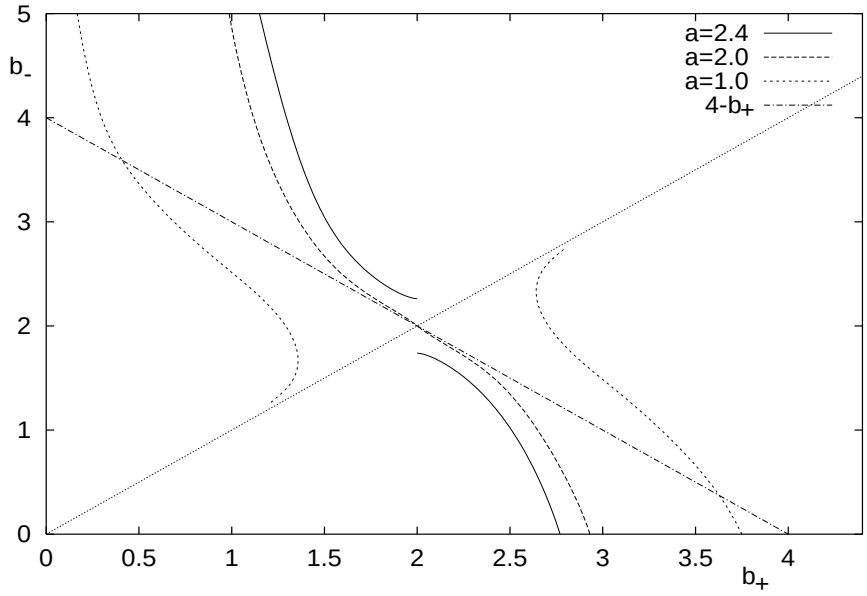

Figure 5.10: Phase diagram of the Bando wave for different sensitivities a. Only for $a < 2$ can they be fitted together to yield the typical jam fronts of unstable flow.

et al [8, 4].

5.4 The Metastable Regime

In the last section, we have linked the nonlinear Bando wave to the fronts of traffic jams in the unstable regime. We can also show that there is another analogy between this wave type and former results of traffic flow simulations.
Kerner [48] found that his model contains a *metastable* regime of the density, in which an initial homogenous, uniform and linear stable flow may become unstable under a sufficient perturbation of finite amplitude. This region of nonlinear instability is adjacent to the unstable region with respect to density, and the critical amplitude of the perturbation increases when moving away from the linearly unstable region. When perturbed sufficiently, the system shows the cluster solution similar to Fig. 2.6. This is not to be confused with the metastable states that the same author observed in traffic data (section 2.1). Here, we deal with a theoretical result of traffic models. However, in full accordance with Kerner's results, there are two metastable regimes in the car-following Bando model. Choosing the sensitivity to be $a = 1.5$, for example, the headway range can be divided correspondingly into

$$b^1_{ms}...b^2_{ms} = 1.45 = b^1_{us}...b^2_{us} = 2.55 = b^3_{ms}...b^4_{ms}, \tag{5.4.1}$$

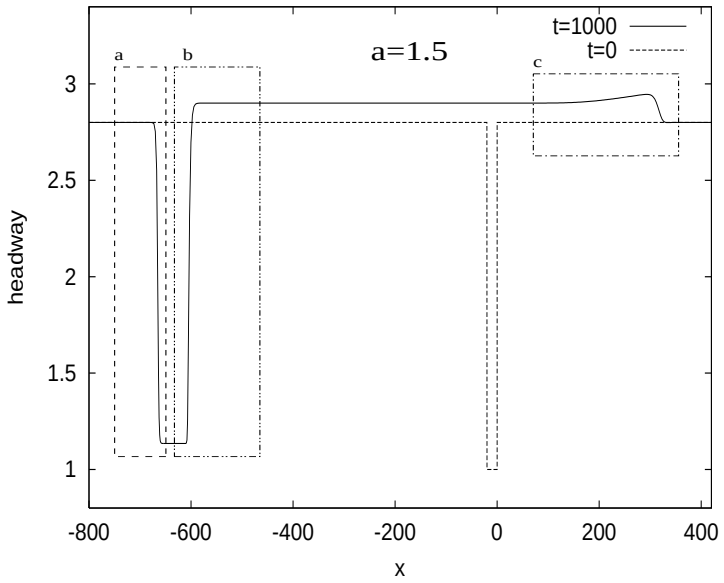

Figure 5.11: The cluster formation in the metastable regime. It consists of two Bando waves (a,b) and another shock wave (c), which matches the downstream headway.

where b^1_{ms} and b^2_{ms} are the boundaries of the metastable region adjacent to the left of the unstable region, whose boundaries are given by b^1_{us} and b^2_{us}. Accordingly, b^3_{ms} and b^4_{ms} are the boundaries of the metastable region adjacent to the right of the unstable region.

If we start from an initial headway distribution as illustrated in Fig. 5.11 for $t = 0$, we can observe cluster solutions ($t = 1000$) for sufficient perturbations. They consist of two growing regions of higher and lower headways, respectively, with respect to the original perturbed headway $b_0 = 2.8$. These regions are connected by three shock waves. A closer examination reveals that the first two, a and b, are actually Bando waves, whereas the latter, c, turns eventually into a shock wave of region I. The structure is fully determined by the original headway due to the unique selection of the Bando wave a and in turn b. The "state" can only be "excited" when there is a sufficient perturbation, so that the solution can lock on to the Bando wave a and accordingly b. Since this solution type is also found in the dimensional Kerner-Konhäuser model (next section), it suggests that it might be a general feature of a traffic model whose fundamental diagram contains a point of inflexion, as well as a linearly unstable and metastable regime.

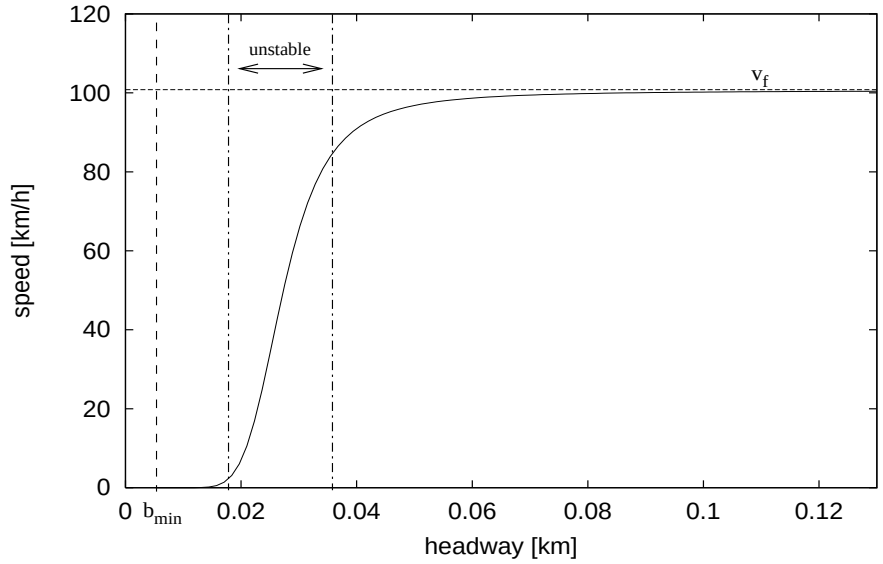

Figure 5.12: The optimal-velocity function $\bar{V}_{kk}(b)$ of the Kerner-Konhäuser model. The flow is unstable for headways 18m $< b <$ 36m. The parameter b_{min} is the average space that cars occupy in a standstill.

5.5 Comparison with other OV Functions

It is of interest to examine whether similar types of transitions occur for other OV functions. This might support the idea that the wave types found in section 5.2 are an intrinsic feature of car-following models with relaxation terms based on an OV function.

Hermann and Kerner considered a Bando type model based on traffic data that does not depend on individual vehicle characteristics and, therefore, averages over all cars to obtain a dynamic equation of the form [38]

$$\dot{v}_n = \frac{1}{T}\left[\bar{V}_{kk}(b_n) - v_n\right], \tag{5.5.1}$$

with an OV function $\bar{V}_{kk}(b_n) = V_{kk}(1/b_n)$ and parameters as in section 3.5.

In comparison to the Bando model, there are three major features which are important: firstly, the speed is only positive for headways bigger than b_{min} (Fig. 5.12) and by analogy, the flow is only positive for densities smaller than ρ_{max} (Fig. 5.13); and secondly, the flow is unstable in a regime $b_{c_1} \approx 18\text{m} < b < 36\text{m} \approx b_{c_2}$. These two features are different from the stable Bando model. On the other hand, one feature that the models have in common is that the flow has a point of inflexion, and this seems to be important for travelling waves, as discussed above in more detail.

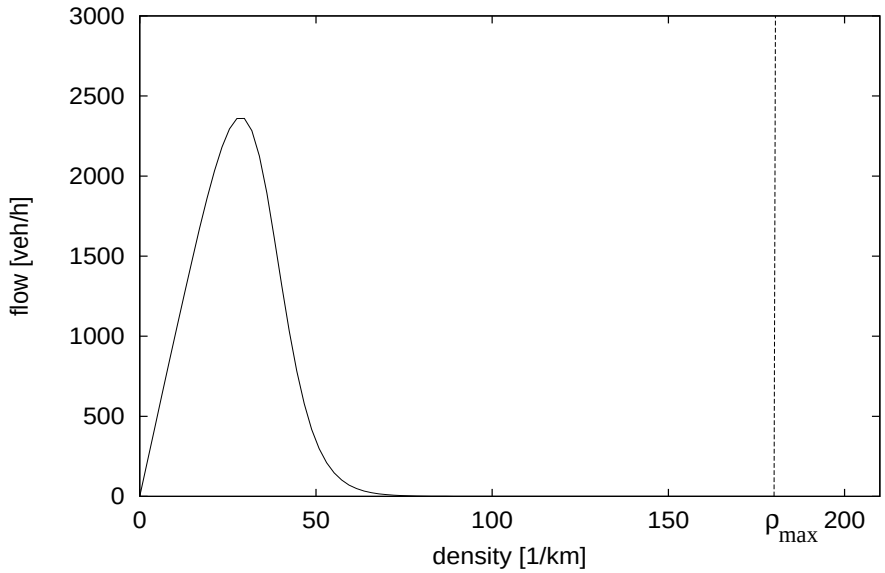

Figure 5.13: Fundamental diagram: the flow vanishes for standstill jams (ρ_{max}). The curve contains a point of inflexion like the Bando model.

Figure 5.14 shows how linearly unstable platoons of cars with headways of 35m and 30m, respectively, merge. After 500 seconds, the flow consists of clusters of vehicles with rapidly oscillating headways, which are followed by the stable jam pattern of stop-and-go traffic between -6km and -2km. The headways of the latter, 48m and 12m, respectively, are not symmetric around the point of inflexion $b_{tp} \approx 26$m ($q''(1/b_{tp}) = 0$) any more, since the corresponding dynamic equation (5.2.5) for the headways is not invariant under an appropriate transformation analogous to Eq. (5.2.6).

However, this system contains Bando waves for suitable up- and downstream headways, as shown in Fig. 5.15. This nonlinear wave is formed very rapidly from the initial conditions, and the Bando wave already appears before the flow becomes unstable and breaks down. Bando waves can also be found for smaller stable upstream headways, as long as the downstream headway remains stable.

In a more detailed numerical study, we found most types of transitions of the stable regime as classified in section 5.2, with the exception of the oscillatory (region II) solutions. This wave type could not be reproduced, even though it is observed in stable traffic flow. An explanation for this discrepancy between the model predictions and the data may be that it is necessary to introduce time delay explicitly into the dynamic equations, regardless of whether they are continuum or car-following models.

In this analysis, the oscillatory waves might not occur since they lie in the unstable

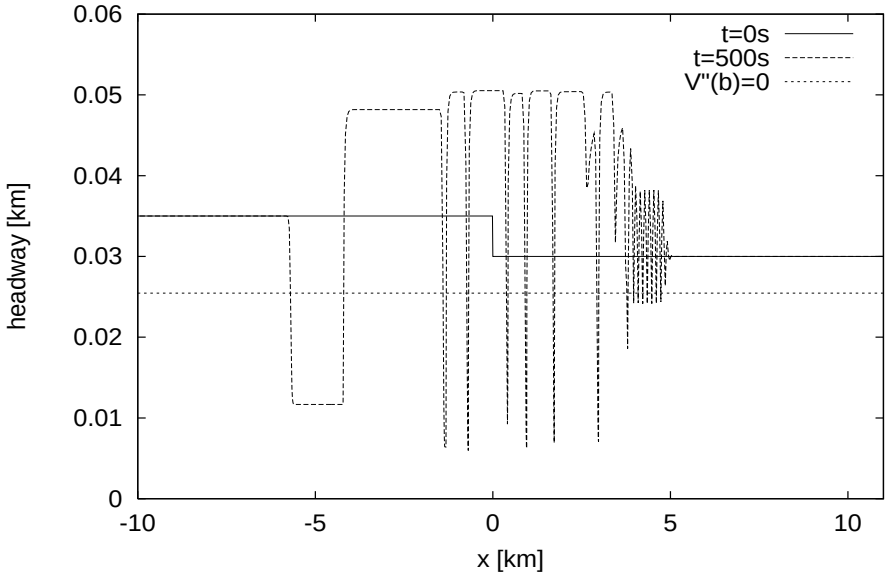

Figure 5.14: The evolution of an initial jump in headway in the unstable regime. The typical jam cluster forms at the tail.

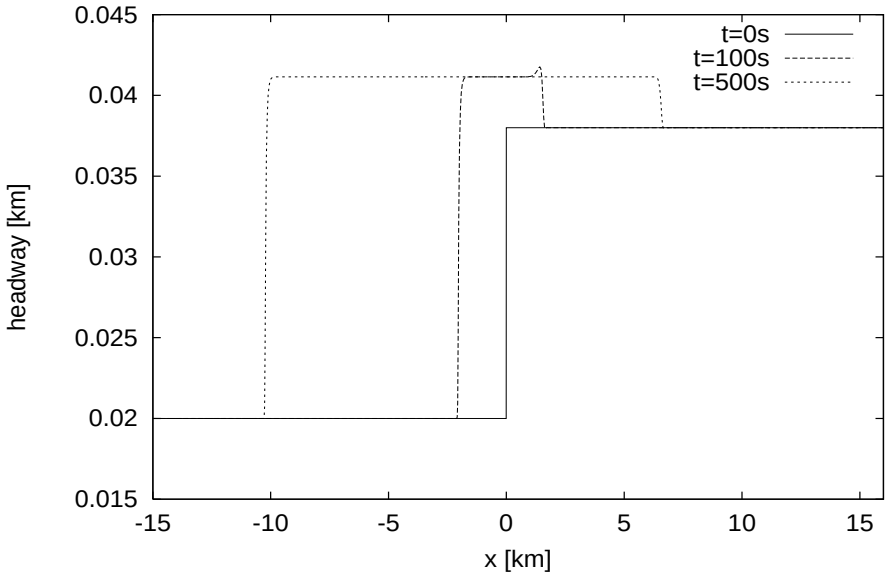

Figure 5.15: Cars can adjust from an upstream to a downstream headway via a Bando wave, even though parts of the headways involved in this transition are unstable.

region.

5.6 Periodic Boundary Conditions

The results presented so far refer to a step-function as an initial condition (Fig. 5.1). It is of interest to know how the profile evolves in the case of periodic boundary conditions. This can be considered either as a train of density pulses along an infinitely long road or as one density pulse on a circular road.
The latter case was investigated by Nagatani [66]. He studied the relaxation process from nonuniform stable flow to uniform steady flow in freely moving traffic on a circular road. Initially, there are two density regions connected by kink-antikink waves. As time evolves, the density profile assumes a triangular shock wave solution whose amplitude decays with time, similar to Fig. 3.15. This solution can be described by a Burger's equation, derived from the original optimal-velocity model Eq. (5.1.1) in the stable regime.
However, a triangular shock wave solution also arises from an initially uniform flow on a straight road that is disturbed by a pulse-like density variation, as illustrated in section 3.7. This shows that, unless we are in the metastable or unstable regime [38], stable wave structures can only be found on straight roads for different values of the upstream and downstream headways ($b_- \neq b_+$). For periodic initial conditions or periodic boundary conditions, as on circular roads, the wave profile eventually assumes a steady uniform flow solution.
This can be explained in the phase diagrams Figs. 5.2 and 5.5. We consider two step functions connecting regions of two different headways, say, b_{high} and b_{low}, as initial conditions. This means that the profile exists of wave solutions (b_{high}, b_{low}) and (b_{low}, b_{high}), respectively, corresponding to two points in the diagrams Figs. 5.2 and 5.5. It can be seen from those that at least one of these two points lies in one of the dispersive regimes. It is not possible to connect a monotonic or oscillatory wave to another one and thus to obtain a stable wave structure. Therefore, dispersion is inevitable, and the wave profile eventually approaches the steady uniform flow solution.

5.7 Multi-species Flow

The advantage of discrete car-following models compared to continuum models shows, when different vehicles on the road are simulated. Clearly, one has to expect new effects, as the impact of a lorry on an autocade of identical cars suggests [61].
Using the Bando model, there are two ways to simulate varying vehicle characteristics: introducing functions a_n for the sensitivity or for the OV function V_n,

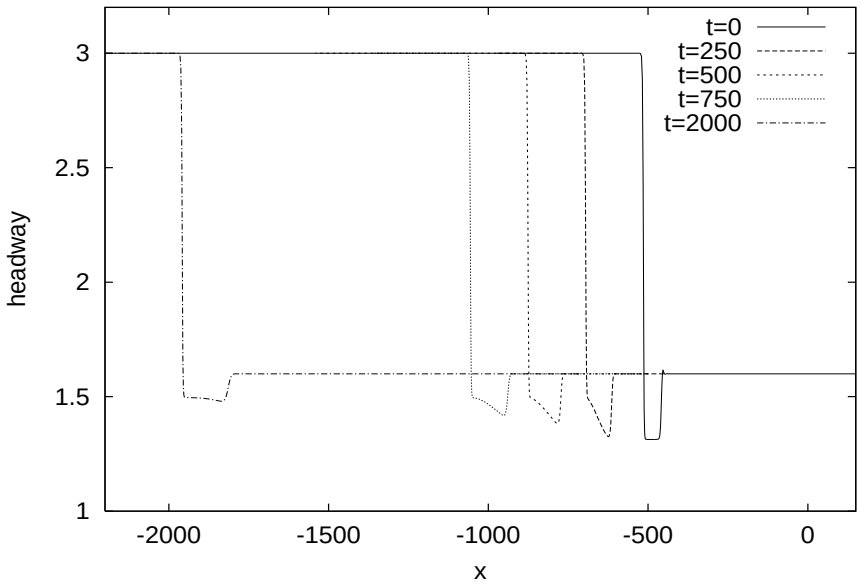

Figure 5.16: Initial ($t = 0$) Bando wave for $a = 2.0$, followed by a convoy of cars with higher sensitivity $a = 2.4$. The Bando wave changes shape but neither dissolves nor assumes an oscillatory shape, as expected from Fig. 5.2.

depending on the vehicle number. Here, we restrict ourselves to varying only the sensitivity a. This is because we can then interpret numerical results by using the diagrams Figs. 5.2, 5.4, 5.5 and 5.6.

By contrast, a continuum model now contains an additional differential equation for the sensitivity, and is more difficult to simulate numerically. The sensitivity $a(x,t)$ must be a function of space and time, since it has to move with the cars and, hence, the flow. As an example, we consider the analogous continuum version of the discrete Bando model. In addition to the coupled, first-order, partial differential equations (PDE) for the density ρ and the speed v

$$\rho_t + (\rho v)_x = 0, \tag{5.7.1}$$

$$v_t + v v_x = a\left[\bar{V}(\rho) - v\right] + a\bar{V}'(\rho)\left[\frac{\rho_x}{2\rho} + \frac{\rho_{xx}}{6\rho^2} - \frac{\rho_x^2}{2\rho^3}\right], \tag{5.7.2}$$

we also obtain a PDE for a. It must be a constant for each car, and we simply find

$$\frac{d}{dt}a(x,t) = a_t + v a_x = 0. \tag{5.7.3}$$

The flow is then determined by the initial conditions

$$\rho(x,0) = \rho_0(x)\ ,\ v(x,0) = v_0(x)\ ,\ a(x,0) = a_0(x). \tag{5.7.4}$$

For slowly varying sensitivities across the autocade, and in the limit of small changes in headway, this model is an accurate first-order approximation to the discrete ver-

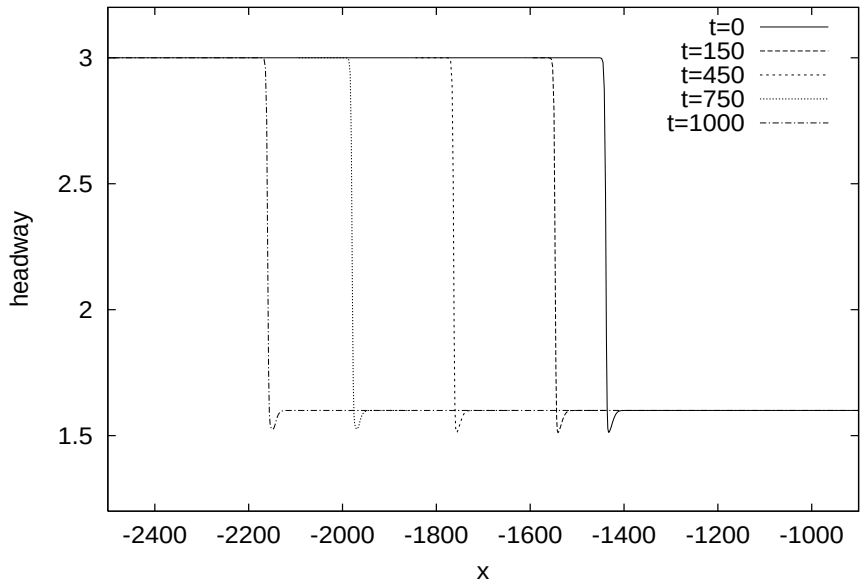

Figure 5.17: Evolution of a transition from $b_- = 3.0$ to $b_+ = 1.6$ with a varying sensitivity $a_n = 2.4 + 0.2\sin(2\pi n/100)$: shape remains oscillatory.

sion. For randomly distributed sensitivities and rapidly changing headways as in real traffic flow, however, the solutions increasingly diverge from this model.

As a classic example, we now consider a single truck of sensitivity a_{tr}, surrounded by cars of sensitivity a_c. Even if the convoy is of almost uniform density and speed, the gradient of the sensitivity $\frac{d}{dx}a(x,t)$ in the continuum picture can be very large near the truck, if the distance to its neighbouring vehicles is small. Even for this simple case, the continuum model will fail to reproduce an appropriate picture of the actual traffic events.

In what follows, we varied the sensitivity as a function of the car-number n in a sinusoidal form

$$a_n = a_0 + \epsilon \sin(2\pi n/N), \tag{5.7.5}$$

and investigated how travelling waves change with time in the car-following Bando model. Even though it seems to be an unrealistic and very special distribution, it reveals that the system can go through an unexpected phase transition: once it has switched to the Bando wave, it does not necessarily assume its initial wave solution again (an oscillatory transition for instance) that corresponds to the average sensitivity a_0. Whether a phase transition occurs or not depends in a complex manner on the parameters a_0, ϵ, n and N.

Figure 5.16 shows an initial Bando wave ($t = 0$) for $a = 2.0$. For $t > 0$, the sensitivity of the upstream cars is constant at $a = 2.4$. From Fig. 5.4 ($a = 2.4$,

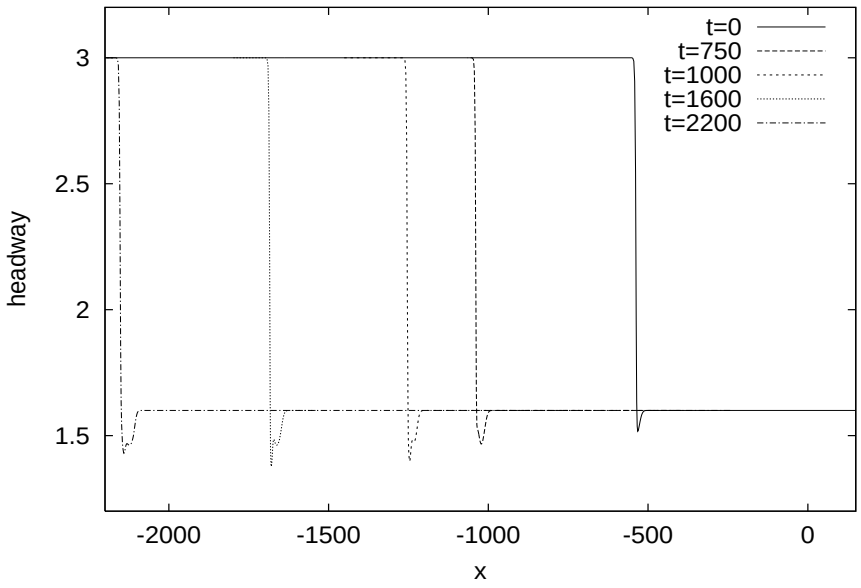

Figure 5.18: Evolution of a transition from $b_- = 3.0$ to $b_+ = 1.6$ with a varying sensitivity $a_n = 2.4 + 0.4\sin(2\pi n/100)$: Bando wave forms.

$b_- = 3.0$, $b_+ = 1.6$), we should eventually expect an oscillatory transition, rather than a Bando wave. However, once the system has assumed this solution consisting of two waves, it cannot return to its initial state, simply because the waves keep going at different speeds. Thus, they do not merge into the state shown in its corresponding diagram. Only the plateau, the intermediate headway, changes its value.

Figures 5.17 and 5.18 give examples of how such a phase transition might occur. The first represents the steady state solution ($t = 0$) of a transition from $b_- = 3.0$ to $b_+ = 1.6$ at a sensitivity $a = 2.4$. For $t > 0$, the sensitivity of the upstream cars varies as in

$$a_n = 2.4 + 0.2\sin(2\pi n/100). \tag{5.7.6}$$

One cycle contains 100 cars, and its mean is obviously $a_0 = 2.4$. After $t = 1000$, we still find an oscillatory transition, even though the stream of cars contains sensitivities analogous to a Bando wave. However, their percentage of the whole cycle is simply not sufficient to switch the state to this nonlinear wave.

This changes if we increase the amplitude in Fig. 5.18 to

$$a_n = 2.4 + 0.4\sin(2\pi n/100). \tag{5.7.7}$$

It still gives the same mean $a_0 = 2.4$, but a higher variance

$$\Delta_a = \frac{1}{100}\sum_{n=0}^{100}(a_n - a_0)^2 \tag{5.7.8}$$

and, hence, a higher percentage of those sensitivities which correspond to a Bando wave. Now there is enough time during a cycle to form a sufficiently wide gap between this wave and its corresponding downstream shock wave that it does not dissolve during the next cycle. Therefore, a growing gap of varying shapes forms that leads to an increase in travel time. An analogous situation appears for accelerating traffic, which results in a decrease in travel time.
These few examples show already that a small fraction of vehicles can cause a phase transition in traffic flow. For randomly distributed sensitivities among the vehicles, the mean a_0 and the variance Δ_a seem to be the two decisive variables in the system that determine what state it will most likely assume eventually. Varying sensitivities might, therefore, explain effects of traffic flow, which have not been reproduced with constant sensitivity a and constant OV function V yet. This stochastic approach delivers plenty of problems and questions for future work.

A final note: another approach to modelling different vehicles in a continuum picture is that the density becomes a N-dimensional vector $\vec{\rho}(x,t)$, where N corresponds to the number of different types of vehicles. The conservation of cars now reads

$$\rho_t^{(i)} + \left(v^{(i)}\rho^{(i)}\right)_x = 0. \tag{5.7.9}$$

In contrast, the dynamical equation has to couple all densities in a complicated multi-dimensional model

$$v_t^{(i)} + v^{(i)}v_x^{(i)} = \frac{1}{T_i}\left[V_i(\vec{\rho}) - v^{(i)}\right] + A_i(\vec{\rho})\rho_x^{(i)} + B_i(\vec{\rho})\rho_{xx}^{(i)} + \dots\ . \tag{5.7.10}$$

This model would be far more complicated than one additional PDE (5.7.3) which takes the variation of the sensitivity along the platoon into account.

5.8 Impact on Bottlenecks and Autonomous Cruise Control Systems

The effects we have discovered have significant implications for speed limits and bottlenecks. They predict that for certain jumps of headway, determined by either of these measures, the traffic flow locks on to a nonlinear wave. The bottleneck determines the downstream (upstream) headway, whereas the type of transition that evolves also depends on the flow further upstream (downstream). The most desirable transition in a bottleneck is the monotonic type. Oscillatory waves cause rapid braking and acceleration, which leads to higher fuel consumption and dangerous traffic situations. The same applies to Bando waves which, in addition, contain a congested region. Therefore, it might be of greater use to set up bottlenecks and speed limits stepwise along the road, depending on the upstream traffic situation.

Each stretch decreases the speed by a moderate and monotonic transition. This can be a safer and more stable method than a localized large decrease in velocity at a speed limit.
This has to be taken into account when implementing ACCS. The main goal of this application is to couple cars in a convoy by electronic control of their speed and acceleration by an algorithm based on a car-following law. This should result in a stable autocade of high safety and flux [77]. However, the major problems of convoy driving are the merging of cars at on- and off-ramps or at lane merging, and the adjustment to bottlenecks and speed limits. All these road features have an impact on the autocade by changing the density of cars locally. From our analysis, we expect transitions between these regions of different headways, travelling up- or downstream along the road. The aim of any control algorithm would be to avoid oscillatory and Bando waves.
As shown in the last section, it only requires a few cars of a multi-species convoy to cause phase transitions in the system, which lead to time delays and harsh braking manoeuvres. The wave type that evolves (monotonic, oscillatory, Bando wave, etc) depends on the composition of the vehicles with regard to their control algorithms. In a multi-species flow, these vary from car to car. It is, therefore, harder to predict what implications a given speed limit or bottleneck might have on a stream of different vehicles. However, the accuracy of the predictions increases when the control algorithms converge.
Speed limits which vary with time can be regarded as a changing bottleneck. They can be adjusted to the current upstream traffic situation. However, there are bottlenecks which have static characteristics such as maximum speed and throughput, given by the road layout, for example. In this case optimal safety, stability and flux might be obtained by dynamic algorithms, which adjust to the downstream bottleneck situation. In-vehicle information of the oncoming traffic situation, as realized by mobile technology or beacons along the road, could deliver the required data.

5.9 Travelling Waves in the Continuum Model

[1]So far, the analysis of the transition types has been carried out in the car-following model. The most important aspect has been the question of whether one travelling wave or another transition structure forms, once the up- and downstream conditions ρ_- and ρ_+ are given. Here, the change from an oscillatory wave type to the Bando wave is of particular interest. As already mentioned, this occurs in the continuum model, when the integration of Eq. (3.4.12) breaks down, and it is this instability

[1]This section contains work that was mainly carried out by and in cooperation with Wilson [87]. It should only be regarded as a brief overview of the continuum analysis of the transition types.

that we will investigate in the following.
If we rewrite Eq. (3.4.12) in terms of the density by using Eqs. (3.4.11) and (3.4.5), it yields

$$-\frac{q_0^2}{\rho^3}\rho_z = a\left[\bar{V}(\rho) - \frac{q_0}{\rho} - c\right] + a\bar{V}'(\rho)\left[\frac{\rho_z}{2\rho} + \frac{\rho_{zz}}{6\rho^2} - \frac{\rho_z^2}{2\rho^3}\right]. \tag{5.9.1}$$

This can be turned into a system of two coupled first-order ordinary differential equations, if a new variable w is introduced. It is simply given by $w = \rho_z$ and, thereby, transforms Eq. (5.9.1) into

$$\rho_z = w, \tag{5.9.2}$$

$$w_z = F(\rho, w) \tag{5.9.3}$$

$$= \frac{6\rho^2}{a\bar{V}'(\rho)}\left\{a\left[\frac{q_0}{\rho} + c - \bar{V}(\rho)\right] - \frac{q_0^2}{\rho^3}w\right\} + \frac{3w^2}{\rho} - 3\rho w. \tag{5.9.4}$$

For any boundary conditions ρ_- and ρ_+, which also deliver the speed c of the travelling wave (if it exists), this system can be linearized around the up- and downstream densities, ρ_- and ρ_+, respectively. An analysis of the phase space of ρ and w and its fixed points then reveals the qualitative shape of the travelling wave, or that it does not exist, but it does not reveal if the travelling wave is stable.
As an example, we consider a wave that connects an upstream density ρ_-, with a downstream density ρ_+^1, as illustrated in Fig. 5.19a[2]. The chord and its gradient represent a travelling wave solution and its speed, respectively. Note that there is a second intersection of the chord with the flow curve and, therefore, a second potential travelling wave with the same wave speed, connecting ρ_- and ρ_+^2. As shown earlier on, when ρ_+^1 moves along the flow curve, the solution turns at first from the monotonic into the oscillatory type before it eventually hits the critical density $\rho_+^1 = \rho_{crit}$, where it locks on to the Bando wave ($\rho_{bw} > \rho_+^2$).
These transitions are explained by the phase space diagram (Fig. 5.19b) of these solutions without a more detailed discussion of the underlying algebra. Roughly speaking, monotonic waves of region I exist when the central state is a stable node and the left hand saddle connects to it. Oscillatory waves of region II form when the central state is a stable spiral and the left hand saddle connects to it. Bando waves are connections from the left hand saddle to the right hand saddle. Here, the central state cannot connect to the left hand saddle in the phase space. This is not a generic effect and explains why these waves lie on a line in the (b_+, b_-) plane.
This analysis does not only predict the transition from a travelling wave to a different wave structure; it may also be used to determine the downstream density ρ_{bw}, of the Bando wave. Wilson verified that the values coincide with those of the car-following model with an accuracy of at least 1 per cent, and this method is still part of much

[2]The flow is scaled by a factor of 2 for purposes of illustration.

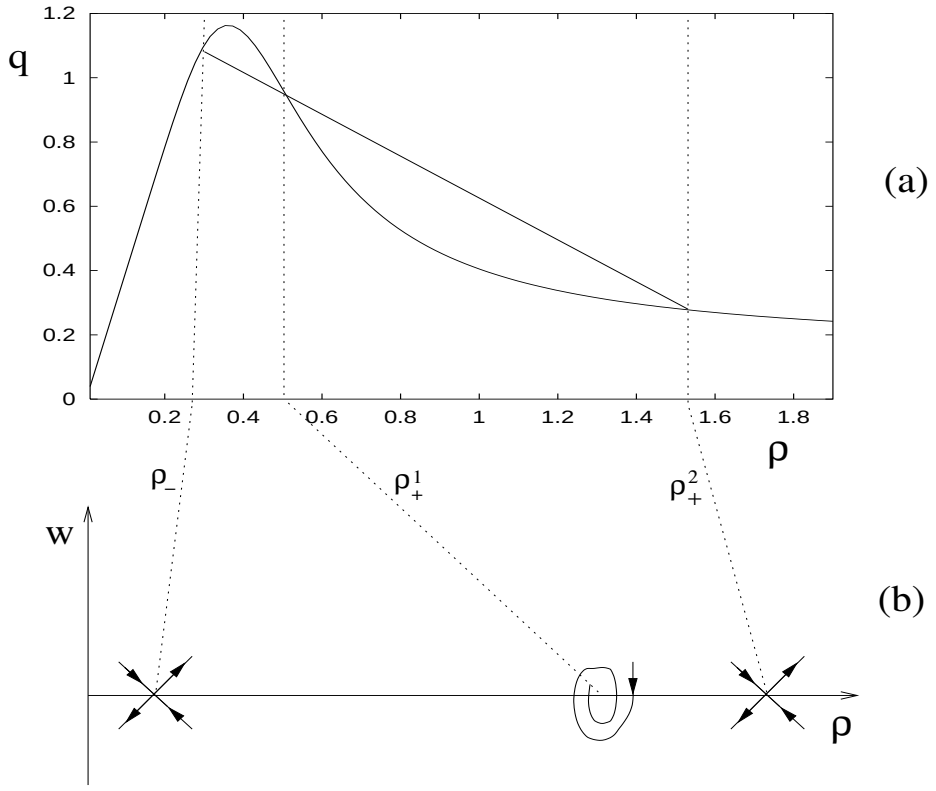

Figure 5.19: a) Scaled fundamental diagram with upstream (ρ_-) and downstream (ρ_+^1, ρ_+^2) densities. b) Phase space diagram of travelling wave solutions: local stability analysis reveals that the upstream state is always a saddle, the centre (downstream) is either a stable node or a stable spiral and the right state (downstream) is always a saddle.

current research [87]. This approach could deliver a much faster method to determine the phase diagram of the transition types like Fig. 5.2 for which no simulation of the flow itself has to be carried out. Moreover, it could also be used to support the idea of Kerner [38] that all traffic flow models with an unstable and metastable regime, as well as a point of inflexion in the fundamental diagram, reproduce similar features. This idea is, therefore, an exciting starting point for future fundamental research.

However, one might argue that infinitely many roots are dropped in the analysis of the local stability of the fixed points when going from the discrete model to the second-order continuum model, and that this method is, hence, not correct. For example, Bevan [15] has shown that a linear stability analysis of Eq. (5.2.5) for the car-following Bando model reveals a delay equation for the downstream headway

perturbation of a travelling wave solution

$$\frac{1}{a}\ddot{b}_n(t) + \dot{b}_n(t) + \operatorname{sech}^2(b_+ - 2)\,[b_n(t) - b_n(t+T)] = 0. \tag{5.9.5}$$

The delay T is given by the up- and downstream headways b_- and b_+, respectively, as follows

$$T = \frac{b_+ - b_-}{\tanh(b_+ - 2) - \tanh(b_- - 2)}. \tag{5.9.6}$$

If we assume a perturbation of the form

$$b_n(t) = A\exp(\lambda t), \tag{5.9.7}$$

it shows that the characteristic equation

$$\frac{1}{a}\lambda^2 + \lambda + \operatorname{sech}^2(b_+ - 2)\,[1 - \exp(\lambda T)] = 0 \tag{5.9.8}$$

has infinitely many roots, of which only two can be positive [15]. The argument that the continuum method nevertheless applies is similar to the agreement of the stability analysis of chapter 3. The continuum and the car-following picture are only analogous descriptions in the limit of small changes of headway. Large gradients do not play an important part in stability analyses, and higher order terms can hence be neglected. This is why the results in both classes coincide.

5.10 Conclusion

We have investigated different types of wave solutions in a stable, optimal-velocity model of road traffic, the car-following Bando model. Once the parameters of the model, the sensitivity and the OV function, are given, the wave types can be represented in a diagram by their up- and downstream headways. There are six possible transitions (Fig. 5.2): monotonic, oscillatory, purely dispersive, Bando wave (a non-generic monotonic travelling wave) plus dispersive tail, Bando wave plus plateau and adjoining dispersive tail, and a Bando wave followed by a second wave.
In the last case, the transitions exist of two monotonic travelling waves of different speeds, with a growing region of congested or free flowing traffic in between. For sufficiently high sensitivities, equivalent to small inertia, the cars react fast enough to the traffic situation, and the wave does not assume this specific solution any more. For these sensitivities, Bando waves and plateaus are not solutions.
For a given upstream headway, the fastest travelling wave predicted from the fundamental diagram is either not accessible, or it only exists for two specific upstream headways in the form of Bando waves. In the first case, its corresponding headways are either part of the dispersive regime or it locks on to a slower Bando wave.

There is a strong connection between Bando waves and travelling jam fronts of stop-and-go traffic of unstable flow. They are analogous, but while Bando waves can be found for various upstream headways for a given sensitivity, these jam fronts are uniquely determined: jam and free flow densities are functions of the sensitivity alone. A similar analysis reveals a correspondence between Bando waves and the clusters of the metastable regimes.
The wave types can be interpreted by the fundamental diagram. The higher the sensitivity, the faster the cars react, and the closer the actual dynamic flow is to the equilibrium flow. However, for small sensitivities, the actual flow may differ significantly from the fundamental diagram. Therefore, an interpretation of the observed transitions is not as straightforward any more.
We have compared our results to another Bando-type car-following model, based on different parameters fitted to traffic data. We have discovered all types of waves apart from the oscillatory transitions, due to the choice of the sensitivity parameter. It shows that the wave types we found may be an intrinsic feature of car-following models with relaxation terms.
The Bando waves play an important role when considering varying sensitivities. Once the system assumes this solution, the growing region of congested traffic between the two waves does not necessarily dissolve when returning to higher sensitivities. Hence, even in a linearly stable system, we can find irreversible phase transitions.
This has to be taken into account when implementing autonomous cruise control systems. The algorithms should be fitted in order to avoid increasing travel times and intense braking manoeuvres. This might be realized by dynamic algorithms, which take the current downstream traffic situation into account.
Finally, we have mentioned that this work, which was carried out in the discrete Bando model, may also be interpreted in its continuum analogue. This does not only save time, it might also be a basis for future research which tries to link various continuum models including a relaxation term. Furthermore, it underlines the thought that traffic models show similar features if they contain an unstable and a metastable density regime as well as a point of inflexion in the corresponding stable fundamental diagram.

Chapter 6

Simulation of an On-ramp in a Car-following Model

Finally, we present an on-ramp simulation of the Bando model, which reveals qualitatively similar results to previous simulations of continuum models carried out by Helbing [32] and by Lee, Lee and Kim [56]. Among various solutions, we discuss the solitary waves in greater detail. They can be approximated by a Kortweg-de-Vries (KdV) equation derived from the analogous continuum version. Hence, this establishes a further link between these two types of traffic simulation, and supports the idea that models of either kind lead to similar predictions when they contain a relaxation term.
Moreover, the results of this chapter uncover some aspects of on-ramps and their impact on the current traffic situation. It might help in implementing controls of the on-ramp flux via traffic lights, for example, which depend on the current flow conditions on the motorway. These systems are already in use at various spots in the Netherlands and Germany, for instance.

6.1 The Model

So far, there have been two attempts to model oncoming vehicles near a ramp. Firstly, Helbing *et al* and Lee *et al* have simulated an on-ramp in their continuum models by introducing a source term to the right hand side of the equation for the conservation of cars

$$\rho_t + (\rho v)_x = q_{in}(x,t). \tag{6.1.1}$$

Secondly, Helbing used a macroscopic model to represent the on-ramp and its vicinity, whereas the remaining stretch of road was simulated by the corresponding microscopic model [30, 80]. Here, the authors leave the question open as to how to

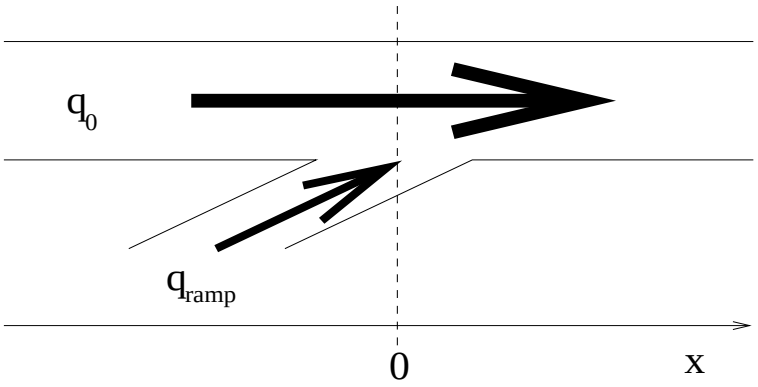

Figure 6.1: A model for the on-ramp.

incorporate the interaction of the two systems near their interfaces.
In contrast to this dual methodology approach, we aim for a direct on-ramp simulation of the discrete Bando model [8]

$$\dot{v}_n = a\,[V_B(b_n) - v_n] \tag{6.1.2}$$

with the monotonic increasing optimal-velocity (OV) function

$$V_B(b_n) = \tanh(b_n - 2) + \tanh(2). \tag{6.1.3}$$

Cars are inserted in an open system ("infinitely" long road represented by 2500 vehicles in the numerical simulations) at $x = 0$, with constant flux q_{ramp} after $t = 0$ (dimensionless running time of programs between 1000 and 2500), as illustrated in Fig. 6.1. Their speed must match the speed of the surrounding cars at the ramp. For $t < 0$, the traffic state consists of equally distributed cars of density $\rho_0 = 1/b_0$ along the road with constant speed $v_0 = V_B(b_0)$. To avoid crashes, vehicles only enter the road if a safety distance d, both to the car in front and behind, is given. It turns out that this is fulfilled in the overwhelming majority of cases.

Since inserting cars at an on-ramp is a discrete process in space and time, the continuum analogue is found by adding a delta function to the right hand side of the equation for the conservation of cars (6.1.1). If the ramp is at $x = 0$ and its flux is constant, it reads

$$\rho_t + q_x = q_{in}(x,t) = q_{ramp}\delta(x)\frac{2}{\omega}\delta[\sin(\omega t)], \tag{6.1.4}$$

where cars are inserted with a frequency $\omega/2$. This equation has clearly no stationary solution, $\rho_t = 0$ and $q_t = 0$, since the right hand side depends on time. This discrete process will be further illustrated by the results of small on-ramp fluxes.
However, if the ramp flux is of a similar order to the upstream flux, or if the system

reacts sufficiently fast to a discrete perturbation caused by the on-ramp, we can expect stationary solutions on a macroscopic scale. In the continuum picture, they correspond to a constant flow q_{ramp} so that Eq. (6.1.4) turns into

$$q_x = q_{ramp}\delta(x). \tag{6.1.5}$$

Integration yields a relation between the upstream, the on-ramp and the downstream flux

$$q_{-\infty} + q_{ramp} = q_{\infty}, \tag{6.1.6}$$

which is another expression for the conservation of cars. A Fourier analysis reveals the shape of q: we write

$$q(x) = q_0 + \frac{1}{2\pi}\int_{-\infty}^{\infty} Q(k)\exp[i(kx)]\,dk, \tag{6.1.7}$$

$$q_{in}(x) = \frac{1}{2\pi}\int_{-\infty}^{\infty} q_{ramp}\exp[i(kx)]\,dk. \tag{6.1.8}$$

$$\tag{6.1.9}$$

Substitution into Eq. (6.1.5) gives

$$\frac{1}{2\pi}\int_{-\infty}^{\infty} ikQ(k)\exp[i(kx)]\,dk = \frac{1}{2\pi}\int_{-\infty}^{\infty} q_{ramp}\exp[i(kx)]\,dk \tag{6.1.10}$$

and, therefore,

$$q(x) = q_0 + \frac{1}{2\pi}\int_{-\infty}^{\infty} Q(k)\exp[i(kx)]\,dk \tag{6.1.11}$$

$$= q_0 + \frac{1}{2\pi}\int_{-\infty}^{\infty} \frac{q_{ramp}}{ik}\exp[i(kx)]\,dk \tag{6.1.12}$$

$$= q_0 + \frac{1}{2\pi}\int_{-\infty}^{\infty} \frac{q_{ramp}}{k}\sin(kx)\,dk \tag{6.1.13}$$

$$= q_0 + \left\{ \begin{array}{rcl} -q_{ramp}/2 & : & x<0 \\ q_{ramp}/2 & : & x>0 \end{array} \right\} \tag{6.1.14}$$

becomes a Heaviside function. This is a rather obvious result, but it does not mean that the density and the velocity jump too. In the latter case, this would correspond to an infinite acceleration or deceleration, whereas in reality, we expect the velocity and the density to assume a continuous profile. It is the discrete on-ramp process that is incorporated into a continuum model, which leads to inconsistencies. Strictly speaking, there are no stationary solutions on the microscopic level.

6.2 Traffic States near On-ramps

We will now summarize the events in the vicinity of an on-ramp for a constant oncoming flow q_{ramp}, which is equivalent to a constant number of vehicles entering

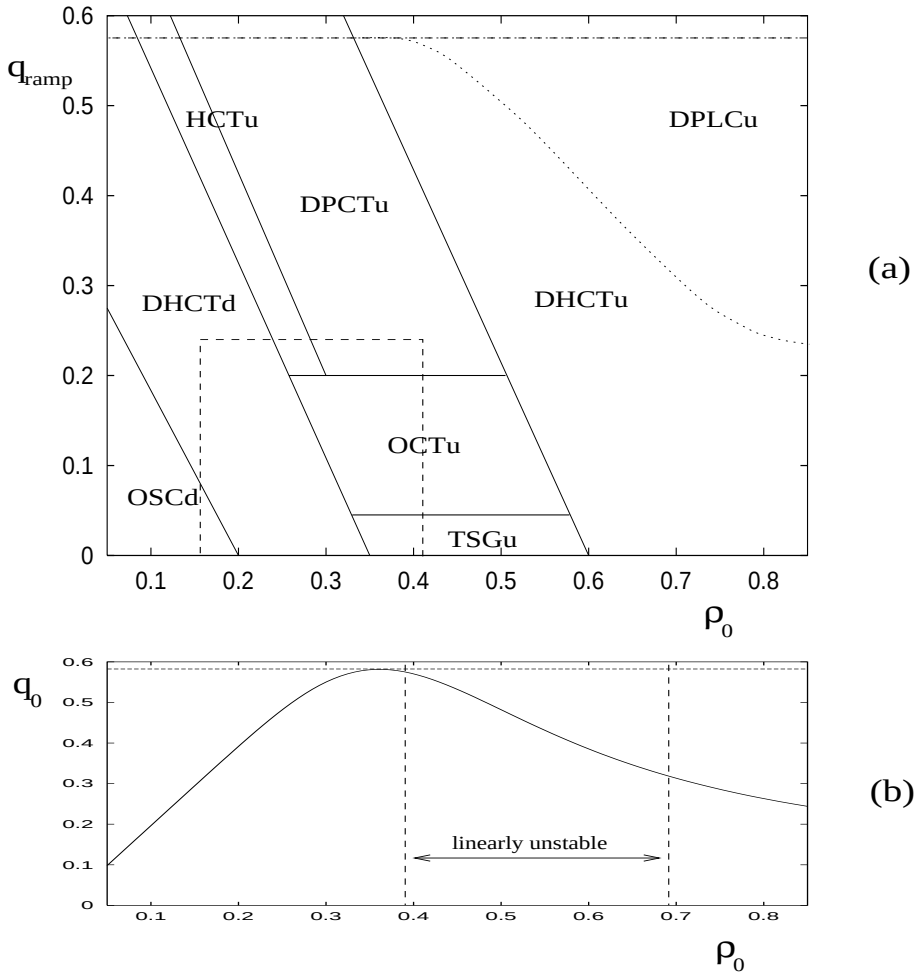

Figure 6.2: a) The traffic states of the on-ramp. The dotted box refers to Helbing's analysis [32]. b) The fundamental diagram for $a = 1.5$, showing the original flow q_0 of density ρ_0 before the on-ramp perturbation sets in, contains an unstable region.

the road per unit time. This might not be particularly realistic, but it gives a first insight into the system, and a foundation for further research regarding time dependent ramp parameters.

To make the simulations a bit more realistic, they are carried out with a *sensitivity* $a = 1.5$ for which the model Eq. (6.1.2) is linearly unstable in a density regime $\rho \in [0.39, 0.69]$. This in turn corresponds to a headway range $b \in [1.45, 2.55]$ (Fig. 6.2b).

Figure 6.2a shows the traffic states that can be found after the on-ramp flux sets in. Depending on the original density ρ_0 and q_{ramp}, we find triggered stop-and-go traffic upstream (TSGu), oscillatory congested traffic upstream (OCTu), homogenous congested traffic upstream (HCTu), "dipole" congested traffic upstream (DPCTu),

dispersive congested traffic downstream (DHCTd) and oscillatory congested traffic downstream (OSCd). These types turn out to be qualitatively the same as in Helbing's continuum model [32], in which the author restricts the analysis to the dotted box shown in Fig. 6.2a. In addition, two more solution types can be revealed when one considers perturbations of highly dense traffic: dispersive homogenous congested traffic upstream (DHCTu), and dispersive peak located congested traffic upstream (DPLCu). It should be mentioned that going from one solution type in the diagram to another is a continuous process. Hence, the lines which separate the regions should not be regarded as phase transitions. Helbing came to the same conclusions, and we will comment on this again later on.
At first sight, it is very surprising that the car-following model reveals the same results as some continuum models. However, in case of the TSGu state, this analogy can be shown explicitly (section 6.3) by using the continuum analogue of the Bando model. In the following, we will discuss all of these types briefly, apart from the TSGu, OCTu and OSCd states, which will be explained in greater detail in sections 6.3 and 6.4. Once again, the fundamental diagram is of great importance in interpreting and classifying the solutions.
Unless otherwise stated, the figures represent the traffic state after $t = 1000$.

6.2.1 Dispersive Homogenous Congested Traffic Downstream (DHCTd)

This solution occurs for various on-ramp flows which perturb a single lane of the free flow regime.
Figure 6.2b shows that the linear wave speed of such a perturbation, the gradient of the fundamental diagram at the corresponding density, is positive. Therefore, as a first-order approach, we can expect information to travel downstream, leaving the upstream headway unperturbed. This in turn results in the profile shown in Fig. 6.3. It contains a jump of headway in the vicinity of the ramp, which is determined by Eq. (6.1.6). The transition back to the original headway further downstream appears as a dispersive wave, as discussed in chapter 5.
The speed varies only gradually across the profile due to the almost constant value of the OV function in this headway regime (Fig. 3.1). Helbing refers to this type as the free traffic state, since the upstream headway is unperturbed, and the downstream flow generally remains in the free flow regime.

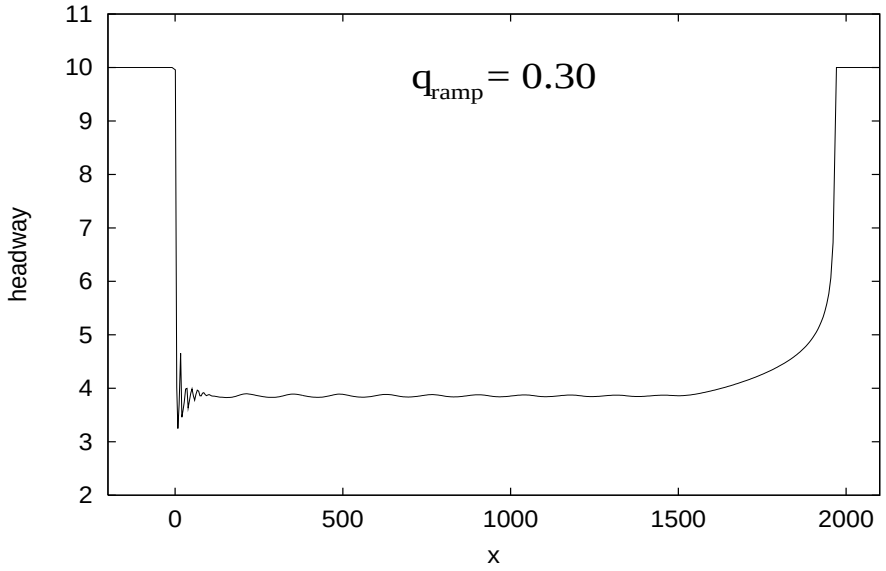

Figure 6.3: Dispersive homogenous congested traffic downstream (DHCTd): the flow jump at the on-ramp is determined by Eq. (6.1.6). The upstream headway remains unperturbed, and the downstream headway is linked to the original headway by a dispersive tail.

6.2.2 Homogenous Congested Traffic Upstream (HCTu)

Adjacent to the DHCTd region, where we find slightly higher ramp flows and original densities ρ_0, the linear wave speed analysis does not apply any longer. The oncoming traffic volume is now too large not to influence the upstream traffic events. The sum of the upstream flow and the ramp flow exceed the maximum flow $q_{max} \approx 0.58$, which leads inevitably to a piling up of cars in front of the ramp.
Another argument is that the downstream density of a DHCTd state would exceed the density of maximum flow $\rho_{max} \approx 0.36$, and the downstream information would travel upstream towards the ramp. This explains why the DHCTd has to vanish eventually, and the HCTu state of Fig. 6.4 takes over.
Now an upstream plateau forms in the vicinity of the ramp, which is linked to the original flow by a shock wave. The jump at the ramp is again determined by Eq. (6.1.6), leaving the question open as to how the downstream headway is selected. In the case of an ideal flow, we could expect that it reacts instantaneously to the traffic situation ($a \to \infty$), so that it assumes the maximum flow downstream of the ramp. All vehicles of the ramp enter the lane and, between these, some of

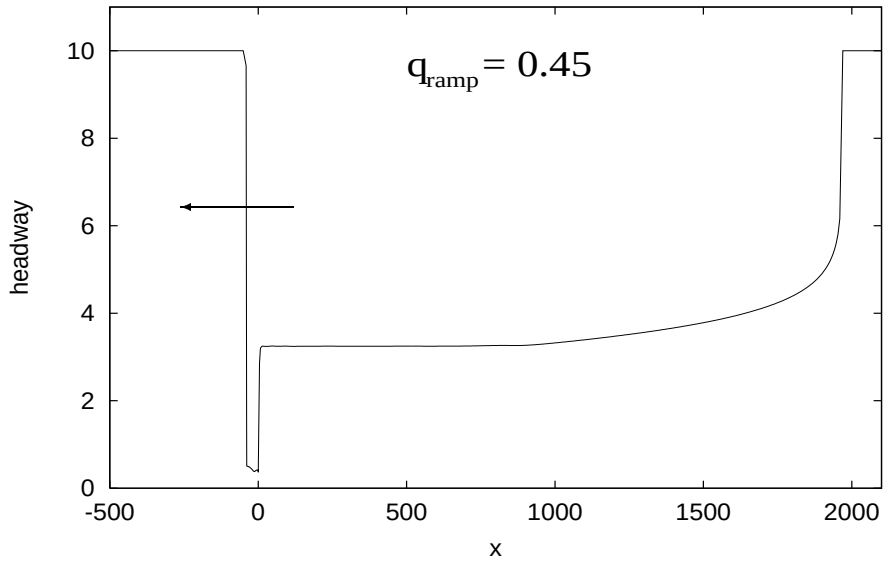

Figure 6.4: Homogenous congested traffic upstream (HCTu): the flow jump at the on-ramp is determined by Eq. (6.1.6). The upstream headway is matched by a shock wave, and the downstream headway by a dispersive tail. The downstream flow in the vicinity of the ramp is close to the maximum equilibrium flow.

the upstream vehicles squeeze in, in order to obtain maximum flow. However, the sensitivity is restricted to $a = 1.5$, leaving a finite inertia of cars. This way, the flow does not react optimally to the ramp events, and the downstream flow differs slightly from q_{max}. The numerical data reveal that for increasing a, the plateau approaches $b = 2.78$, the headway of maximum flow. Correspondingly, the boundary between DHCTd and HCTu is identical to the curve defined by $q_0 + q_{ramp} = q_{max}$ only in the limit $a \to \infty$.
However, the downstream transition back to the original headway appears again as a dispersive tail.

6.2.3 Dipole Congested Traffic Upstream (DPCTu)

In this regime, the sum of the original flow q_0 and the ramp flow q_{ramp} still exceeds the maximum flow. We would, therefore, expect a solution similar to HCTu. However, the jump in headway of the first shock wave becomes so large that we now observe a Bando wave. This is represented in Fig. 6.5 by the dotted box. The downstream plateau of the Bando wave influences, in a complicated manner, the other headways. However, the jump at the ramp is given as usual by Eq. (6.1.6), and the downstream plateau in the vicinity of the ramp approaches the headway of

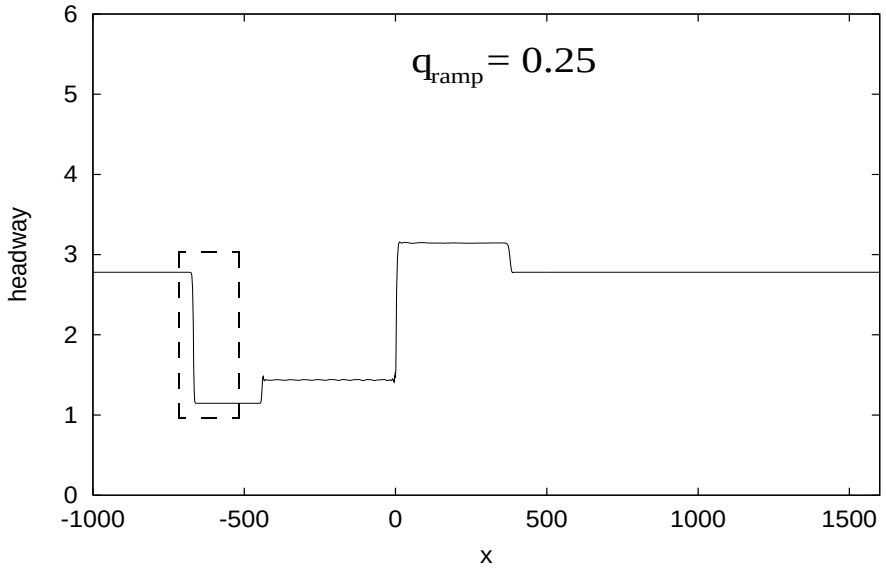

Figure 6.5: Dipole congested traffic upstream (DPCTu): the flow jump at the on-ramp is determined by Eq. (6.1.6). The downstream flow in the vicinity of the ramp is again close to the maximum equilibrium flow. This determines the upstream flow in the vicinity of the ramp, which can only be matched by a Bando wave (dotted box) and, hence, a further plateau.

maximum flow for $a \to \infty$.
Kerner refers to this profile, which is similar to the cluster solution of the metastable regime, as a "dipole" structure. On the other side, Helbing also calls the DPCTu state homogenous congested traffic, which occurs in front of the on-ramp as the simulation time grows.

6.2.4 Dispersive Homogenous Congested Traffic Upstream (DHCTu)

When the original density is increased even further, it turns out that any perturbation can only travel upstream. In Fig. 6.6, the downstream headway is unperturbed, whereas vehicles in front of the ramp form a congested state, whose headway is once again given by Eq. (6.1.6).
The transition from the original headway to this plateau occurs once more as a dispersive tail in accordance with the results of chapter 5.
This state leads to a piling up of cars in front of the ramp, which might eventually cause a flow breakdown. Hence, in this regime, on-ramp metering must carefully monitor the motorway situation.

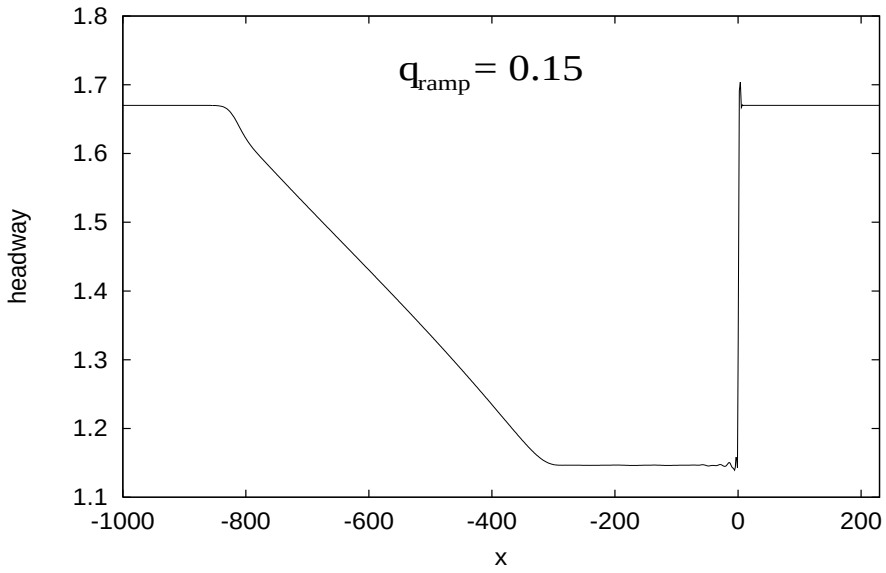

Figure 6.6: Dispersive homogenous congested traffic upstream (DHCTu): the flow jump at the on-ramp is determined by Eq. (6.1.6). The downstream headway is unperturbed, and the upstream headway is linked to the original headway by a dispersive tail.

6.2.5 Dispersive Peak Located Congested Traffic Upstream (DPLCu)

If the oncoming traffic volume is further increased to a level where it matches the original flow, a new wave type appears. The downstream flow of vehicles is now fully provided by the on-ramp, so that the upstream cars come to a standstill and pile up in front of the ramp. This leads to a notch, shown in Fig. 6.7, since the length of the cars was assumed to be zero. A finite length of cars would result in a plateau, which spreads out in front of the ramp. However, this standstill is linked to the original headway by a dispersive tail.

The curve that separates the regions DHCTu and DPLCu, should ideally be the stretch of the fundamental diagram in the corresponding density regime represented by the dotted line in Fig. 6.2a. However, it is hard to tell from the numerical data where this line really lies, depending on the process, as to whether the vehicles come to a temporary or a permanent standstill. One has to be careful in interpreting these numerical results.

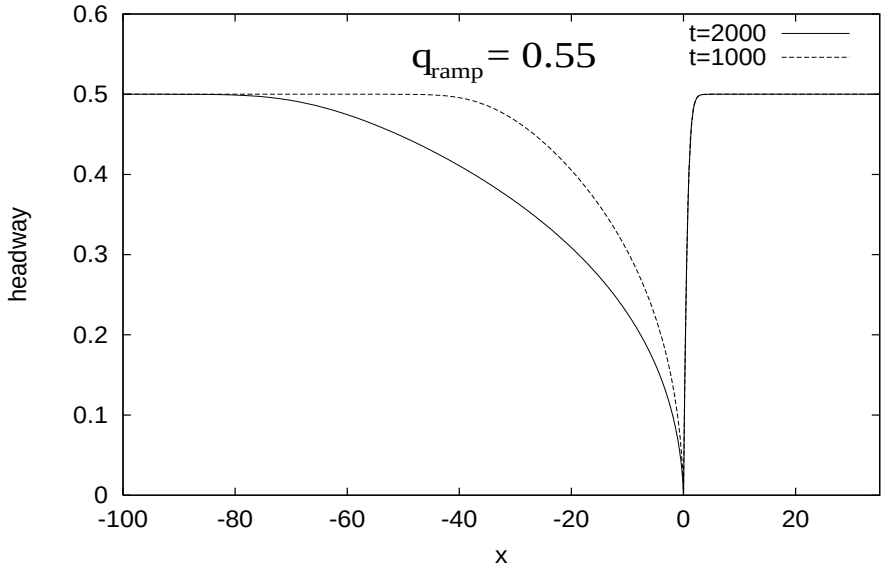

Figure 6.7: Dispersive peak located congested traffic upstream (DPLCu): a dispersive tail, matching the upstream headway, ends in a total halt of cars at the on-ramp. The downstream headway is unperturbed.

6.3 Triggered Stop-and-go Waves and Solitons

There is one case where the correspondence between the car-following and the continuum simulations can be shown analytically: the triggered stop-and-go state of Fig. 6.8, which is also interpreted as synchronized flow due to its high flux and its slowly varying speed [56]. We can prove that the TSGu solution can be approximated using the continuum analogue of chapter 3

$$v_t + v v_x = a\left[\bar{V}(\rho) - v\right] + a\bar{V}'(\rho)\left[\frac{\rho_x}{2\rho} + \frac{\rho_{xx}}{6\rho^2} - \frac{\rho_x^2}{2\rho^3}\right], \tag{6.3.1}$$

$$\bar{V}(\rho) = V_B(1/\rho). \tag{6.3.2}$$

In the following, we neglect the nonlinear term in ρ_x^2, since the same wave type also occurs in the previously mentioned continuum models, which do not include it. Moreover, inclusion of ρ_x^2 would not allow for an analytical solution any longer. On the other hand, neglecting it could lead to a solution that deviates from the numerical data, depending on its order in comparison with the other terms.
Being in the linearly stable regime (Fig. 6.2b), we can try to interpret the solitary wave type in Fig. 6.8 as an upstream travelling wave away from the on-ramp. Hence, there will be no source term on the right hand side of Eq. (6.1.1).
Since the waves resemble *cnoidal waves*, which are solutions of the Kortweg-de-Vries

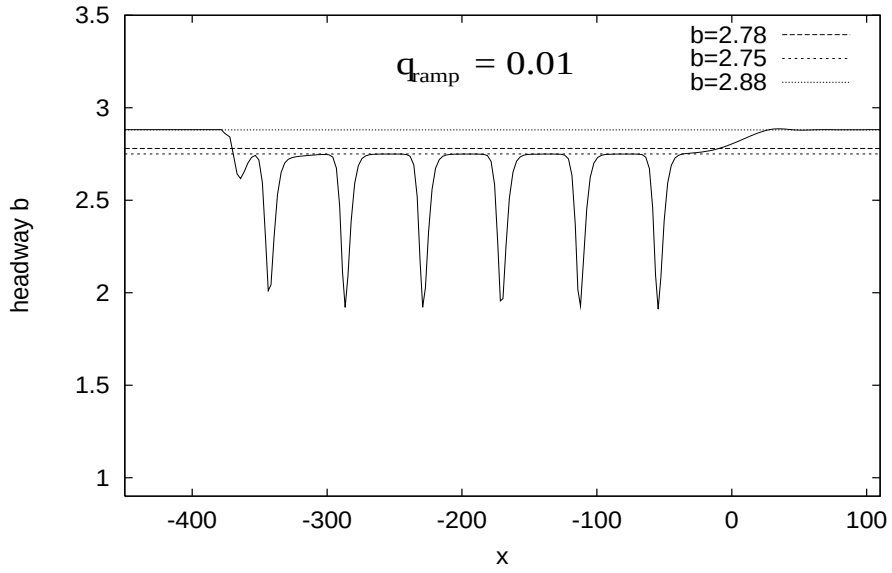

Figure 6.8: The triggered stop-and-go state (TSGu) resembles the *cnoidal waves* solution of the KdV equation.

(KdV) equation

$$\rho_t + (\alpha + \beta\rho)\rho_x + \rho_{xxx} = 0, \tag{6.3.3}$$

we are motivated to try and extract a KdV equation from Eqs. (6.1.1) and (6.3.1) by balancing nonlinear and dispersive effects, as well as neglecting the dissipation in the first place.

If we consider travelling wave solutions away from the on-ramp and change to the reference system of the wave by introducing the coordinate

$$z = x - ct \tag{6.3.4}$$

with the wave speed c, the system of Eqs. (6.1.1) and (6.3.1) turns into

$$-c\rho_z + q_z = 0, \tag{6.3.5}$$

$$-cv_z + vv_z = a\left[\bar{V}(\rho) - v\right] + a\bar{V}'(\rho)\left[\frac{\rho_z}{2\rho} + \frac{\rho_{zz}}{6\rho^2}\right], \tag{6.3.6}$$

with the flow q being the product of the density and the speed

$$q = \rho v \Rightarrow v_z = \frac{c\rho_z}{\rho} - \frac{q\rho_z}{\rho^2}. \tag{6.3.7}$$

This way, the dynamic equation Eq. (6.3.6) can be written as

$$-\frac{\rho_z}{\rho^3}q^2 + \left(\frac{2c\rho_z}{\rho^2} + \frac{a}{\rho}\right)q = a\bar{V} + \left(\frac{a\bar{V}'}{2\rho} + \frac{c^2}{\rho}\right)\rho_z + \frac{a\bar{V}'}{6\rho^2}\rho_{zz}. \tag{6.3.8}$$

We then approximate the flow q to lowest order as

$$q = \rho\bar{V} + a_1\rho_z + a_2\rho_{zz}. \tag{6.3.9}$$

The leading term $\rho\bar{V}$ represents the fundamental diagram Fig. 6.2b, which describes homogenous stationary stable flow q of density ρ and speed $\bar{V}(\rho)$. The parameters a_1 and a_2 can be found by substitution of Eq. (6.3.9) into Eq. (6.3.8) as

$$a_1 = \frac{\bar{V}'}{2} + \frac{1}{a}\left(\bar{V}^2 - 2c\bar{V} + c^2\right), \tag{6.3.10}$$

$$a_2 = \frac{\bar{V}'}{6\rho}, \tag{6.3.11}$$

which leads to

$$q = \rho\bar{V} + \left[\frac{\bar{V}'}{2} + \frac{1}{a}\left(\bar{V}^2 - 2c\bar{V} + c^2\right)\right]\rho_z + \frac{\bar{V}'}{6\rho}\rho_{zz}. \tag{6.3.12}$$

If the second term in ρ_z can be neglected in comparison to the third term in ρ_{zz}, we can rewrite the equation for the conservation of cars Eq. (6.3.5) as

$$-c\rho_z + \left(\rho\bar{V}\right)_z + \frac{\bar{V}'}{6\rho}\rho_{zzz} = 0. \tag{6.3.13}$$

If we consider perturbations of the density

$$\rho(x,t) = \rho^* + \hat{\rho}(x,t) \tag{6.3.14}$$

near the maximum flow $q_{max} = q(\rho_{max} = 1/2.78) \approx 0.58$, $\rho\bar{V}$ can be approximated by the first terms of a Taylor series

$$\rho\bar{V} = \rho^*\bar{V}(\rho^*) + \left(\rho\bar{V}\right)_\rho\Big|_{\rho=\rho^*}\hat{\rho} + \frac{1}{2}\left(\rho\bar{V}\right)_{\rho\rho}\Big|_{\rho=\rho^*}\hat{\rho}^2 + \dots . \tag{6.3.15}$$

Inserting this into Eq. (6.3.13) yields (dropping the "hat")

$$-c\rho_z + \left[\left(\rho\bar{V}\right)_\rho + \left(\rho\bar{V}\right)_{\rho\rho}\rho\right]\rho_z + \frac{\bar{V}'}{6\rho}\rho_{zzz} = 0, \tag{6.3.16}$$

which is the KdV equation that we were looking for. This equation is only a good approximation under the assumption $|a_1\rho_z| \ll |a_2\rho_{zz}|$. One way to show this is to derive the solution of Eq. (6.3.16), and then to examine how accurately this condition is fulfilled.

We first transform the KdV equation into a standard form found in most books about this topic [19]. In order to do so, we introduce a new variable

$$u(z) = \frac{1}{6}\left[\left(\rho\bar{V}\right)_\rho + \left(\rho\bar{V}\right)_{\rho\rho}\rho\right]. \tag{6.3.17}$$

Now Eq. (6.3.16) turns into (c and $\frac{V'}{6\rho}$ negative)

$$-(-c)u_z - 6uu_z + \left(-\frac{\bar{V}'}{6\rho}\right)u_{zzz} = 0. \tag{6.3.18}$$

A coordinate transformation

$$\bar{z} = \sqrt{-\frac{6\rho}{\bar{V}'}}z \tag{6.3.19}$$

yields

$$-(-c)u_{\bar{z}} - 6uu_{\bar{z}} + u_{\bar{z}\bar{z}\bar{z}} = 0, \tag{6.3.20}$$

which is the standard form whose solution is

$$u(\bar{z}) = \frac{1}{2}c\ \mathrm{sech}^2\left(\frac{1}{2}\sqrt{-c}\bar{z}\right). \tag{6.3.21}$$

This in turns delivers

$$\rho(x,t) = \frac{3c}{\left(\rho\bar{V}\right)_{\rho\rho}}\ \mathrm{sech}^2\left[\frac{1}{2}\sqrt{\frac{6c\rho}{\bar{V}_\rho}}(x-ct)\right] - \frac{\left(\rho\bar{V}\right)_\rho}{\left(\rho\bar{V}\right)_{\rho\rho}}, \tag{6.3.22}$$

which has to be added to ρ^*. Therefore, we end up with two parameters to be fitted, the wave speed c and ρ^*. They are not independent of each other, since they should ideally fulfill the *flow conservation criterion*: the downstream flow must equal the sum of the on-ramp flow and the average flow of the upstream soliton-like profile. This is how the soliton is selected.

However, ρ^* determines all remaining parameters in Eq. (6.3.22) by taking their values at $\rho = \rho^*$. An analysis of the individual terms reveals that the solution does not vary much, with ρ^* being close to the maximum of the flow curve.

One way to determine the two parameters, is to use the numerical results, which deliver both the wave speed

$$c = -0.64 \pm 0.03 \tag{6.3.23}$$

and the density

$$q^* = 0.301 \pm 0.001\ . \tag{6.3.24}$$

These lead to a soliton solution, as shown in Figure 6.9, which illustrates that the analytical solution does not quite reach the right amplitude or width. This might be based on the fact that due to its high amplitude, higher order terms such as ρ_x^2 come into play that have been neglected in this analysis. Furthermore, dissipation may broaden the distribution. Nevertheless, the analytical solution can be regarded as a good first-order approach, even though the flow criterion cannot be exactly fulfilled. This is different for the fit, which shows in addition that the numerical data really has the shape of a sech^2-soliton.

If we now consider the values of a_1 and a_2 as shown in Fig. 6.10, it becomes clear that the soliton solution appears in the regime where the dissipation term becomes negligible, and $|a_1(\rho \approx 0.365)\rho_z| \ll |a_2(\rho \approx 0.365)\rho_{zz}|$ applies. Therefore, as a first-order approach, we can neglect this term and the KdV equation is justified. Nevertheless, dissipation would also contribute an asymmetric correction term that explains the discrepancy between the left hand and the right hand side of the maximum in

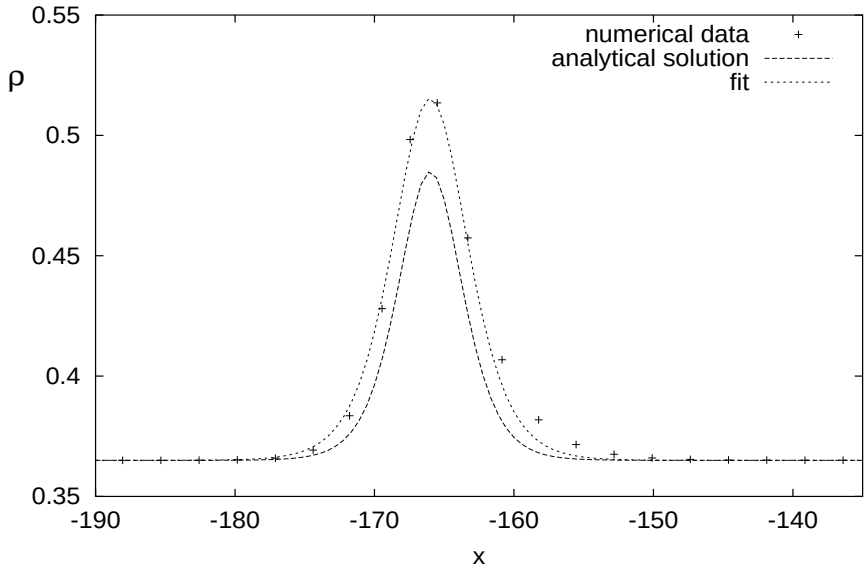

Figure 6.9: The solitary wave solution of the car-following simulation (TSGu) is only partly matched by the analytical solution (6.3.22) due to higher order and dissipative effects. The latter reaches about 82 per cent of the actual amplitude represented by the sech^2-fit.

Fig. 6.9 [43]. It can be treated as a small perturbation $a_2\rho_{zz}$ to the KdV equation (6.3.16), and the solution is then found by introducing multiple time scales [43]. This comprehensive method goes beyond the scope of this dissertation.
Another effect, which might explain further discrepancies, is that we assumed $a_2 = V'/6\rho$ to be constant. In fact, it varies with ρ between -2.2 and -1.2 across the density range of the soliton solution. If the term depends on ρ, it will not allow an analytical solution any longer. Similar arguments hold for the other parameters in Eq. (6.3.22).
As mentioned above, the results of this section coincide with earlier publications that consider various OV models. It, therefore, supports the idea that OV models which contain an unstable density region in the fundamental diagram lead to similar predictions of on-ramp states. However, it does not imply that all states of Fig. 6.2a can actually be found in real traffic [31, 45]. It has to be regarded as a purely mathematical theory, whose predictions might not fully cover real traffic events, since it lacks stochasticity, varying vehicle parameters and time delay. Hence, it is doubtful if the TSGu state can really be interpreted as synchronized flow just because of its high flux and slowly varying speed [56].

The oscillatory state **OSCu** of Fig. 6.11 was considered by Helbing as an individual state. However, it occurs more plausible to regard it as the limit of the TSGu state, when the wavelength of the cnoidal wave solution is shrinking. The maximum

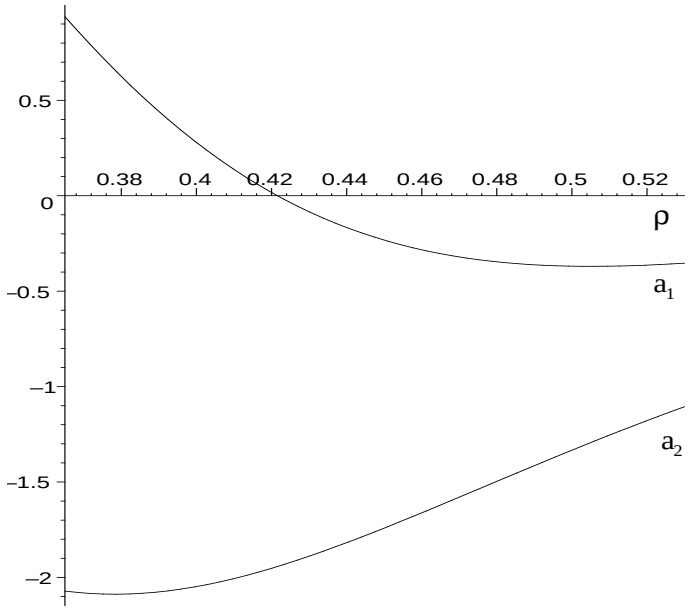

Figure 6.10: The coefficients of the expansion Eq. (6.3.9) in the density range of the soliton solution. The solitons form in the regime of negligible dissipation.

headway $b \approx 2.76$ of the solution which, in analogy to the TSGu state, is close to the headway of maximum flow, is a strong hint for this. This also corresponds to the finding of the author that there is no strict boundary between these two phases.

6.4 Downstream Oscillations

In the free flow regime, which is equivalent to small densities ρ_0, we can find downstream oscillations (OSCd) for small on-ramp flows, as illustrated in Fig. 6.12. The upstream headway is again unperturbed due to the positive wave speed of the free flow regime, whereas the downtream headway eventually assumes a level (plateau) given by the upstream and the ramp flow. The oscillations in the vicinity of the ramp decay more slowly when these two parameters tend to zero.
The solution evolves due to the discretization of the model, which is most obvious in this regime. This is because the OV function varies only gradually with the headway and, so, the governing equation for the headway of the downstream plateau Eq. (5.2.5)

$$\ddot{b}_n + a\dot{b}_n + aV(b_n) = aV(b_{n-1}) \tag{6.4.1}$$

can be approximated by a Taylor expansion ($b = b_p + \hat{b}$) of the OV function to first order (dropping the "hats")

$$\ddot{b}_n + a\dot{b}_n + aV'(b_p)b_n = aV'(b_p)b_{n-1}. \tag{6.4.2}$$

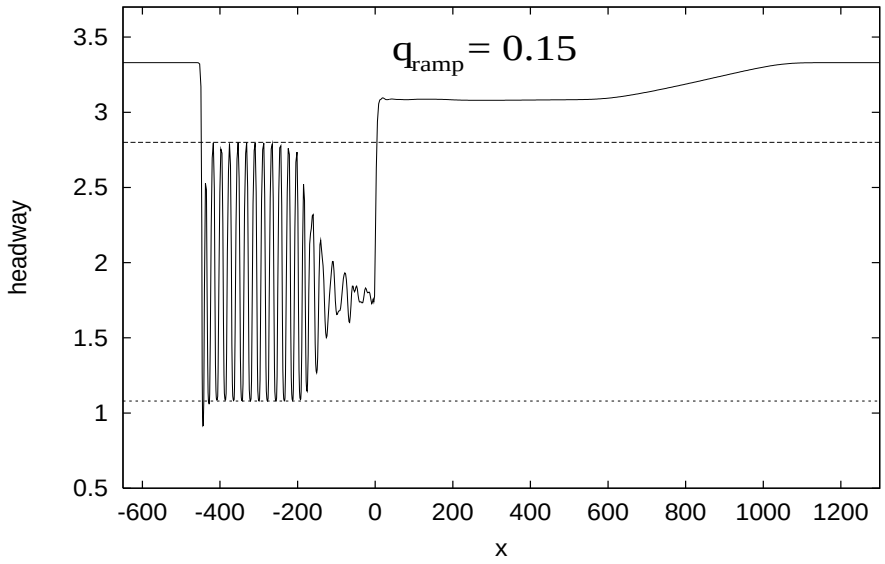

Figure 6.11: Oscillatory congested traffic upstream (OSCu).

Looking for solutions for the n-th car

$$b_n(t) = b_p + B\exp(\lambda t) \tag{6.4.3}$$

following the $(n-1)$-th car, for which we assume a constant headway

$$b_{n-1}(t) = b_p, \tag{6.4.4}$$

we find for $V' \ll a$

$$\lambda_1 = -V' - \frac{V'^2}{a} + \dots , \tag{6.4.5}$$

$$\lambda_2 = -a - \lambda_1. \tag{6.4.6}$$

For $t \to \infty$, the first root will dominate, and we see that the adjustment takes place on a time scale

$$T = \frac{1}{V'} \overset{b_0 \to \infty}{\to} \infty, \tag{6.4.7}$$

which explains the growing adjustment time with increasing plateau headway caused by small upstream and ramp flows.

We can now try to interpret the OSCd type with the help of the continuum version. We have already seen how this solution might be triggered in the car-following model, by considering individual vehicles which are inserted in between two cars of the free flow regime. A disadvantage of this analysis is that it does not deliver any spatial length scales or periods of this traffic pattern.

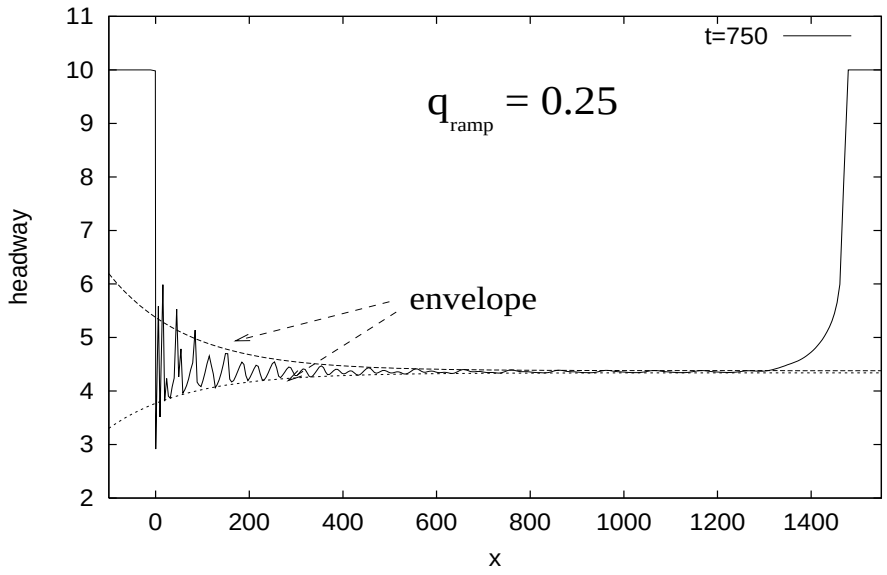

Figure 6.12: Oscillatory congested traffic downstream (OSCd): the envelope is stationary, and the plateau is determined by Eq. (6.1.6).

To work out these values, we look for solutions of the continuum model around the plateau of the form

$$\hat{\rho}(x,t) \sim \exp(kx-\omega t) = \exp(k_r x - \omega_r t)\exp\left[i(k_i x - \omega_i t)\right], \quad (6.4.8)$$

$$\hat{v}(x,t) \sim \exp(kx-\omega t) = \exp(k_r x - \omega_r t)\exp\left[i(k_i x - \omega_i t)\right], \quad (6.4.9)$$

with

$$\omega = \omega_r + i\omega_i, \quad (6.4.10)$$

$$k = k_r + ik_i. \quad (6.4.11)$$

In accordance with the numerical data, we make two assumptions: the envelope is stationary, which equals $\omega_r = 0$, and the wave speed c_p of the oscillations coincides with its linear pendant

$$c_p = \frac{\omega_i}{k_i} = q_\rho(1/b_p). \quad (6.4.12)$$

Hence, one variable can be expressed by the other one, once the downstream plateau of headway b_p is determined. This leaves us with two unknown real variables, k_r and k_i.

One way to find these out is to insert the asymptotic expressions (6.4.8) and (6.4.9) into the linearized continuum model of chapter 3, Eqs. (3.3.6) and (3.3.7), and to solve for k_r and k_i by setting the determinante to zero analogous to the stability analysis of the continuum model.

It turns out that there are no real roots, k_r and k_i, neither for the example in Fig. 6.12 nor in other cases. Therefore, this asymptotic analysis fails, and it seems more reasonable to assume that the solution cannot be approximated in terms of harmonic functions. This is not very surprising, since the pattern only shows in the regime where the discrete nature of the model is most obvious. It is this discrete process in the free flow regime which cannot be described by the continuum analogue.

6.5 Conclusion

We have classified various traffic states in a car-following model which occur in the vicinity of an on-ramp for both constant upstream and constant ramp flow. They are in good agreement with Helbing's results [32], and further support the idea that car-following and continuum models reproduce similar features if they contain a relaxation term. In the case of a solitary wave train – the triggered stop-and-go waves (TSGu) – this analogy can be verified analytically. This type represents a solution of a KdV equation, and is the product of nonlinear wave steepening and dispersive effects near the maximum flow.
It should be stressed that the transition between the various types in the phase diagram Fig. 6.2a is smooth and does not occur as a phase transition of any kind. It is indeed very hard to say in what regime one is near the boundaries.

Kerner argued that the on-ramp triggers numerous solutions of single lane flow. Accordingly, some types covered in this chapter have already occured in the analysis of the transition types in chapter 5: DHCTd consisting of a shock wave and a dispersive wave, HCTu consisting of two shock waves and a dispersive tail, DPCTu containing the cluster solution of metastable states, DHCTu consisting of a dispersive and a shock wave, and DPLCu, which is a dispersive adjustment wave from dense traffic to a standstill. Here, the difference lies in the location of these transitions. They appear as stationary solutions, which are bound to the ramp, rather than structures moving up or down the road. However, the TSGu, OSCu and OSCd states are not found in single lane simulations. They have to be *triggered* by the on-ramp in the sense that it pushes the trajectory of the vehicles towards a limit cycle of the corresponding phase space, which results in oscillatory behaviour.
Helbing has found a similar phase diagram for bottlenecks, which suggests that it is a general feature of road inhomogenities [80]. These results are part of much current research, comparing theoretical predictions to empirical data, which might contain additional traffic states.[1]

[1] At this date, the relevant publications by Kerner and by Helbing are still in preparation.

Chapter 7

Summary and Outlook

This dissertation establishes a link between microscopic car-following models and macroscopic continuum models of traffic flow, which have so far been considered as different deterministic systems. This is achieved by the derivation of a transformation that relates the headway and density, which are the analogous parameters in these models.

Special attention should be drawn to the optimal-velocity type, represented ultimately by the car-following Bando model, since it is the most popular and promising type of model used in recent research. Upon application, the transformation delivers a second-order continuum model, which resembles those of Kühne [53] and Kerner-Konhäuser [48]. It demonstrates that the occurrence of *pressure* and diffusive terms can be characterized as an implicit feature of the discrete model, rather than as a merely stochastic term of the continuum counterpart caused by random fluctuations of the flow.

The analogy between the two models is further supported by stability analysis and comparison of their travelling wave solutions. This correspondence increases, furthermore, with the number of terms that are kept throughout the transformation. However, the same stability criterion holds already true for a second-order model and, moreover, the travelling wave solutions' description is sufficiently accurate, even in the occurrence of the steepest gradients, which is what we call Bando waves. In addition, traffic data suggest that higher order terms do not add remarkable contributions, so that higher order models are of no further interest.

The transformation and its inverse enable the derivation of a variety of analogous models, both for the car-following and continuum types. Here, the time delay of certain discrete models causes problems when working out the continuum counterpart. The result, a partial differential delay equation, is far from practical and suitable. On the other hand, when going from the continuum form to the car-following analogue, spatial derivatives of discrete variables, in particular the headway, are difficult

to interpret. This comparison reveals the superiority of car-following models when it comes to time delay and the simulation of different driver and vehicle characteristics among the platoon.
The results of the travelling wave analysis of chapter 5, and the on-ramp simulation of chapter 6, do not only further support the analogy between car-following and continuum models. They couple with the suggestion that optimal-velocity models of the microscopic and the macroscopic type produce similar traffic features when they contain a linearly unstable and adjacent metastable density regime. A variation of the OV function, whether it is dimensionless or not, changes the phase diagrams quantitatively, but not qualitatively.
The results of this work are vital for flow simulations and the implementation of autonomous cruise control systems. By relating discrete and continuum models and discussing various flow situations, some intrinsic effects of these formulations have been uncovered. Among these is the range of transition types between different flows. The analysis of these transitions has revealed a wider understanding of how they are triggered, what terms dominate and when nonlinearity is apparent. The identification of real flow patterns with these theoretical predictions might help in assessing why, when and whether traffic simulations and control algorithms lead to sensible solutions, last but not least, by the prediction of the qualitative results.

Whatever results a traffic model reveals, it is imperative that they are compared with traffic data to assess its accuracy. It can only be regarded as a fundamentally sound model if it reproduces specific traffic features. Most of these are quite well understood by now, apart from synchronized flow on highways [44]. It is still unclear whether the latter can be described in the framework of the current models or whether higher order models, stochasticity, or time delays are necessary to match the empirical findings.
Despite this, traffic flow modelling delivers a powerful tool in providing insight into the intrinsic effects of the system. An example might be in the recent discovery of Helbing [32, 80] that bottlenecks, on-ramps, speed limits and spatial variations of the road characteristics have similar impacts on the flow condition in the sense that they trigger the same traffic states in his simulations. This and the hypothesis that all traffic models predict similar behaviour if they fulfill certain criteria, might be a light at the end of the tunnel after the proposal of increasingly more models. However, the combination of empirical research and theoretical modelling in recent years suggest that this highly random system can only partly be described by deterministic mathematical models and that its features have to be considered as a result of the stochasticity and the nonlinearity of the flow. Here, one of the most challenging tasks remains as to how to relate analytically stochastic cellular automata and deterministic car-following models, as described aptly by Nagel [67]. This project

goes beyond the scope of this dissertation; on the other hand, our results provide some background knowledge in how to tackle this problem.
In this framework, it would also be of interest to investigate whether the combination of random variables describing multi-species traffic [61], reaction time and temporally changing driver characteristics lead to a more realistic reproduction of traffic data, possibly including synchronized flow. However, in addition to the comprehensive numerical effort, the problem with this approach might be the lack of a deeper understanding of the system due to the greater amount of parameters.

Appendix A

Cellular Automata

In some situations, traffic is very similar to granular flow. However, since granular motion describes interacting particles whose movements depend on physical contact, the theory cannot be applied straightforwardly. Nevertheless, cellular automata (CA) models have proved to be a useful means to simulate congested flow, city traffic including junctions, and lane-changing. In contrast, the free flow regime of motorways is unlikely to be well modelled this way, because there is little or no interaction among the vehicles, due to the low density.
The granular flow theory of traffic encountered a great boost with the introduction of a stochastic (discrete) automaton model by Nagel and Schreckenberg [68]. A road

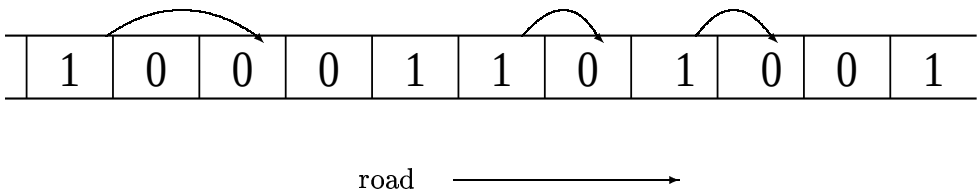

Figure A.1: Cell hopping in a cellular automata models. '0': free cell; '1': occupied cell.

is divided into cells, approximately the size that a car occupies in a jam. Each site may either be empty, or occupied by a vehicle. Each car has an integer velocity with values between 0 and v_{max}. The update of the traffic situation is then based on a fixed number of rules which allow a car to hop to one of the next free cells ahead, as in Fig. A.1:

- If the velocity v of the car is lower than v_{max}, and the distance to the next car ahead is larger than $v + 1$, the speed is increased by one.

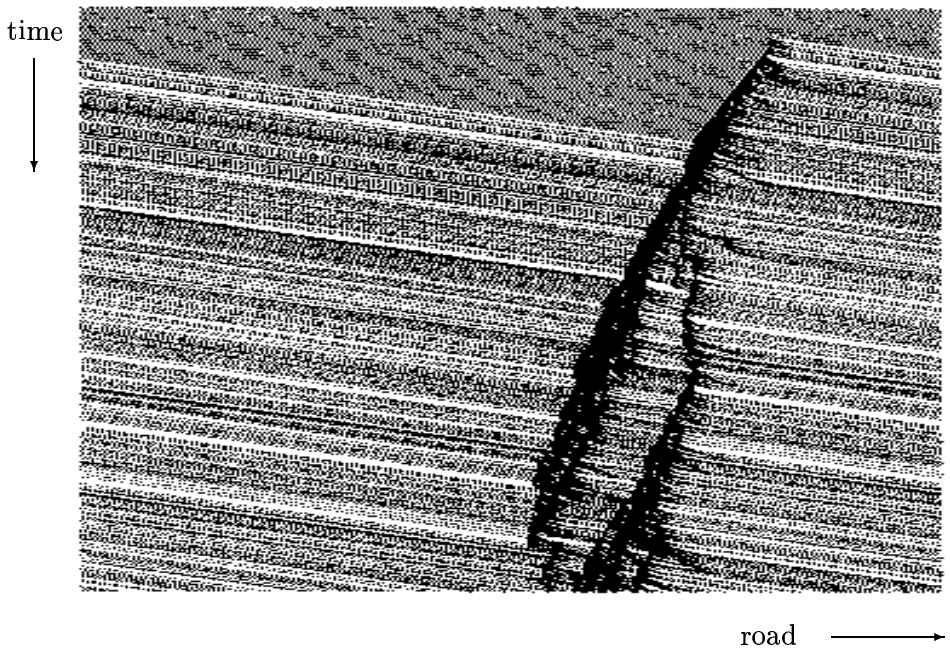

Figure A.2: Trajectories of vehicles in a cellular automaton model of road traffic [67]: formation of an upstream running shock wave and the secession of a second shock wave from the original one.

- If a driver at site i sees the next vehicle at site $i + j$, with $j < v$, she reduces its speed to $j - 1$.
- The velocity of each vehicle (if greater than zero) is decreased by one with probability p ("dawdling").
- Each vehicle is advanced by v sites.

Since each vehicle in a CA model hops with some probability, depending on the distance to the car in front, it is also regarded as a car-following model. However, in this dissertation we refer to car-following models as being deterministic, and ignore CA models.

Monte-Carlo simulations of the model show a transition from laminar flow to start-stop-waves with increasing vehicle density, as observed in real freeway traffic. Figure A.2 presents how a shock wave might arise from an initial homogenous unstable flow. Here, the upper bound of the car density in the clusters is obviously given by the length of the cell.

The advantage of these models clearly lies in their quick realization of numerical simulations. Real time online simulations can be carried out, and compared to their continuous analogues [67]. However, the problem of these models is the difficulty of extracting analytical results due to the discretization of space and time, which is one

major reason why we consider only the deterministic continuum and car-following models in this dissertation.

Appendix B

Inappropriate Inverse Transformation

In chapter 3, we derived the inverse transformation successfully in two different ways. In the following, a method will be presented by which the inverse transformation cannot be derived. At first sight, it may seem to be counterproductive to concentrate on an example that does not succeed. However, it gives even more insight into the relation between the traffic parameters headway and density.
Analogous to the integral representation Eq. (3.2.3) of the headway, another obvious approach to produce the inverse transformation might be

$$\int_x^{x+1/\rho(x,t)} 1/b(x',t)dx' = \int_0^{1/\rho(x,t)} 1/b(x+y,t)dy \equiv 1. \tag{B.0.1}$$

By proceeding as in chapter 3, one obtains an asymptotic series or, in other words, another differential equation

$$\frac{1}{\rho b} + \frac{1}{2\rho^2}\left(\frac{1}{b}\right)_x + \frac{1}{6\rho^3}\left(\frac{1}{b}\right)_{xx} = 1, \tag{B.0.2}$$

but this time for b instead of ρ. However, this method fails for different reasons. One is that the conservation of cars is not fulfilled any longer, and since this equation is dropped by going from the continuum model with two coupled equations to the car-following model with one governing equation, this violation leads to inconsistencies in the discrete model.

Total differentiation of Eq. (B.0.1) with respect to time yields

$$\begin{aligned} 0 &= \int_x^{x+1/\rho} \left[\frac{1}{b(x')}\right]_t dx' && \text{(B.0.3)} \\ &+ \left[x_t + \left(\frac{1}{\rho}\right)_t\right] \frac{1}{b(x+1/\rho)} - x_t \frac{1}{b(x)} \\ &= \int_x^{x+1/\rho} \left[\frac{1}{b(x')}\right]_t dx' + \frac{v(x+1/\rho)}{b(x+1/\rho)} - \frac{v(x)}{b(x)} && \text{(B.0.4)} \\ &= \int_x^{x+1/\rho} \left\{\left[\frac{1}{b(x')}\right]_t + \left[\frac{v(x')}{b(x')}\right]_{x'}\right\} dx'. && \text{(B.0.5)} \end{aligned}$$

From the transformation Eq. (3.2.10), we know that $1/b$ might be written as

$$\frac{1}{b} \sim \rho + \frac{\rho_x}{2\rho} + \frac{\rho_{xx}}{6\rho^2} + \dots \,. \tag{B.0.6}$$

Moreover, the integral must vanish for any function $b(x,t)$

$$\left[\frac{1}{b}\right]_t + \left[\frac{v}{b}\right]_x = 0. \tag{B.0.7}$$

Inserting Eq. (B.0.6) and taking the conservation of cars Eq. (3.1.4) into account, Eq. (B.0.7) reads

$$\left(\frac{\rho_x}{2\rho} + \frac{\rho_{xx}}{6\rho^3}\right)_t + \left[v\left(\frac{\rho_x}{2\rho} + \frac{\rho_{xx}}{6\rho^3}\right)\right]_x = 0, \tag{B.0.8}$$

which does not hold for every function $\rho(x,t)$. Therefore, given the transformation Eq. (3.2.10) that relates car-following models to their continuum counterparts, the ansatz Eq. (B.0.1) leads to inconsistencies and is, for this reason, not a proper method for deriving the inverse transformation.

Moreover, there is the second argument that this method does not succeed. Equation (B.0.2) is equivalent to Eq. (3.2.5), if one considers the substitutions

$$\begin{aligned} b(x,t) &\longrightarrow 1/\rho(x,t), && \text{(B.0.9)} \\ \rho(x,t) &\longrightarrow 1/b(x,t), && \text{(B.0.10)} \end{aligned}$$

so effectively making use of $b\rho \approx 1$. As in chapter 3, we proceed to gain an expression for ρ in terms of b, b_x and b_{xx}, and straightforward calculation gives

$$\rho = \frac{1}{b} - \frac{b_x}{2b} - \frac{b_{xx}}{6} + \text{higher order terms.} \tag{B.0.11}$$

This differs obviously from the inverse transformation (3.8.10), which was derived from the original asymptotic series Eq. (3.2.5). In accordance, it can be shown that under this inappropriate inverse transformation, the continuous Bando model does not transform into its original discrete analogue. It now includes higher order terms in b_x and b_{xx}

$$\dot{v_n} = a\left[V_B(b_n) - v_n\right] - \frac{(b_n)_x}{b} - \frac{7}{12}(b_n)_{xx}\,. \tag{B.0.12}$$

The problem that arises here is how to interpret the spatial derivatives of the headway (chapter 4).

Appendix C

Differential Delay Equations

In this appendix, a brief introduction into the theory of differential delay equations (DDE) is given. We restrict ourselves to the discussion of ordinary DDE (ODDE) rather than partial DDE (PDDE).
A first-order ordinary differential equation (ODE) usually takes the form

$$u'(t) = f(t, u(t)), \tag{C.0.1}$$

and describes the rate of change of a variable u, depending on its current state and time. However, in many systems in nature, the current process depends on the *history* of the system. Examples are nuclear reactions, control systems, population growth, economic growth, epidemiology and traffic flow [18, 20, 59, 85, 86].
The evolution of the current state $u(t)$ may then depend on the state $u(t-T)$ a time T ago, a number of different states at different times in the past $u(t-T_1),\ u(t-T_2), ...,\ u(t-T_n)$, or even on the states during a time interval $[t-T; t]$ where $T \in [0; \infty)$.
In the first case, the governing equation might now read

$$u'(t) = f(t, u(t), u(t-T)), \tag{C.0.2}$$

where T is called the **time delay**. In traffic flow modelling this term corresponds to the driver's reaction time. Even though it is the simplest ODDE, it already reveals interesting phenomena.
Before we discuss those, it should be mentioned that single time delay as in Eq. (C.0.2) and multiple time delay (numerous linear terms $u(t-T_1),\ u(t-T_2), ...,\ u(t-T_n)$ on the right hand side of Eq. (C.0.2)), are special cases of a time interval dependency

$$u'(t) = f\left(t, u(t), \int_{-\infty}^{\infty} K(t, t')u(t-t')\ dt'\right), \tag{C.0.3}$$

by specifying the kernel to be

$$K(t, t') = a_1\delta(t'-T_1) + a_2\delta(t'-T_2) + ... + a_n\delta(t'-T_n). \tag{C.0.4}$$

However, the kernel often takes the form of a Gaussian function.
To illustrate the basic difference between ODDE and ODE, we consider the example

$$u'(t) = -u\,(t-T) \quad , \quad T = \frac{\pi}{2}. \tag{C.0.5}$$

For the initial condition $u(0) = 0$, we can find infinitely many oscillatory solutions

$$u(t) = A\sin(t) \quad , \quad A \in \mathrm{R}. \tag{C.0.6}$$

This is different from the corresponding ODE ($T = 0$), which shows exponential decay

$$u(t) = A\exp(-t) \quad , \quad A \in \mathrm{R}, \tag{C.0.7}$$

and does not provide any non-trivial function which satisfies the initial condition.
We see that the initial condition of an ODDE must be given on a *history window* $[t_0 - T; t_0]$, where T is the time delay, in order to determine the solution uniquely. In general, the dependency on those initial conditions is crucial, and its analysis is usually quite demanding. Moreover, we can expect the *phase space* to contain more function types, some of them with fundamentally different behaviour. One way to illustrate this is Eq. (C.0.5) for arbitrary T. The characteristic equation reads

$$\lambda + \exp(-\lambda T) = 0, \tag{C.0.8}$$

which, in general, has an infinite amount of roots and, hence, an infinite amount of independent solutions, whereas for $T = 0$, there is only the exponential function (C.0.7) as a fundamental solution.
Therefore, one should not try to expand the term $u(t-T)$ as a finite Taylor series

$$u(t-T) = \sum_{n=0}^{N} \frac{(-T)^n}{n!} \frac{\partial^n}{\partial t^n} u(t) \tag{C.0.9}$$

of order N. This leads to an ODE of the same order, which can only have N independent solutions.
This example shows that a Taylor series approach usually fails, and it might be an analogous differential equation for very small time delays only. This has to be be discussed for every single problem [20]. However, if autonomous cruise control systems (ACCS) reduce the time delay of their algorithms to a margin, they might as well be approximated by a Taylor series. This shows the basic research that has to be done before implementing ACCS [41].
Apart from the characteristic equation of linear ODDE with constant coefficients, there is no recipe to solve ODDE. In general, it is much harder to determine these solutions than for the corresponding ODE. In particular, nonlinear terms as in a Bando model with explicit time delay

$$\dot{v}_n(t+T) = a\left[\tanh(b_n - 2) + \tanh(2) - v_n\right], \tag{C.0.10}$$

complicate the analysis. However, the asymptotic behaviour can be extracted for some problems [20].

Time delay seems to be a natural part of traffic flow due to the driver's retarded reaction towards traffic situations. In deterministic models, the delay has to be regarded as an averaged quantity. However, a major question is why it has not yet been included in continuum models. The discussion of analogous models in chapter 4 clearly shows that it should be done in order to incorporate the microscopic driver behaviour. This certainly opens up a new field of research.

Appendix D

Numerical Techniques

The simulations in this dissertation were carried out in *C*. It turns out that the programs run faster this way than for standard integration programs such as *MATLAB*. Where possible, appropriate calculations were supported by *MAPLE*. The stability analysis of chapter 3 is one example.

Both car-following and continuum models can be simulated in **real time**, if dimensions are incorporated. In the first case, real time refers to a certain number of cars on the road, whereas for the latter to a stretch of road of a certain length.
The equivalent of a few thousand cars was considered in this work, typically $N = 2000$. For an average headway of about 25m, this equals a stretch of road about 50km long. The large number of cars is necessary to investigate the long-time behaviour of traffic for any given initial condition, such as a jump in headway (chapter 5) or a pulse (section 3.7).
There are two main advantages of car-following simulations over continuum modelling. Firstly, every car can be simulated individually with its own characteristic features (section 5.7). Secondly, rapidly changing headways in space do not cause problems during integration, because only discrete variables are involved in the governing equations. This differs from the continuum models, which typically contain spatial derivatives such as ρ_x and v_{xx}. When discretized, the accuracy of their approximations decreases with increasing spatial step-size and spatial gradients.
However, for the simulations considered, a **fourth-order Runge-Kutta algorithm** proved to be sufficiently accurate for both the car-following models and the travelling wave analysis of the continuum models. Here, car-following models in particular are integrated simply and efficiently. Nevertheless, the parameters of integration such as step-sizes of time and space have to be matched for every single problem.

The dimensionless Bando model was integrated with a fourth-order Runge-Kutta

algorithm of step-size $\Delta t = 0.005$. Large time-steps can lead to crossings of car trajectories, and smaller time-steps to unacceptably long CPU times.
On a 233MHz Pentium, a program for the simulation of 1000 cars over a time $t = 1000$ takes about 15 minutes. About 500 of those runs were required to obtain the phase diagram Fig. 5.2.
For the dimensional model of section 3.5, the step-size was $t = 0.01$s. This enables real-time simulations of up to $N = 1000$ cars, where the number N depends obviously on the available computer power.
The need for numerical simulations is shown when the critical headways b_{crit} of Bando waves are determined. In this work, this value and the corresponding headway of the Bando wave b_{bw} were only obtained numerically, either by running a car-following simulation or by integrating the travelling wave solution Eq. (3.4.12). Decreasing the downstream headway, b_{crit} is given by the latter method, when integration breaks down. b_{bw} is the global minimum of the oscillatory solution on the verge of integration breakdown [15].

The advantage of continuum models is apparent, when travelling waves are analysed. The integration of Eq. (3.4.12), for example, takes only 5 seconds. In contrast, travelling waves in the car-following model can only be obtained by running the corresponding program for a sufficiently long time (Fig. 3.4). On the other hand, the **shooting method** of the continuum model is very sensitive towards the spatial step-size, initial speed gradient $v_x|_{x\to-\infty}$ and density gradient $\rho_x|_{x\to-\infty}$. This complicates the determination of the correct travelling wave solution and the headways b_{crit} and b_{bw}. Moreover, the instability of the travelling wave occurs only in the car-following model. The shooting method delivers solutions without a linear or nonlinear stability criterion.

In the numerical simulations of the car-following model, the cars were represented by a linked list. This way, the insertion of a vehicle at an on-ramp becomes a rather straightforward task. In addition, it saves time compared with an array structure, in which the upstream cars have to be moved down the array every time a car enters the lane.

Publications

Several parts of this dissertation have been published as follows:

- Chapter 3:

  Continuum approach to car-following models,
  Peter Berg, Anthony Mason and Andrew Woods,
  Physical Review E, Volume 61, 2000

  and

  Relating car-following and continuum models of road traffic,
  Peter Berg and Andrew Woods,
  In: *Traffic and Granular Flow '99*,
  D. Helbing, H.J. Herrmann, M. Schreckenberg and D.E. Wolf,
  Springer, 2000

- Chapter 5:

  Traveling waves of an optimal-velocity model of freeway traffic,
  Peter Berg and Andrew Woods,
  Physical Review E, Volume 63, 2001

  and

  Travelling waves in a linearly stable, optimal-velocity model of road traffic,
  Peter Berg and Andrew Woods,
  In: *Progress in Industrial Mathematics at ECMI 2000*,
  M. Anile, V. Capasso and A. Greco,
  Springer, 2001

- Chapter 6:

  On-ramp simulations and solitary waves of a car-following model,
  Peter Berg and Andrew Woods,
  Physical Review E, Volume 64, 2001

Bibliography

[1] W.F. Adams. Road traffic considered as a random series. *Journal of the Institute of Civil Engineers*, 1936.

[2] Highways Agency and Transport Research Laboratory. M25: controlled motorways monitoring. Final report, 1996.

[3] AP. Beckstein: Staus kosten jährlich 200 Milliarden Mark. *Süddeutsche Zeitung*, 22 May, 1999.

[4] A. Bachem, M. Schreckenberg, and D.E. Wolf. *Traffic and granular flow.* World Scientific, 1996.

[5] R.G.V. Baker. On the kinematics and quantum dynamics of traffic flow. *Trans. Res. B*, 17, 1982.

[6] M. Bando, K. Hasebe, K. Nakanishi, and A. Nakayama. Analysis of optimal velocity model with explicit time delay. *Phys. Rev. E*, 58:5429–5435, 1998.

[7] M. Bando, K. Hasebe, K. Nakanishi, A. Nakayama, A. Shibata, and Y. Sugiyama. Phenomenological study of dynamical model of traffic flow. *J. Phys. I France*, 5:1389–1399, 1995.

[8] M. Bando, K. Hasebe, A. Nakayama, A. Shibata, and Y. Sugiyama. Dynamical model of traffic congestion and numerical simulation. *Phys. Rev. E*, 51:1035–1042, 1995.

[9] H. Baum. Volkswirtschaftliche Kosten und Nutzen des Verkehrs. Technical report, Forschungsgesellschaft für Strassen- und Verkehrswesen Köln, 1998.

[10] E. Ben-Naim and P.L. Krapivsky. Maxwell model of traffic flows. *Phys. Rev. E*, 59:88–97, 1999.

[11] P. Berg, A. Mason, and A.W. Woods. Continuum approach to car-following models. *Phys. Rev. E*, 61:1056–1066, 2000.

[12] P. Berg and A.W. Woods. On-ramp simulations and solitary waves of a car-following model. *Phys. Rev. E*, 64, 2001.

[13] P. Berg and A.W. Woods. Travelling waves in a linearly stable, optimal-velocity model of road traffic. In *Progress in Industrial Mathematics at ECMI 2000*. Springer, 2001.

[14] P. Berg and A.W. Woods. Travelling waves of an optimal-velocity model of freeway traffic. *Phys. Rev. E*, 63, 2001.

[15] J. Bevan. Travelling waves in the Bando model of road traffic. Master's thesis, University of Bristol, 1998.

[16] R.E. Chandler, R. Herman, and E.W. Montroll. Traffic dynamics: studies in car-following. *Opns. Res.*, 6:165–184, 1958.

[17] C.F. Daganzo. Requiem for second-order fluid approximations of traffic flow. *Trans. Res. B*, 29, 1995.

[18] O. Diekmann, S.A. van Gils, V. Lunnel, and H.O. Walther. *Delay Equations: Functional-, Complex-, and Nonlinear Analysis*. Springer, 1995.

[19] P.G. Drazin and R.S. Johnson. *Solitons: an introduction*. Cambridge University Press, 1989.

[20] R.D. Driver. *Ordinary and Delay Differential Equations*. Springer, 1977.

[21] Bundesministerium für Verkehr. *Verkehr in Zahlen 1998*. Deutscher Verkehrs-Verlag, 1998.

[22] D.C. Gazis, R. Herman, and R.B. Potts. Car-following theory of steady-state traffic flow. *Opns. Res.*, 7:499–505, 1959.

[23] D.C. Gazis, R. Herman, and R.W. Rothery. Nonlinear follow-the-leader models of traffic flow. *Opns. Res.*, 9:545–567, 1961.

[24] B.D. Greenshields. A study of traffic capacity. *Highway Research Record*, 14:448–477, 1934.

[25] H. Hassheider. Nutzen und Finanzierbarkeit transeuropäischer Verkehrsnetze, Diploma thesis, University of Münster, 1997.

[26] H. Hayakawa and K. Nakanishi. Theory of traffic jam in a one-lane model. *Phys. Rev. E*, 57:3839–3845, 1998.

[27] D. Helbing. Theoretical foundation of macroscopic traffic models. *Physica A*, 219:375–390, 1995.

[28] D. Helbing. Empirical traffic data and their implications for traffic modeling. *Phys. Rev. E*, 55:R25–R28, 1997.

[29] D. Helbing. Fundamentals of traffic flow. *Phys. Rev. E*, 55:3735–3738, 1997.

[30] D. Helbing. From microscopic to macroscopic traffic models. In *A perspective look at nonlinear media*, pages 122–139. Springer, 1998.

[31] D. Helbing. Traffic and related self-driven many-particle systems. *to appear in: Rev. of Mod. Phys.*, 2001.

[32] D. Helbing, A. Hennecke, and M. Treiber. Phase diagram of traffic states in the presence of inhomogeneities. *Phys. Rev. Lett.*, 82:4360–4363, 1999.

[33] D. Helbing, H.J. Herrmann, M. Schreckenberg, and D.E. Wolf. *Traffic and granular flow '99*. Springer, 2000.

[34] D. Helbing and B.A. Huberman. Coherent moving states in highway traffic. *Nature*, 396:738–740, 1998.

[35] D. Helbing and B. Tilch. Generalized force model of traffic dynamics. *Phys. Rev. E*, 58:133–138, 1998.

[36] D. Helbing and M. Treiber. Gased-kinetic-based traffic model explaining observed hysteretic phase transition. *Phys. Rev. Lett.*, 81:3042–3045, 1998.

[37] R. Herman, E.W. Montroll, R.B. Potts, and R.W. Rothery. Traffic dynamics: analysis of stability in car-following. *Opns. Res*, 7:86–106, 1958.

[38] M. Herrmann and B.S. Kerner. Local cluster effect in different traffic flow models. *Physica A*, 255:163–188, 1998.

[39] E.N. Holland. *Continuum and car-following models of road traffic.* PhD thesis, University of Cambridge, 1995.

[40] E.N. Holland and A.W. Woods. A continuum model for the dispersion of traffic on two-lane roads. *Trans. Res. B*, 31:473–485, 1997.

[41] S. Hooper. Modifications of Bando's car-following model of highway traffic. Master's thesis, University of Bristol, 2000.

[42] S. Hume. The energy crisis and us. *Vancouver Sun*, 2 June, 2001.

[43] R.S. Johnson. A non-linear equation incorporating damping and dispersion. *J. Fluid Mech.*, 42:49–60, 1970.

[44] B.S. Kerner. Congested traffic flow: observations and theory. *Trans. Res. Record*, 1678:160–167, 1999.

[45] B.S. Kerner. title tba. *to appear in: Networks and spatial economics*, 2001.

[46] B.S. Kerner, S.L. Klenov, and P. Konhäuser. Asymptotic theory of traffic jams. *Phys. Rev. E*, 56:4200–4216, 1997.

[47] B.S. Kerner and P. Konhäuser. Cluster effect in initially homogenous traffic flow. *Phys. Rev. E*, 48:2335–2338, 1993.

[48] B.S. Kerner and P. Konhäuser. Structure and parameters of clusters in traffic flow. *Phys. Rev. E*, 50:54–83, 1994.

[49] B.S. Kerner and H. Rehborn. Experimental properties of phase transitions in traffic flow. *Phys. Rev. Lett.*, 79:4030–4033, 1997.

[50] B.S. Kerner and H. Rehborn. Messungen des Verkehrsflusses: charakteristische Eigenschaften von Staus auf Autobahnen. *Internat. Verkehrswesen*, 5:196–203, 1998.

[51] A. Klar and R. Wegener. A hierarchy of models for multilane vehicular traffic. Part 2: numerical investigations. *SIAM*, 59:1002–1011, 1999.

[52] T.S. Komatsu and S. Sasa. Kink soliton characterizing traffic congestion. *Phys. Rev E*, 52:5574–5582, 1995.

[53] R. Kühne. Macroscopic freeway model for dense-stop-start waves and incident detection. In *9th Int. Symp. on Transp. and Traffic Theory*, pages 21–42. VNU Science Press, 1984.

[54] R. Kühne. Verkehrsablauf auf Fernstraßen. *Phys. Bl.*, 47:201–204, 1991.

[55] D.A. Kurtze and D.C. Hong. Traffic jams, granular flow and soliton selection. *Phys. Rev. E*, 52:218–221, 1995.

[56] H.Y. Lee, H.W. Lee, and D. Kim. Origin of synchronized traffic flow on highways and its dynamic phase transitions. *Phys. Rev. Lett.*, 81:1130–1133, 1998.

[57] W. Leutzbach. *Introduction to the theory of traffic flow.* Springer, 1998.

[58] M.J. Lighthill and G.B. Whitham. On kinematic waves II: a theory of traffic flow on long crowded roads. *Proc. Roy. Soc. Lond. A*, 229:317–345, 1955.

[59] G. Mainardus and G. Nürnberger. *Delay Equations, Approximation and Application.* Birkhäuser-Verlag, 1985.

[60] A.D. Mason. *Mathematical problems of road traffic and related problems.* PhD thesis, University of Cambridge, 1998.

[61] A.D. Mason and A.W. Woods. Car-following model of multispecies systems of road traffic. *Phys. Rev. E*, 55:2203–2214, 1997.

[62] P.G. Michalopoulos and P. Yi. Continuum modelling of traffic dynamics for congested freeways. *Trans. Res. B*, 27:315–332, 1993.

[63] P.K. Munjal and L.A. Pipes. Propagation of on ramp density perturbations on unidirectional two- and three-lane freeways. *Trans. Res. B*, 5:241–255, 1971.

[64] T. Nagatani. Modified KdV equation for jamming transition in the continuum models of traffic. *Physica A*, 261:599–607, 1998.

[65] T. Nagatani. TDGL and MKdV equations for jamming transition in the lattice models of traffic. *Physica A*, 264:581–592, 1999.

[66] T. Nagatani. Density waves in traffic flow. *Phys. Rev. E*, 61:3564–3570, 2000.

[67] K. Nagel. Particle hopping models and traffic flow theory. *Phys. Rev. E*, 53:4655–4672, 1996.

[68] K. Nagel and M. Schreckenberg. A cellular automaton model for freeway traffic. *J. Phys. I. France*, 2:2221–2229, 1992.

[69] K. Nakanishi, K. Itoh, Y. Igarashi, and M. Bando. Solvable optimal velocity models and asymptotic trajectory. *Phys. Rev. E*, 55:6519–6532, 1997.

[70] G.F. Newell. Nonlinear effects in the dynamics of car-following. *Opns. Res.*, 9:209–229, 1960.

[71] H.J. Payne. FREFLO: a macroscopic simulation model of freeway traffic. *Transp. Res. Record*, 722:68–77, 1979.

[72] L.A. Pipes. Car-following models and the fundamental diagram of road traffic. *Trans. Res.*, 1:21–29, 1967.

[73] I. Prigogine and F.C. Andrews. A Boltzmann-like approach for traffic flow. *Operat. Res.*, 8, 1960.

[74] H.W. Richardson. A note on the distributional effect of road pricing. *JTEP*, pp. 82-85, 1974.

[75] P. Ross. Traffic dynamics. *Transp. Res.*, 22B:421–435, 1988.

[76] M. Schreckenberg and D.E. Wolf. *Traffic and granular flow '97*. Springer, 1998.

[77] H. Schuh. Freie Fahrt in der Kolonne. *Die Zeit*, 17 June, 1999.

[78] Y. Sugiyama and H. Yamada. Simple and exactly solvable model for queue dynamics. *Phys. Rev. E*, 55:7749–7752, 1997.

[79] M. Treiber, A. Hennecke, and D. Helbing. Derivation, properties and simulation of a gas-kinetic-based, nonlocal traffic model. *Phys. Rev. E*, 59:239–253, 1999.

[80] M. Treiber, A. Hennecke, and D. Helbing. Congested traffic states in empirical observations and microscopic simulations. *Phys. Rev. E*, 62:1805–1824, 2000.

[81] J. Treiterer. Investigations and measurement of traffic dynamics. Technical report, Appx IV of the final report EES 202-2, Colombus Ohio State University, 1965.

[82] J. Walters. UK set choke on glut of cheap cars. *The Observer*, 25 July, 1999.

[83] D. Wanfahrt. Alternative Verkehrskonzepte und politische Massnahmen zur Verringerung der externen Effekte des motorisierten Individualverkehrs. Technical report, University of Bielefeld, 1997.

[84] G.B. Whitham. *Linear and nonlinear waves.* John Wiley & Sons, 1974.

[85] R.E. Wilson. Introduction to differential delay equations. Technical report, University of Bristol, 2000.

[86] R.E. Wilson. An analysis of Gipps' car-following model of highway traffic. *IMA J. Appl. Math.*, 66:509–537, 2001.

[87] R.E. Wilson and P. Berg. Existence and classification of travelling wave solutions of second order highway traffic models. In *Traffic and granular flow '01.* Springer, 2002.